THE CATALYTIC SOLVENTLESS SYNTHESIS OF DISILOXANE USING GOLD NANOPARTICLES SUPPORTED BY REDUCED GRAPHENE OXIDE

MUHAMMAD NUR IMAN BIN AMIR

FACULTY OF SCIENCE
UNIVERSITI MALAYA
KUALA LUMPUR

2023

THE CATALYTIC SOLVENTLESS SYNTHESIS OF DISILOXANE USING GOLD NANOPARTICLES SUPPORTED BY REDUCED GRAPHENE OXIDE

MUHAMMAD NUR IMAN BIN AMIR

THESIS SUBMITTED IN FULFILMENT OF THE REQUIREMENTS FOR THE DOCTORATE PHILOSOPHY PHD

DEPARTMENT OF CHEMISTRY
FACULTY OF SCIENCE
UNIVERSITI MALAYA
KUALA LUMPUR

2023

UNIVERSITI MALAYA

ORIGINAL LITERARY WORK DECLARATION

Name of Candidate: **MUHAMMAD NUR IMAN BIN AMIR**

Registration/Matric No: **SVA180020 or 17027736/2**

Name of Degree: **Doctor of Philosophy (PhD)**

Title of Project Thesis ("this Work"): **THE CATALYTIC SOLVENTLESS SYNTHESIS OF DISILOXANE USING GOLD NANOPARTICLES SUPPORTED BY REDUCED GRAPHENE OXIDE**

Field of Study: **Chemistry (Physical Chemistry)**

I do solemnly and sincerely declare that:

(1) I am the sole author/writer of this Work;
(2) This Work is original;
(3) Any use of any work in which copyright exists was done by way of fair dealing and for permitted purposes and any excerpt or extract from, or reference to or reproduction of any copyright work has been disclosed expressly and sufficiently and the title of the Work and its authorship have been acknowledged in this Work;
(4) I do not have any actual knowledge nor do I ought reasonably to know that the making of this work constitutes an infringement of any copyright work;
(5) I hereby assign all and every rights in the copyright to this Work to the Universiti Malaya ("UM"), who henceforth shall be owner of the copyright in this Work and that any reproduction or use in any form or by any means whatsoever is prohibited without the written consent of UM having been first had and obtained;
(6) I am fully aware that if in the course of making this Work, I have infringed any copyright whether intentionally or otherwise, I may be subject to legal action or any other action as may be determined by UM.

Candidate's Signature Date: 28/8/2022

Subscribed and solemnly declared before,

Witness's Signature Date: 28/8/2022

Name:

Designation:

THE CATALYTIC SOLVENTLESS SYNTHESIS OF DISILOXANE USING GOLD NANOPARTICLES SUPPORTED BY REDUCED GRAPHENE OXIDE

ABSTRACT

Most of the synthetic chemical reactions are involved in the application of various organic solvents. However, some of the toxic solvents are mainly used specifically in the chemical industry and research laboratory. These toxic solvents have caused major environmental pollution and degradation of worker's physical and health. Therefore, the green chemistry approach is important to provide an alternative chemical process either by reducing or eliminate the usage of harmful solvents during reaction. Subsequently, the key aspect of the green artificial method is to utilize sustainable products, safe chemical and to carry out the chemical process under solventless conditions. Consequently, the catalytic design is important to produce an efficient and effective catalyst that can produce high conversion and selectivity in a solventless reaction. This project was focused on the synthesizing and characterizing gold (Au)-based catalyst because Au has electrochemical stability in strong acid conditions and remarkable selectivity for dehydrogenative coupling reaction. Au synthesized in this project was present as nanoparticles sized as confirmed by XRD and HR-TEM analysis. It was found that, the gold nanoparticles (AuNPs) have good interaction with reduced graphene oxide (rGO) support as XPS analysis demonstrated the interaction of Au-O-C. The catalyst of AuNPs/rGO was synthesized with different molarity of Au solution by using trisodium citrate ($Na_3C_6H_5O_7$) as a reducing and capping agent in one pot synthesis method prior to its solidification in freeze drier process. Then, the catalyst was tested in both solvent and solventless in oxidation reaction of dimethylphenylsilane (DMPS) into 1,3-diphenyltetramethyldisiloxane. The reaction with benzaldehyde solvent showed 100% conversion after one hour whereas reaction without solvent showed 70% conversion after 12 hours because the substrate's viscosity in solventless reaction was higher than solvent reaction. However, the solventless reaction showed 100% selectivity compared to 84%

selectivity in solvent reaction. Different reduction agent catalysts were tested and reaction parameter of the catalyst weight, Au concentration and temperature had been varied in the reaction. It was found that 4 wt% mM AuNPs/rGO was the optimizing catalyst in dehydrogenative coupling of hydrosilanes. The catalytic activity of 4 wt% mM Au was higher than other Au concentration possibly due to lower precursor deposition compared to higher Au concentration of catalyst that led to lower catalytic activity. The catalytic activity of AuNPs/rGO synthesis from sodium borohydride ($NaBH_4$) reduction agent was higher than citrate reduction agent because $NaBH_4$ is a stronger reduction agent that possibly created strong bonding between BH_4^- with the core of AuNPs. The AuNPs/rGO catalyst reusability was tested for five times with small decrease of conversion because no significant functional and structure of the catalyst was changed based on FTIR and XRD analysis.

Keywords: gold nanoparticles, reduce graphene oxide, disiloxane, solventless, dehydrogenative coupling.

PEMANGKINAN TANPA PELARUT SINTESIS DISILOXANE MENGGUNAKAN ZARAHNANO EMAS DISOKONG OLEH PENGURANGAN GRAFIN OKSIDA

ABSTRAK

Lazimnya tindak balas kimia sintetik terlibat dalam penggunaan pelbagai pelarut organik. Walau bagaimanapun, terdapat beberapa pelarut yang toksik digunakan adalah tertumpu di dalam industri kimia dan makmal penyelidikan. Pelarut toksik ini telah menyebabkan pencemaran alam sekitar yang besar dan kemerosotan terhadap fizikal dan kesihatan pekerja. Oleh itu, pendekatan kepada kimia hijau adalah penting untuk menyediakan alternatif untuk proses kimia sama ada dengan mengurangkan atau menghapuskan terus bagi penggunaan pelarut yang berbahaya semasa proses tindak balas. Seterusnya, aspek utama kaedah buatan hijau adalah untuk menggunakan produk yang mampan, bahan kimia yang selamat dan menjalankan proses kimia dalam keadaan tanpa pelarut. Oleh itu, reka bentuk bermangkin adalah penting bagi menghasilkan pemangkin yang cekap dan berkesan serta yang dapat menghasilkan pengubahan dan kepilihan yang tinggi di dalam tindak balas tanpa pelarut. Projek ini tertumpu bagi mensintesis dan mencirikan pemangkin yang berasaskan emas (Au) kerana Au mempunyai kestabilan elektrokimia di dalam keadaan asid kuat dan keterpilihan yang luar biasa untuk tindak balas gandingan penyahhidrogenatif. Au yang disintesis dalam projek ini hadir sebagai partikel bersaiz nano yang telah melalui pengesahan oleh analisa XRD dan HR-TEM. Didapati, partikel nano emas (AuNPs) mempunyai interaksi yang baik dengan sokongan pengurangan grafin oksida (rGO) disokong melalui analisa XPS yang menunjukkan saling tindak Au-O-C. Pemangkin AuNPs/rGO telah disintesis dengan kemolaran berbeza larutan Au dengan menggunakan trinatrium sitrat ($Na_3C_6H_5O_7$) sebagai agen penurun dan penyekat dalam kaedah sintesis satu periuk sebelum pemejalan dalam proses pengeringan beku. Mangkin telah diuji dalam kedua-dua pelarut dan tanpa pelarut dalam tindak balas pengoksidaan dimethylphenylsilane

(DMPS) kepada "1,3-diphenyltetramethyldisiloxane". Tindak balas dengan pelarut benzaldehyde menunjukkan pengubahan 100% selepas satu jam manakala tindak balas tanpa pelarut menunjukkan pengubahan 70% selepas 12 jam kerana kelikatan substrat dalam tindak balas tanpa pelarut adalah lebih tinggi daripada tindak balas pelarut. Walau bagaimanapun, tindak balas tanpa pelarut menunjukkan keterpilihan 100% berbanding keterpilihan 84% dalam tindak balas pelarut. Telah diuji bagi perbezaan agen pengurangan pemangkin serta parameter tindak balas berubah bagi berat pemangkin, kepekatan Au dan suhu dalam tindak balas. Ia didapati 4 wt% mM AuNPs/rGO adalah pengoptimuman pemangkin dalam gandingan penyahhidrogenatif hidrosilanes. Keaktifan bermangkin melalui 4 wt% mM Au adalah lebih tinggi daripada kepekatan Au yang lain sama sekali disebabkan oleh pemendapan pelopor yang lebih rendah berbanding kepekatan Au yang lebih tinggi terhadap pemangkin itu yang membawa kepada keaktifan bermangkin yang lebih rendah. Keaktifan bermangkin oleh AuNPs/rGO yang disintesis melalui agen pengurangan natrium borohidrida ($NaBH_4$) adalah lebih tinggi daripada agen pengurangan sitrat kerana $NaBH_4$ ialah agen pengurangan yang lebih kuat yang sama sekali mewujudkan ikatan kuat antara BH_4^- dengan teras AuNPs. Kebolehgunaan semula oleh pemangkin AuNPs/rGO telah diuji selama lima kali melalui pengurangan pengubahan yang kecil kerana tiada fungsi dan struktur pemangkin yang ketara telah diubah berdasarkan analisa FTIR dan XRD.

Kata kunci: zarahnano emas, zarah grafin oksida, "disiloxane", tanpa pelarut, gandingan penyahhidrogenatif.

ACKNOWLEDGEMENTS

Thanks, Allah, for my wife (Siti Nazifah binti Elias) and all my family for the support throughout my PhD journey. This thesis would not have been possible without the efforts and support of people at the Universiti Malaya (UM). I have learned a lot and really enjoyed working on this thesis. I would like to send my humble gratitude to all the people who helped me with their valuable support throughout the process of completing this research project. I would like to acknowledge and express my deepest gratitude to my supervisors, Dr. Azman bin Ma'amor and Dr. Nurhidayatullaili binti Muhd Julkapli for their helpful guidance, advises, clear explanation and encouraging supervision throughout the course of this work. I deeply express my thanks to them in helping me in editing the contents and wording of this thesis. Without the guidance from them, I would be in nowhere to complete my PhD study.

Next, I would like to send my gratitude to my postgraduate senior, Ahmed Halilu for sharing his experience, generous assistance, and great moral support that was truly necessary as an encouragement for me throughout the execution of this project. Most importantly, I would also like to acknowledge my colleagues greatly also in UM and all my dearest friends in NANOCAT. I deeply appreciated their precious ideas and support throughout the entire study. I am also truly thankful to all Chemistry Department lecturers and supporting staff members for all the help and patience in guiding me.

Additionally, this project would not be possible without the research grants provided by UM. This research was supported by a grant from the Universiti Malaya Research Grant (UMRG) and Postgraduate Research Fund (PPP) for the sources of funding through this study. I gratefully acknowledge UM for financial supporting that helped me in this study. Lastly, I would like to take this opportunity to express my deepest gratitude to my beloved parents, wife and all family members through their encouragement and support me to continue studying.

TABLE OF CONTENTS

LIST OF FIGURES

LIST OF TABLES

LIST OF SYMBOLS AND ABBREVIATIONS

AC	: Active carbon
Ar	: Argon
AuNPs@SIL-g-G	: AuNPs in supramolecular ionic liquids grafted on graphene
EPPG	: Benchmarked against pristine graphene
BCO	: Bicyclo[2.2.2]octene
C	: Carbon
CNTs	: Carbon nanotubes
C_3N_4NTs	: Carbon nitride nanotubes
C4A5	: Calix[4]amidocrown-5
CO	: Carbon monoxide
COOH	: Carboxylic
F	: Capacitance (standard unit farad)
CaO	: Calcium oxide
CeO_2	: Cerium(IV) oxide
CVD	: Chemical vapor deposition
$HAuCl_4$	: Chloroauric acid
cb	: Conduction band
Cu	: Copper
CYs	: Cotton yarns
CN	: Cyanide
CV	: Cyclic voltammogram
SH	: Cysteamine
DI	: Deionized
DMPS	: Dimethylphenylsilane
e^-	: Electron
EA	: Electronic affinity
hv	: Energy (photon)
EDS	: Energy dispersive spectrometer
FESEM	: Field emission scanning electron microscope
FID	: Flame ionization detection
FTIR	: Fourier transform infrared
C60	: Fullerene
GC	: Gas chromatography

GLC	:	Glassy carbon
Au	:	Gold
AuNPs	:	Gold nanoparticles
g	:	Gram
GO	:	Graphene oxide
GQDs	:	Graphene quantum dots
GON	:	GO nanosheets
G	:	Graphene
GRC	:	Graphite
GOQDs	:	Graphene oxide quantum dots
HR	:	High Resolution
HR-TEM	:	High-resolution transmission electron microscopy
H	:	Hydrogen
OH	:	Hydroxyl
IP	:	Ionization potential
Fe	:	Iron
L	:	Liter
LPE	:	Liquid phase exfoliation
MS	:	Mass spectroscopy
MgO	:	Magnesium oxide
MNPs	:	Metal nanoparticles
µm	:	Micrometer
mL	:	Milliliter
MIP	:	Molecular imprinted polymer
MWCNs	:	Multi-walled carbon nanotubes
mM	:	Millimolar
NGO	:	Nitrogen-doped graphene oxide
NMR	:	Nuclear magnetic resonance
TMPD	:	N, N, N′ ,N′- Tetramethyl-p- phenylenediamine
O	:	Oxygen
p-	:	p-aminothiophenol
KCl	:	Potassium chloride
h^+	:	Positive hole
BPPG	:	Plane-/basal plane pyrolytic graphite
PDMS	:	Polydimethylsiloxane

POM	:	Polyoxometalate
PtNPs	:	Platinum nanoparticles
rGO	:	Reduced graphene oxide
rGOCY	:	Reduce graphene oxide-coated cotton yarn
rAu-PtNPs	:	Rod gold-platinum nanoparticles
RuNPs	:	Ruthenium nanoparticles
rGO	:	Reduce graphene oxide
SiO_2	:	Silicon dioxide
Ag	:	Silver
$NaBH_4$	:	Sodium borohydride
SERS	:	Surface-enhanced Raman Spectroscopy
TEOS	:	Tetraethoxysilanes
TMOS	:	Tetramethoxysilane
TCD	:	Thermal conductivity detector
TGA	:	Thermal gravimetric analyzer
TiO_2	:	Titanium dioxide
$Na_3C_6H_5O_7$	:	Trisodium citrate
UV	:	Ultraviolet
UV-vis	:	Ultraviolet-visible
vb	:	Valence band
W	:	Work function
XRD	:	X-Ray diffraction
XPS	:	X-Ray photoelectron spectroscopy
ZnO	:	Zinc oxide

LIST OF EQUATIONS

CHAPTER 1: INTRODUCTION

1.1 Research background

Catalysis stays prominent within contemporary life. It has been well acknowledged that at least one catalytic phase is involved in 85–90% of commercial chemical processes (Védrine, 2017). The primary goals of using a catalyst are to achieve high activity, high reactant conversion, and high selectivity to targeted products. This characteristic of the catalyst prevents or restricts the separation or purification of our product, necessitating important considerations, especially in terms of cost and overall environmental issues. Numerous approaches have been used for synthesis of symmetrical siloxanes Chojnowski et al. (2005) that employed Lewis acid by using perfluorotriphenylboron, as a catalyst to generate symmetrical siloxanes via a hydrosilane-alkoxysilane coupling process or by using intermolecular silanol condensation (Hackel & McGrath, 2019). Although various methods have been reported in literature, disiloxane synthesis by using transition metal catalysts is widely applied. Indium(III) was reported to be used as a catalyst in air oxidation of hydrosilanes (Sridhar et al., 2009). Other than indium (Sridhar et al., 2009) and nickel (Lv et al., 2019), transition metals such as cobalt (Pattanaik & Gunanathan, 2019) also was reported in synthesis of siloxanes.

Siloxanes which have a Si-O-Si linkage are unique in nature and play important roles in silicone industries, microelectronic industries, beauty products, liquid crystal display element, and sensor fabrication. It was also been used in the medicine industries such as muscle relaxants (Lv et al., 2019). These silicon (Si) derivatives was used in Hiyama-coupling reactions. Siloxane derivatives, such as 1,3-bis(phenylethynyl) tetramethyldisiloxane, was used as key components for the preparation of macrocycles (Kuciński et al., 2022; Mézailles et al., 2001).

Nevertheless, with ever increasing environmental regulations, organosilicon derivatives are gaining momentum as viable alternatives to other materials. Many conventional chemical processes make use of large amounts of volatile organic solvents (VOS) and toxic chemicals (Nazari & Shabanian, 2014; Radwan & Abbas, 2009). One of the priorities towards the main goals of green chemistry is to replace of such a hazardous reaction solvent (Karthikeyan et al., 2012; Lancaster, 2020; Sekhar et al., 2013; Sharma & Sharma, 2009; Siddiqui et al., 2011). This study applied the fifth green chemistry principle by using heterogenous catalyst in organic reaction synthesis. With respect to the global environmental awareness, the design of solventless green processes has gained noticeable attention many researchers (Adib et al., 2007; Calvino et al., 2006; Sheldon, 2018). By huge awareness of this environmental concern, many reactions with solid-state or solventless conditions have been designed to reduce the cost and importantly follow up with the pollution decrease. These reactions are much easier to proceed cleanly, less subproduct and efficiently with procedure work up, hence in short span of time these reactions gained viral in popularity and vital importance in future (Anastas et al., 2000; Anastas & Kirchhoff, 2002; Lancaster, 2020). In 1990, the green chemistry campaign had been initiated in the United States under pollution prevention legislation by keeping in view that organic substances could be produced an environmentally clean manner (Lancaster, 2020).

The perspectives based on Hutchings and Haruta (2005) about the catalytic activity of gold (Au) has opened many potential in nanotechnology research and chemical synthesis. Interestingly, from that there are three major lines of approach in Au catalysts. First, gold nanoparticles (AuNPs) are capable of being a very active catalyst for many reactions, especially at temperatures below 200 °C. New green routes for efficient processes and chemical syntheses related to hydrogen energies are being explored (Haruta, 2003). Second, AuNPs combined with a variety of support materials, for examples graphene (G),

zeolites and activated carbon can present a wide range of environmental applications. Especially, they are the most effective in cleaning contaminated air under humid conditions and at ambient temperature without consuming heating energy. A useful way for an approach in this field of applications maybe mixing with other noble metal catalysts deposited on different metal oxide supports (Okumura et al., 2003). The third important component according to many researchers are the particle size of Au must be present in nanometer to give promising catalytic activity (Hutchings & Haruta, 2005).

The use of G as support is expected to increase the reaction rates because the adsorption capacity of G bringing substrates and reagents near the active metal nanoparticles (MNPs). Copper (Cu) (Ansari & Bhat, 2019) and palladium (Pd) (Khan et al., 2020) nanoparticles (NPs) supported on G have been tested in the dehydrogenative coupling of alcohol with hydrosilanes and dehydrogenative coupling of hydrosilanes and amines (Ansari & Bhat, 2019; Khan et al., 2020). For both processes, it was found that G was working very well as a support that could lead to a more efficient catalyst compared to the MNPs that are deposited on other material oxide supports (Ganesh & Ramakrishna, 2020; Nasrollahzadeh et al., 2018).

The use of appropriate catalysts for any reactions involved has been approached in a variety of methods to produce at fast conversion rates for reaction rates while also improving selectivity products. The activity of MNPs supported on G is superior to the activity of MNPs on other oxide supports because G modulates the electronic density on the MNPs that can result in lowering MNP size growth and develop a strong metal–support interaction necessary to avoid metal leaching especially during catalyst synthesis or during severe reaction conditions (Ganesh & Ramakrishna, 2020; Redón et al., 2021). The use of G or graphene oxide (GO) especially as support is expected to increase the reaction rates because the adsorption capacity of G bringing substrates and reagents near

the active MNPs. This is occurred due to tunable electrical properties present on the G structure itself. In addition, its ultrahigh thermal conductivity and high chemical stability may possibly promote high loading of that catalytically active sites (Guo et al., 2019; Papiya et al., 2019).

It is known that dimethylphenylsilane (DMPS) is recognised with a chemical properties as clear colorless liquid. The substrate has physical properties as boiling point at 157 °C, 744 mmHg and density about 0.889 gcm^{-3}. Most common use of this chemical as reagent for enol ether synthesis and used as a precursor by plasma deposition processes in optical emission spectroscopy. While in hydrosilylation reaction, the substrate is used as reagent with a transition metal catalyst as the hydrosilane that adds to carbon–carbon double or triple bonds to give alkenylsilanes or alkylsilanes (Komiyama et al., 2017; Roy, 2007).

This research project is considered a novel since still not much research and literature report Au supported on G catalyst in aldehyde hydrosilylation. Au catalysts have recently been intensively studied in relation to many important organic transformations and hydrogenation as Au's uniquely excellent selectivity toward the target product exceeds that of other noble metals (i.e., Pd, Pt, Ru,), making it environmentally attractive due to being good in reproducibility that can be used multiple times and highly efficient catalyst (Naeimi & Farahnak Zarabi, 2018; Pocklanova et al., 2016; Sawama et al., 2016). AuNPs supported on a series of different Au loading are prepared by supported with G materials that undergo freeze-drying process and the used of reducing agent throughout the process are chosen to complete the synthesis catalyst.

In this work, the catalysts were performed in dehydrogenative coupling of hydrosilanes where the reaction temperature, residence time, catalyst loading with different type of Au based catalysts. This reaction also common as the type of reaction used in the formation

of Si-Si bonds. The reaction is proceeded with metals catalyst or other organic compounds. While this research study of using the inorganic heterogenous catalyst with the desired properties and the process conditions were chosen for catalyst and reaction optimization. The final reaction product, disiloxane was the targeted material which had been observed further.

1.2 Problem statement

Typically, many common solvents such as toluene was used to synthesis disiloxane. Throughout the last couple decades, the idea of sustainable development has become widely tolerated, particularly in the chemical industry. The extensive and broad use of solvents in the fine chemical and pharmaceutical industries is one of the most significant waste disposal problems which has led to production of tones of aqueous waste per year contaminated with organic solvents (Zhou et al., 2019). The fine chemical and pharmaceutical sectors have already been identified as substantial contributors of chemical waste. Large quantities of organic solvents, relative to reagents, are usually essential for chemical reactions to proceed. In addition, many extractions, purifications, and cleaning processes also depend on solvents, with large excesses necessary to achieve sufficient product purity. By giving one of the examples through the process used in the manufacture of the most widely used in herbicide by glyphosate that used brand such as Roundup. This reaction uses the sodium salt of 2,2'-iminodiethanoic acid as one of the intermediates. This is made in a series of reactions from ammonia, methanal (formaldehyde) and hydrogen cyanide. Although hydrogen cyanide is a very useful reagent, it is extremely toxic. A recent innovation has been the introduction of a new route to sodium salt. The starting materials are epoxyethane together with ammonia and produce target product that was 2,2'-iminodiethanol (diethanolamine) (Humans, 2013). Other solvents wastes may finally end up in landfill and this is the point at which to create

an idea to the waste that is significant and it might be dangerous towards environment and human beings.

Furthermore, the annual industrial scale for organic solvents production was estimated at 20 million metric tons (Clarke et al., 2018). Due to the concern toward environment, it was important in this work to create a green method to prepare disiloxane with minimum use of solvent and auxiliaries which persist with the fifth principle of Green Chemistry. Besides that, the utilization of catalysts plays a huge part in the development of more sustainable processes to produce chemicals. There are many advantages in developing and using catalysts for industrial reactions, some important ones being they influence the necessary circumstances, often decreasing energy demand by lowering the pressure and temperature used. The use of catalyst also enables alternative reactions to be used which have significantly reduce waste and indirectly give better in atom economy. It is possible to reduce unwanted side products, more precisely to control the reaction pathways and make it easier to purify and separate the required product.

Most industrial applications of hydrosilylation are catalyzed by the used of late transition metals, which are toxic and expensive (Huang et al., 2014; Marciniec et al., 1992). Heterogeneous catalysis would involve a reaction directly when the substrate molecules are adsorbed to the surface of the catalyst. Specifically, supported AuNPs of heterogenous catalyst possess a significant specialty in the application of Au heterogeneous catalysis in numerous reactions. The interfaces and surface of heterogeneous catalysts are essential with their performance as they are often considered to be active sites for catalytic reactions. The catalytic cycle involves Au^{3+} and Au^{+}. While the catalytically active species is Au^{3+}. Carbon that used to support Au catalysts are now industrially produced for this reaction and the use of a highly toxic mercury chloride catalyst can thereby be avoided (Haruta & Daté, 2001; Ishida et al., 2019). The use of

nanoparticle size with wide distribution of Au is important that contributes of higher catalytic activity even at low temperature. Nevertheless, higher MNPs loading can also increases the tendency towards particle agglomeration and sintering thus reduces the catalytic performance (Ji et al., 2021). Based on research done by Anwar et al. (2022), the study observed that when the Au loading increased from the void of smaller particles size and there has high tendency for agglomeration at high temperature.

Other perspective feature of supported Au catalysts is that the catalytic activity of Au strongly depends on the kind of support. From the point of view of practical applications, it is important to select the suitable support to stabilize AuNPs and to optimize contact structure between AuNPs with support (Corma & Garcia, 2008; Takei et al., 2012). Based on Ishida et al. (2019), there are several reviews to give a general overview of supported catalysts using AuNPs. Therefore, this project presented a novel method to synthesis the disiloxane by oxidative coupling of hydrosilane in a solventless reaction and to improvised for a new catalyst regarding with the used of current catalyst such as transition metal catalyst complexes that are not stable. The research is using precious metals catalyst AuNPs to be supported with GO. The reaction of hydrosilylation would be characterized with reducing production cost and high recyclability of catalyst used for the reaction. Herein we report our study on the dehydrogenative coupling of hydrosilanes with benzaldehyde and the most important part is by solventless reaction that further used with catalyzed by AuNPs on reduced graphene oxide (AuNPs/rGO).

This is considered as new and novel method in catalytic process for hydrosilylation reaction and targeting of selectivity of the product while advantages of this approach include the ease of that reaction. This research project also promoted low production cost for the industry as the reaction was performed solventless. Therefore, reaction cost was reduced since solvent was not used, the separation step between product and solvent was

removed, reduced safety hazards and obviously eliminated the generation of solvent waste. Overall, hydrosilylation reaction established in this work was a green and environmentally friendly catalytic system. In this project, AuNPs/rGO was used as a heterogeneous catalyst to run the reaction. As this project's concern is to minimize usage of solvents, heterogeneous catalysts are easier to recover dry by oven or filtration and obviously recycle without the need of any solvent extraction methods. For this current study, the solventless reaction would be focused on AuNPs-rGO catalyst as illustrated in Figure 1.1.

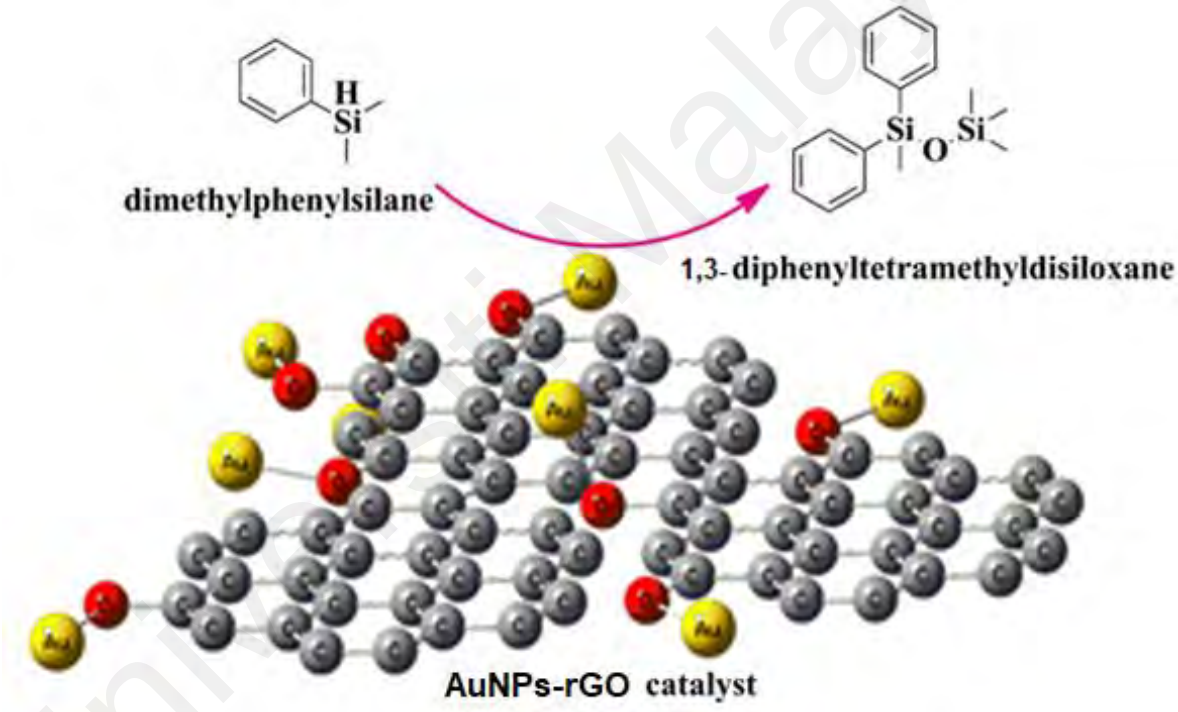

Figure 1.1: Possible arrangement of AuNPs-rGO catalyst.

1.3 Scope of work

Most industrial applications using chemical reactions are catalysed by late transition metals, which are toxic and expensive. Considering the vast number of generated products in chemical industries it is of great importance to circumvent negative impact on the environment. The use of catalysts opens the possibility for the adoption of less harmful reagent and cut down on generated waste products, promoting in more atom economic transformations which are more chemo selective or even unattainable without catalysts.

Most current effort is aimed at replacing heavy late transition metal complexes for less expensive and more environmentally benign early metals, such as Ti_2, Zr_3, and Mo_4, Mo_5, or first d-series metals[6], metals[7], particularly Fe_8 and Cu_9. Catalysts are characterized by different parameters such as selectivity, stability and activity. This research was using a catalyst with precious metals of AuNPs supported with GO. In the beginning of catalyst synthesis, most of the studies used a reducing agent with citrate-stabilized method. Because this reducing agent process has been the most popular method introduced by Turkevich in which trisodium citrate dihydrate is mixing into boiling chloroauric acid together with vigorous stirring (Sudhakar & Santhosh, 2017).

The main focus of this research is to develop an efficient catalyst to be used in the synthesis of disiloxane. Therefore, the scope of this research is outlined as below:

i. The synthesis of reduced graphene oxide (rGO) material from GO (that previously prepared using graphite (GRC) material under improved Hummer's method) as supporter for AuNPs in 5 different concentrations.
ii. Characterization on the physicochemical properties of synthesized AuNPs/rGO catalysts using FESEM-EDS, HR-TEM, UV-Vis, XRD, RAMAN, FTIR, TGA and XPS.
iii. Catalytic properties determination using the synthesized AuNPs/rGO catalyst for the oxidative coupling of hydrosilane under solvent and solventless reaction for the synthesis of disiloxane.
iv. The optimization of solventless reaction and final product analysis using GC-MS and NMR spectroscopy.

1.4 Research novelty

The Si-O bond is the linkage that is most encountered in nature between heteroatom to Si. This is due to the strong nature of this bond, resulting in, e.g., Si-C bonds being

replaced by Si-O bonds and, eventually, the formation of oligomeric siloxane structures. Such structures show higher flexibility and are more inert chemically in comparison with analogous systems, based on chains constituted by C-C bonds. These properties, among others, are the reason for the significant research interest in polysiloxane and other organosilicon compounds (Glosz et al., 2020). Although various methods and reactions have been reported in literature. There are reactions related to disiloxane synthesis by using transition metal catalysts that have been widely applied. However, the reactions especially reactions of silicon has only received marginal attention in the academic world. (Bailey & Rochow, 1994; Lewis & Rethwisch, 1993).

The novelty of this study is the application of the newly developed catalyst in the solventless reaction process. As applications of Au in catalysis increased dramatically over years, there are many studies conducted on catalysis of AuNPs supported on G materials. In these studies, AuNPs supported with rGO exhibit successful conversion under solventless reaction. In addition, there is lack of study focusing on solventless reaction with AuNPs/rGO catalyst due to much research that have less concern and multicomponent reactions still require a solvent to properly promote them. This requirement makes the knowledge of all advantages and drawbacks of each solvent a central issue when trying to optimize multicomponent reactions. Only a few studies with actual evidence of solvent effects on this vital response have been published (Neto et al., 2022). Moreover, there are many advantages using the solventless reaction for production of desirable products and one of it is the ease of handling the final product after reaction. It was only to separation product from catalyst due to higher in obtaining one selectivity with no side products after reaction.

The excellent conversion showed by AuNPs/rGO is due to the nature of support which contains oxygen moiety and moderate graphitic character and the catalyst also derivatives

proved to be excellent in many reactions (Sachdeva, 2020; Samantara et al., 2021). Most of the heterogeneous supported Au catalysts can be recovered and reused easily making them environment and eco-friendly catalysts (Balwe et al., 2019; Guria et al., 2016). From the excellent activity of AuNPs supported on reduced graphene oxide rGO, it is expected to contribute positive outcomes in our research in oxidative coupling of hydrosilane reactions to synthesis disiloxane. The research work presented a green catalyst synthesis method of metal nanoparticles supported with carbon materials of AuNPs/rGO, which was investigated for the process under solventless reaction. The optimizations of the new catalysts synthesis between GO that has been reduced were used as support with metal based AuNPs catalyst which has been contributing to many new scientific findings in the research community.

The basic principles especially in organic synthesis focus on the goals for obtaining a new synthetic strategy through production by utilization of atom-economical processes with minimal use of solvents and to reduce the potential waste. At the same time, production with the use of non-hazardous reagents. In addition, this can be applied using the production with economical energy sources that should not rely on fossil fuel combustion. Lastly, it is important to maximize the yield with the utilization of catalyst when appropriate (Zangade & Patil, 2019). Most of the reactions that used a suitable condition such as multicomponent reactions that are also gain special importance to the organic chemists are carried out under solventless. The merger of industrial imperatives and fundamental academic interests has enabled us, during this PhD research project, to develop a practical and scalable solution to important processes such as the regioselective in oxidative coupling of hydrosilane in a solventless reaction for synthesis of disiloxane.

1.5 Research hypothesis

It is hypothesized here that this project has led to a successful, green synthesis method of producing the AuNPs/GO catalyst, which was investigated for the process of solventless reaction applications. Even though reaction without solvent, possibly produce lower catalytic activity and this reaction possibly showed a high selectivity compared to reaction with solvent. Reaction without solvent can reduce the formation of side products thus reduced the industrial process in separating main product and side products compounds. Therefore, the use of solventless conditions on a solid catalyst is very convenient from the green chemistry perspective. Contrarily, solvent catalytic reaction showed higher conversion or reaction rate due to diffusion between solvent and reactant with catalyst compared with solventless that have contain reactant substrate only with catalyst in the reaction.

This study came up with a novel method of oxidative coupling of hydrosilane in a solventless reaction for synthesis of disiloxane. However, this theme has grown out of its original shell to gradually become, with the advent of selective catalysts, an important research area for organic synthesis.

1.6 Research objectives

The objectives of this study are described as follows: -

1. To prepare reduce GO (rGO) support using modified Hummer's method and synthesize AuNPs/rGO catalyst with different Au concentration.
2. To use AuNPs/rGO catalyst for solvent and solventless experiments in the dehydrogenative coupling reaction of dimethylphenylsilane (DMPS) into 1,3-diphenyltetramethyldisiloxane.
3. To test the reusability of AuNPs/rGO catalyst in terms of its catalytic activity in disiloxane synthesis.

1.7 Organization of Thesis

This thesis has been divided into 5 chapters with description as follow:

Chapter 1 - Consists of a general review about the overall research background including the problem statement, scope of work, research novelty and hypothesis, research objectives and together with the specific research objectives.

Chapter 2 - Highlighted on the literature review of the previous and latest research background of the theoretical foundations with related research study involved. Explaining about the materials, mechanism of chemical reaction of solventless and explore about the nanohybrid of the catalyst with any related chemical reactions.

Chapter 3 – Describe the specifications of the raw materials used, research methodology used to perform synthesis of materials that further used for the reaction analysis and the characterizations.

Chapter 4 - Presenting and discussing the characterization of synthesized catalyst and overall reaction analysis.

Chapter 5 - Summarized the overall conclusions and recommendation for future research proposal of this study.

CHAPTER 2: LITERATURE REVIEW

2.1 Theoretical background

It is estimated that around 80% of the industrial processes are catalytic, as are many of the reactions of modern organic synthesis (Okuhara, 2002; Pascanu et al., 2019; Yoo et al., 2020). The catalyst's mission is to provide reaction mechanisms with adequate activation energies that make chemical transformation possible (Hattori, 2001; Koledina et al., 2019; Pascanu et al., 2019). The role of the catalyst in a reaction to provide an alternative mechanism whose energy profile is lower than that of other routes by facilitating the transformation of reagents in products with decreasing the activation energy (Ea) of the process. Industrial catalysis is currently dominated using transitional metals as active centers that generally correspond to noble metals such as Au, silver (Ag) or platinum (Pt) (Loza et al., 2020; Mashayekhi et al., 2014; Suchorski & Drachsel, 2007). Other transition metals used are considered critical raw materials because there are very limited resources or because these resources are in geographical areas subject to political and/or economic problems. There is an initiative by the European Union (EU) to replace critical or expensive raw materials for other materials that are abundant and affordable. This EU initiative explicitly mentions metal catalysis as one of the keys and extremely vulnerable industrial sectors because of its high dependence on these costly or limited resources (Hernandez et al., 2018). For example, processes as important as catalytic reform, which provides approximately almost 40% of all automotive fuel and more than 90% of the raw material for the polymer industry, require of bifunctional catalysts based on acidic zeolites containing Pt and in less proportion of other metals (Yoshimura et al., 2001). Similarly, it occurs with oxidation processes such as the conversion of ethylene into ethylene oxide, which is carried out in millions of tons per year, and which is based on the use of silver/argentum (Ag), chromium (Cr) or other metals (Stegelmann et al.,

2004). To these processes are added the reactions of complement, widely used in organic synthesis, both at laboratory level and for obtaining compounds in fine chemistry with applications in the pharmaceutical industry, plant protection products and electronics, and which come require the use of palladium (Pd) as a catalyst (Lyons & Sanford, 2010). In general, transitional metals can act as catalysts in organic reactions by two more mechanisms. In the first of these the metal acts as an acidic center of Lewis, while the second of these majority mechanisms corresponds to a redox mechanism that implies a change in the oxidation state of the metal element during the reaction.

2.1.1 Gold Catalyst in organosilicon reactions

Among other noble metal-catalyzed hydrosilylation of aldehydes, Au has been shown to be an active catalyst in this reaction. In 2000, the first homogeneous Au(I) catalyst was reported for hydrosilylation of aldehydes. The homogeneous complex was [$(Ph_3P)AuCl$] (3 mol%) and Bu_3P was used to reduce catalyst deactivation. The catalyst showed active hydrosilylation of benzaldehyde, some aryl aldehydes, and aliphatic aldehydes to give a yield up to 94% (Ito et al., 2000).

According to Corma et al. (2007), they reported that AuNPs with average size of 4 nm supported on cerium(IV) oxide (CeO_2) catalyze hydrosilylation of ketones, aldehydes, alkenes, imines, and alkynes for study of Au/CeO_2 catalyst. The catalyst could be used up to 4 times without loss of activity and selectivity as no Au metal leaching was observed. It was stated that the Au/CeO_2 catalyze the reaction due to the presence of stabilized Au(III) on the catalyst surface. It was reported Au/CeO_2 was the most active catalyst for hydrosilylation of heptanal and high yield. In hydrosilylation of cinnamaldehyde, which contains a conjugated double bond at the carbonyl group, it produced up to 95% yield with high chemo-selectivity (Corma et al., 2007). Later on, the study done by Vasilikogiannaki et al. (2014) have reported Au catalyst supported on

titanium dioxide (TiO_2) for hydrosilylation of aldehydes. This catalyst contains approximately 1% wt. of Au with an average size of 2-3 nm. In this experiment, aldehydes and ketones were reacted with Et_3SiH and $PhMe_2SiH$ with excess hydrosilylation agent to complete the reaction at a reasonable time scale. Based from the experiment, the catalyst produced 100% yield as all the carbonyl groups were consumed in the reaction. Overall (Au/TiO_2) served as excellent catalyst for hydrosilylation of aldehydes even with a sterically hindered group in the substrate. It was also reported the Au catalyst can be separated from the reaction mixture at the end of the reaction and reused with a little deterioration of its activity (Vasilikogiannaki et al., 2014).

This development of Au catalysts proofs that Au can be used as an excellent heterogeneous catalyst for silicon (Si) containing organic reactions. One of the advantages of heterogeneous Au catalyst is its reusability and low Au leaching during reaction. However, till now no study has been reported about the oxidative coupling of hydrosilane (for example DMPS) in solventless reactions with mild conditions. In addition, the catalyst used of AuNPs/rGO by more research study is believed to produce excellent selectivity.

2.1.2 Gold as catalyst in oxidation of hydrosilane into silanol and synthesis of disiloxane

As reported in a study by Mitsudome et al. (2009), AuNPs supported on hydroxyapatite (Au/HAP) has been used for oxidation of silane into silanol using water as solvent and oxidant. The reaction was conducted at 80°C. Most of the reactions have both conversion and yield at 99%. DMPS is converted into respective silanol in just three hours with 99% conversion and yield. Only 0.1 g of catalyst was used in the reaction (Mitsudome et al., 2009).

The catalyst was recovered and reused using triethyl silane as a substrate, and it showed no loss of activity. This proves that supported AuNPs have big potential in catalysis of oxidation of silanes. Catalytic oxidation of silanes by Au nanohybrids into carbon nanotubes (AuCNT) have been reported by John et al. (2011). The reaction was conducted with THF as solvent, and air as oxidant at room temperature. DMPS was converted into dimethylphenylsilanol (98% yield) in just 45 minutes with catalysts loading of 0.1 mol% where the substrate used is 0.2 mmol. The lowest yield percentage was 93% for conversion of triisopropylsilane in 60 minutes (John et al., 2011).

2.1.3 Gold and several other transition metals as Catalysts for Synthesis of Disiloxane

Oxidative coupling of hydrosilane by using carbon (C) to support Au (C/Au) have been reported by Sawama et al. (2016). In this study they have only used one substrate known as DMPS for the reaction. The group suggested several steps in reaction mechanism using C/Au-catalyzed oxidation. Initially, the continuous oxidative coupling of the hydrosilane moieties by dihydromethylphenylsilane (1o) was completed mainly giving a mixture of tetramers to octamers (2o) in Equation (2.1). As the result based on Equation (2.2), Au/C that was tested without any metal leaching in 1a can be recycle for five times (Sawama et al., 2016). The catalyst used from 1a was $H_2{}^{18}O$ that acts as oxidant source in the whole reaction to have the ^{18}O-labeled 2a, which is clearly referred in Equation (2.3). The desired oxidation of 1a to 2a about 80% or 86% is proceeded and the reaction intermediate of 3a produces a small amount of silanol about 15% or 11% after the reaction stop for a period range 5 or 15 min in Equation (2.4). However, the dehydration of 3a by Au/C-catalyzed was comparatively not completed within 3 hours even under either atmospheric H_2 or Ar due to slow in reaction based on Equation (2.5) (Sajiki et al., 2005; Sawama et

al., 2016). While the oxidation of 1a into 2a by C/Au-catalyzed was completed within 3 hours. Based on these results analysis, two patterns of reaction pathways have been considered. Firstly, the production of disiloxane based on dehydration of silanol from the generation of transition metal-catalyzed through hydration of hydrosilane (Chauhan et al., 2009; Ison et al., 2005). Other option also can confirm these disiloxane by the following hydrolytic oxidation of the disilane from the first dehydrogenative coupling of the hydrosilane into disilane (Gryparis & Stratakis, 2012; Gualco et al., 2012). In the presence of catalyst Au/C in H_2O, the quantitative yield disiloxane (2a) is effectively produced from disilane (4a) in Equation (2.6). Sawama et al. (2016) also justify that the production of disiloxane from silanol is slow in Equation (2.4). They have proposed this mechanism by the process of dehydrogenative coupling of the hydrosilane into disilane (4a) that further produce disiloxane predominantly continues through oxidation of hydrosilane (1a) into disiloxane (2a).

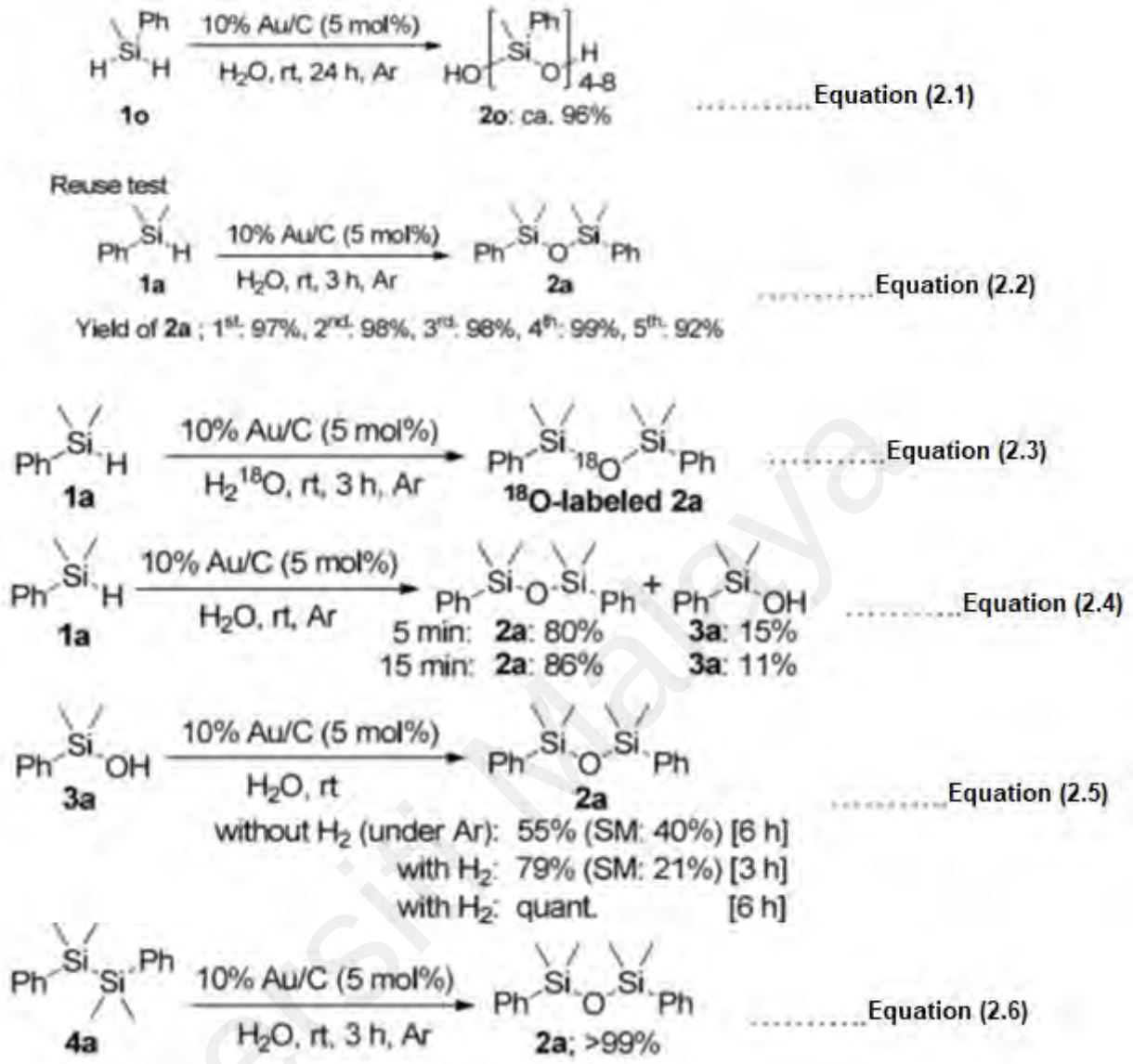

Figure 2.1: The mechanism of disiloxane synthesis (Copyright with permission *(Sawama et al., 2016)*).

The reaction was conducted at room temperature with water as a solvent and oxidant under argon gas atmosphere around 3 and 24 hours by referring on the Figure 2.1. C/Au catalyst used in the reaction showed conversion and yield at 100% and 97%, respectively. In this work, they reported the same reaction with other precious metals such as Pd and Pt that yield percentage was about 87% and 86%, respectively. Thus C/Au showed better performance compared to Pt and Pd.

While, based on current study done towards oxidative coupling of hydrosilane by Fritz-Langhals et al. (2020), the group developed the novel catalytically active

cationic Ge(II) and Si(II) compounds that isolated and synthesized in pure form. The study proved that using Ge(II) based compounds were stable against moisture, air and therefore could be handled very easily. In addition, no significant excess of any of the reactants was required. It demonstrated the suitable method on both synthesis of symmetrical for siloxanes and ethers. Based on their observation, it showed both cationic catalysts compounds were catalytically active and no pronounced influence of the anionic counterion on the catalytic activity. All compounds efficiently catalyzed the oxidative coupling of hydrosiloxanes with ketones and aldehydes as oxidation reagents. Furthermore, the reactions were done at temperature of 40 °C within 30 minutes or more. Besides that, ketones showed less reactivity and therefore, aldehydes were preferred as coupling reagents for siloxanes. It was found that the cationic Ge(II) compounds were completely stable toward air and moisture and readily available, making the compounds particularly useful under synthetic aspects (Fritz-Langhals et al., 2020).

The study from Lv et al. (2019) reported a zero valent nickel (Ni) compound catalyzed oxidation of organosilanes by air as an oxidant. Based on the bis(cyclooctadiene) nickel(0) [Ni $(COD)_2$] catalyst study, the reaction was conducted with toluene as solvent at 70°C temperature with 3,4,7,8-tetramethyl-1,10-phenanthroline as a ligand. The catalyst contributed to 97% yield in four hours of reaction time. This was the first zero valent nickel catalyst reported for oxidation of silane to disiloxane. The catalyst showed good catalytic activity for most of the substrates used in the studies. However, there was no test performed on the reusability of the catalyst.

According to Pattanaik and Gunanathan (2019), the reported cobalt (Co) catalyst for the synthesis of disiloxane showed good activity and selectivity with 99% yield

produced when using DMPS as substrate. The reaction proceeds with 2 mol% catalyst loading, 4 mol% of potassium tert-butoxide, dioxane and water. This catalyst also worked well with other sterically hindered substrate triphenyl silane with 89% yield. There was no test done on reusability of the catalyst. The comparison of Au, Ni, and Co catalyst for synthesis of disiloxane by using DMPS as substrate is shown in Table 2.1.

Table 2.1: The comparison of Au and other metal catalysts in synthesis of disiloxane.

Catalyst	Solvent	Temperature (°C)	Time (h)	Catalyst loading (mol%)	Yield (%)	References
Si(II)	Aldehydes and ketones	40	0.3	0.06	96	(Fritz-Langhals et al., 2020)
Ge(II)	Aldehydes and ketones	40	0.5	0.06	>95	(Fritz-Langhals et al., 2020)
$Ni(COD)_2$	Toluene	70	4	5	97	(Lv et al., 2019)
NNN^{HtBu} Co(II) pincer complex	H_2O	60	2	2	99	(Pattanaik & Gunanathan, 2019)
Au/C	H_2O	Room temperature	3	5	97	(Sawama et al., 2016)

Based on the comparison shown in Table 2.1, Ge(II) and Co metal-based catalysts showed high catalytic activity. Unfortunately, both catalysts was presented as homogeneous catalysts which was difficult to recover after reaction. While the Ni catalyst has the same yield percentage with Au catalyst, the Ni based catalyst was a complex catalyst and must be prepared under inert conditions. Thus, the Ni based catalyst is very sensitive to air in the environment and not robust during reaction.

Thus, Au catalyst that used by Sawama et al. (2016) is the best option as it is robust and relatively easy to prepare.

2.1.4 Comparison between Rochow Process and Oxidative Coupling of Hydrosilane

Other than oxidative coupling of hydrosilanes, another conventional method to obtain silicone monomers is known as Rochow-Müller Process. Rochow-Müller was one of the most convenient ways to produce silicone monomers. The Rochow-Muller process, also called Direct Process is a copper catalyzed reaction of Si with organic chloride where organo chlorosilanes are produced. The comparison of Rochow-Muller process and oxidative coupling reaction is shown in Table 2.2.

Table 2.2: Differences between Rochow-Müller Process and oxidative coupling reaction.

Aspects	**Rochow-Müller process** (Kalchauer & Pachaly, 2008)	**Oxidative coupling** (Sawama et al., 2016)
Catalyst	Copper based catalyst such as copper and copper(I) chloride	AuNPs/C
Starting material	Chloromethane and Si	Hydrosilane and oxidant (water)
System	Heterogeneous system (Gas-Solid) using solid Si that react with chloromethane gas	Heterogeneous system (Liquid-Solid)
Temperature	Between 540 K to 590 K and under pressure at 0.99 to 4.94 atm	Under mild conditions at room temperature at 1 atm
Product	Organochlorosilanes	Disiloxane

Based on the comparison study show in Table 2.2, it can be seen that, oxidative coupling reaction by AuNPs that supported on carbon is a better option where it can catalyze the reaction under mild conditions.

2.1.5 Solventless reaction catalyzed by AuNPs

As the research study is going towards sustainable development, the scientists are trying to reduce the utilization of solvents according to the fifth Green Chemistry Principle which is using safer solvents and auxiliaries. According to Abad et al. (2007), the solventless oxidation of allylic alcohols catalyzed by supported using AuNPs. When supported Au catalyst with Pd catalyst was compared in the reaction, supported Au catalyst was superior to Pd catalyst in terms of selectivity. For solventless oxidation reaction with 1-octen-2-ol, Au/CeO_2 catalyst showed good yield at 99%. The reaction was conducted with P_{O2} at 1 atm, O_2 flow through the vessel at a rate of 35 ml min^{-1}, reaction temperature 120 °C, alcohol 12.5 mmol.

AuNPs supported on Al_2O_3, SiO_2, and TiO_2 for oxidation of benzyl alcohol under solventless reaction medium was reported (Gualteros et al., 2019). The research group performed the reaction with only 0.08-0.05 mol% of the catalyst loading with oxygen (O_2) as an oxidant. The reaction was conducted at 4 bar O_2 in 100°C. The result showed the highest activity of the turnover frequency (TOF) based on that research at 443,624 h^{-1} when Au/Al_2O_3 catalyst was used within that temperature. Excellent catalytic activity was observed due to the nature of Al_2O_3 support.

2.2 Evolution of nanohybrid catalysts

The global chemical demand for domestic and industrial applications is escalating every day. Taking into account with the advances in science and engineering, the use of a sustainable nanohybrid catalyst can form a bridge between the global demand for chemical products and their means of production. Therefore, the search for new nanohybrid materials that can serve chemical production purposes effectively and efficiently becomes inevitable. A nanohybrids and a good instance of GO specifically was designated common chemistry abbreviation and acronyms in all fields of science.

For nanohybrid, it implies incorporating two dissimilar or similar components usually almost ~ 100 nm scale, making a single entity with either enhanced or completely new properties (Ferrari et al., 2015). Usually, mankind guided by the artistic curiosity to develop efficient materials happens to introduce the term nanohybrid toward nanocomposites (Drisko & Sanchez, 2012; Merhari, 2009). These combinations span across the unlimited possible combinations of the distinct properties of organic, inorganic or even bioactive components in a single material, either in molecular or nanoscale dimensions (Liu et al., 2012). Consequently, the nanohybrid advances have provided the opportunity to create a vast number of novel materials with well-defined structures and functions.

The unique properties of the advanced nanohybrid provide many advantages in different fields such as the biomaterials, optical materials, electronic materials, coating, energy storage, catalysis, and sensing (Davies et al., 2019; Halilu et al., 2016; Halilu et al., 2019; Koga et al., 2011; Wang et al., 2019). Already note that, the role of nanohybrid materials as a catalyst is an interesting field of study en-route to the development of new materials. The focus on the nanomaterials that are photoactive for instance has been on metal oxides such as TiO_2 and zinc oxide (ZnO) hybrid materials (Agrawal et al., 2009; Boucle & Ackermann, 2012; Xi et al., 2011). Besides, to improve the activity of generating pure hydrogen (H) from the hydrolysis process of sodium borohydride ($NaBH_4$) for example and to reduce that cost, it is needed to synthesize the highly quality nanohybrid containing both high and low-cost metals in rational proportion dispersed on to a support (Saha et al., 2014).

Previously, the surface-functionalized method, thermal evaporation, compartmentalized hydrolysis, bi-functional linker has been applied to functionalize the surface of nanomaterials (Gondal et al., 2015). Veziroglu et al. (2017) used AuNPs loaded

with $ZnO\text{-}CeO_2$ nanohybrid structures to reveal the beneficial features of using both mixed oxide structure and metallic NPs for catalytic applications. Wen et al. (2017) reported that; the enhanced photocatalytic activity of the nanohybrid could be attributed to the presence of rGO, an excellent electron acceptor for improving the active transfer of photogenerated electrons of ZnO to the rGO sheet. This promotes retardation of the charge carrier recombination, thus enhancing the charge separation properties. Also, the AuNPs-GO catalyst finds suitable application in chemical synthesis particularly, hydrogenation and oxidation of organic compounds. Also, it is known that C based metal nanocomposites poses interesting magnetic, optical, and electrical properties that are superior to ordinary C or metal species (Han et al., 2011; Okpala, 2013). However, G which is carbon-based, coupled with Au and other nanocomposites are beneficial in the chemical industry but mostly they are being used in sensor applications; some of these nanohybrids are listed in Table 2.3.

Table 2.3: Nanohybrid of AuNPs supported on carbon materials or graphene as catalysts.

Materials	Application properties	References
C_3N_4NTs@GQDs	Sensitive electrochemical determination of Chlorpyrifos	(Yola & Atar, 2017)
rAu-PtNPs/AETGO	Electrochemical performances for methanol oxidation	(Yola et al., 2016)
PtNPs/NSrGO/GCE	Highly active electrocatalysts for methanol oxidation	(Akyıldırım et al., 2016)

C_3N_4NTs = carbon nitride nanotubes
GQDs = graphene quantum dots
rAu-PtNPs = rod gold-platinum nanoparticles
PtNPs = platinum nanoparticles
AETGO = 2-aminoethanethiol functionalized graphene oxide
NSrGO = nitrogen and sulfurdoped reduced graphene oxide
GCE = glassy carbon electrode

By combining these advantages of C materials with those of nanostructured materials and C-based nanomaterials including C nanofibers, highly ordered mesoporous Cs, CNTs and others, much more attention have been drawn because of the unusual electronic properties and the ability to improve catalytic properties (Hu et al., 2010). GO is normally reduced by thermal treatment or chemical reduction to form rGO (Bagheri et al., 2018). The rGO has been used for fuel cells, drug detection, and sensors. While AuNPs are utilized as an electrode surface for sensors to increase the surface area and the rate of electron transfer in the catalyst system (Yola et al., 2015). The AuNPs have attracted considerable attention recently because of their unique electronic and optical properties. Besides that, the use of AuNPs synthesized with rGO will give long-term cycle stability and high specific gravimetric capacity for anode material in lithium-ion battery (Atar et

al., 2015). In addition, the potential applications can be seen in different industrial fields, including optics, nanoelectronics, bio-diagnostics, catalysis, and others. Recently, there are only a small number of examples for AuNPs–rGO nanohybrid, such as the AuNPs grown on the surface of functionalized rGO by directly adsorbed on the rGO surface and chemical reduction of $AuCl_4$ ions (Hu et al., 2010).

2.2.1 Gold nanoparticles-graphene oxide nanohybrid

There are many synthesis approaches constructed through lego-like chemistry to synthesize the AuNPs with GO. Nanosized building blocks with self-assemblies into complex dense or porous structures are made (Khalil et al., 2016). These use different kinds of nanoparticles such as Au, Ag, CeO_2 or even copper (Cu) combined with GO. However, more research works have been done by using Au or Ag nanoparticles on GO because of their specific applications in photocatalysis, sensors, electrochemical capacitor, solar cell, surface-enhanced Raman spectroscopy (SERS), drug-resistant cancer treatment, magnetic hyperthermia therapy and antimicrobial etcetera (Hareesh et al., 2016).

2.2.1.1 Synthesis of gold nanoparticles-graphene oxide nanohybrid

2.2.1.1 (a) Chemical vapor deposition (CVD)

Considering the mass-production of GO, the CVD method is effective in fabricating a large amount of GO while limiting the number of planar defects (Yin et al., 2015). The list form Table 2.4 with a current variety of methods or techniques with their characteristic itself for the synthesis of AuNPs.

Table 2.4: Synthesis of AuNPs and their characteristic.

Methods	Characteristic	References
Chemical method	Synthesis with no aggregation (uniformly) of AuNPs and various particles size	(Hussain et al., 2020; Jingyue & Bernd, 2015)
Turkevich method	Leads to the production of AuNPs with small size with diameters ranging from 15 to 150 nm and narrow size distribution	(Kimling et al., 2006; Ojea-Jiménez et al., 2011)
The Brust-Schiffrin method	Generate a formation of AuNPs through an air and thermally stable with controlled size and low dispersity	(Araki et al., 2006; Zhu et al., 2013)
Electrochemical method	The size of the AuNPs can be controlled in the range 58.3 to 8.3 nm.	(Huang et al., 2006; Song et al., 2013)
Seeding growth method	Particle size can be controlled by the changeable ratio of seed to Au salt and obtained every size in the range 5 to 40 nm with sizes in a broad range and multiple shapes	(Jana et al., 2001; Zhao et al., 2013)
Biological method	Cost-effective and eco-friendly procedures for the synthesis of AuNPs that results of average height of the particle roughness to 60.0 nm and particle sizes from 53 67 nm)	(Mittal et al., 2013; Singh et al., 2013)
Sono-chemical method	Can produce a very small nanoparticles with rapid reaction rate and tend to have wide size distributions (to reduce it using surfactants and alcohols)	(Herizchi et al., 2016; Park et al., 2006)

Therefore, GO obtained using the CVD method have carrier mobility values as high as ~2000−4000 $cm^2\ V^{-1}\ s^{-1}$. It is anticipated that the combination of AuNPs and CVD-grown GO can enhance electrochemical performance in catalysis. However, the strength of the attachment between AuNPs and GO significantly affects the electrocatalytic activity of the nanohybrid (Khalil et al., 2016). For instance, Ding et al. (2013) reported that the interactions of AuNPs with defect-free GO is very weak due to the inert nature of covalently bonded sp^2 C atoms on the basal plane of GO. However, Ding et al. (2013) also reported that the strong interactions between GO and AuNPs occurred due to the in-plane defects of GO, including non-hexagonal rings and vacancies. These possibilities inspire the necessity to produce desirable access to enhance the interactions between AuNPs and CVD grown GO. It is worth mentioning that the suspended and wrinkled GO structures always form near the gaps of nanoparticles. This makes GO–metal nanohybrids easily promoted defects and nonuniform structure of GO–metal hybrids. By way of characterizing the GO–metal hybrids, a reduction in the homogeneity and reproducibility of the SERS substrates could be evident. It is satisfactory to apply the CVD method at a directly grown thin layer of GO on the surface of nanoparticles. However, it is difficult to grow high quality GO on the Au or Ag substrate without the CVD method (Xu et al., 2015).

The process of CVD method has been demonstrated by Oznuluer et al. (2011) where they grew GO on Au surface at ambient pressure. The schematic representation of the steps of the preparation of the Au foils involves the deposition and transfer process of the G layers on dielectric substrates (Figure 2.2). About 25 µm thick Au foils was obtained by pressing high purity Au plates (99.99% sourced from Vakıf Bank) was used. To remove impurities and reconstruct the single crystalline surface, the Au foils was annealed with an H flame for about 20 minutes before use. Owing to the fast heating and cooling rates, H flame annealing provides more complete crystallization of the Au foil than the

furnace annealing. The result of this treatment was a polycrystalline Au surface partially (111) oriented, with a roughness lower than a few nanometers. After the annealing step, the Au foil is placed in the quartz chamber and the chamber is flushed with argon (Ar) gas for 5 min. The foil is heated up to 975 °C under Ar and H_2 flow (240 sccm and 8 sccm, respectively). Methane gas with a rate of flow of 10 sccm was channeled into the chamber for 10 min. After stopping the methane flow, they cooled the chamber with a natural cooling rate of ~10 C/sec. They also developed a transfer printing method to transfer the G from the Au foil to insulating dielectric substrates. After the deposition, an elastomeric 4 stamp polydimethylsiloxane (PDMS) was applied to the G coated Au foil. The Au layer was etched by diluting the Au etchant using type TFA. Then complete etching of the Au foil, the G layer of PDMS was applied on a 100 nm silicon dioxide (SiO_2) coated Si wafers. Peeling the PDMS releases the G on the dielectric surface.

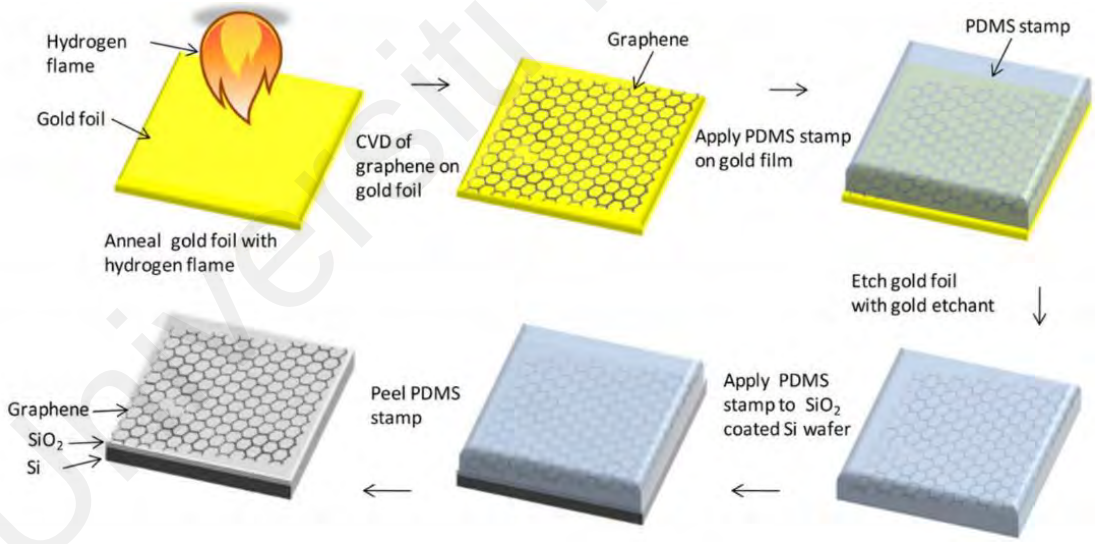

Figure 2.2: CVD synthesis and transfer process of G growth on Au film (Copyright with permission *(Oznuluer et al., 2011)*).

2.2.1.1 (b) Electrochemical

The electrochemical method of AuNPs-GO nanohybrid synthesis is an effective technique singled out for its environmental friendliness. The process is widely preferred because it has been used as a simple one-step method to form coatings on metal substrates (Sun et al., 2002). The process allows effective control of the physical and chemical properties of the coatings. Therefore, it is much easier to scale it up for industrial production (Daniel & Astruc, 2004). Generally, electrochemical synthesis is a powerful tool for the formulation of bulk materials and thin films and obviously for substrate cleaning and surface modification. It is especially suited for surface modification of metals, films and fibers (Iroh et al., 2003).

Electrochemical methods are widely used for the detection of nitrite due to their specific advantages including compactness, relatively low-cost, reliability, sensitivity and real-time analysis (Rajkumar et al., 2016). The synthesis of AuNPs-GO nanohybrid samples has been done by Rajkumar et al. (2016) for as-prepared GO–C60 composite that was redispersed in DI water by sonication for 30 min. Approximately, 8 mL (optimum) of GO–C60 dispersion (1:2 of v/v%) was dropped cast on a pre-cleaned GCE and dried at room temperature. Then, the GO–C60 composite modified electrode was transferred to a pH 3 solution containing 5 mM chloroauric acid ($HAuCl_4$) to $3H_2O$. A constant potential of -1.4 V was applied for 200 s, and this led to the formation of rGO–C60/AuNPs composite. Finally, the rGO–C60/AuNPs composite modified electrode was gently rinsed in deionized (DI) water and dried at room temperature. An illustration of the fabrication of rGO–C60/AuNPs composite is shown in Figure 2.3.

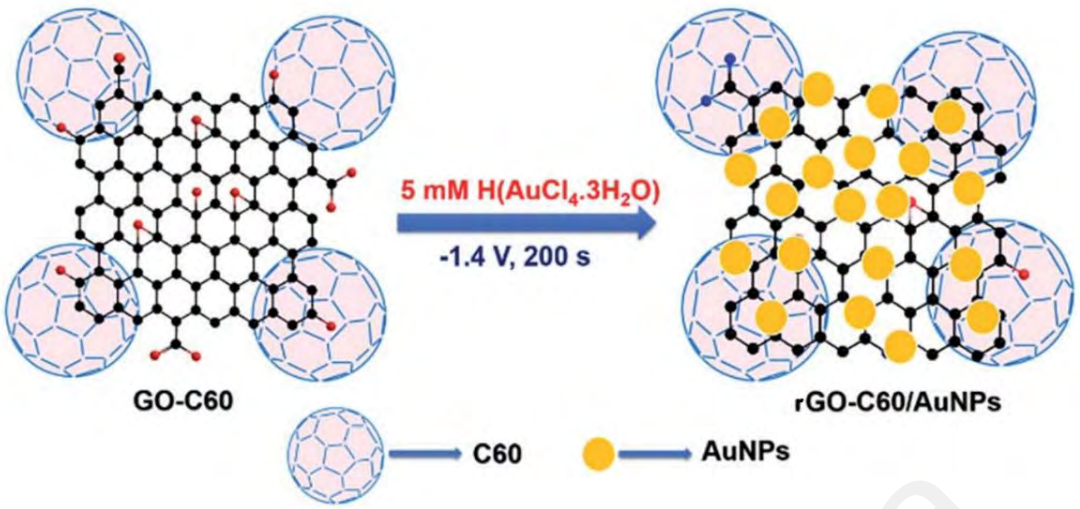

Figure 2.3: Electrochemical preparation of rGO–C60/AuNPs composite (Copyright with permission *(Rajkumar et al., 2016)*).

The electrochemical deposition is an efficient and green technique for the synthesis of AuNPs–rGO nanocomposites by the simultaneous process of electrochemical reduction and electrodeposition of AuNPs onto rGO (Turcheniuk et al., 2015). The attachment of AuNPs onto conductive substrates by electrochemical deposition has generated considerable attention due to its spanning fundamental nanostructures to practical devices. This is in addition to its great importance as well as the capability for controlling the structure-property relationships of as-deposited nanostructures via the adjustment of electrochemical parameters. Due to the large volumes of metal precursors and GO that are required for the electrochemical method, some challenges remain toward the efficient synthesis process (Govindhan & Chen, 2015).

2.2.1.1 (c) Sol-gel processing

The sol–gel method is one of the well-established synthetic approaches to prepare novel metal oxide NPs as well as mixed oxide composites. This method has potential control over the textural and surface properties of the materials. Based on research done by Rao et al. (2017), the sol-gel method principally follows a few stages to convey the final metal oxide protocols. The series of steps are including condensation, drying process and hydrolysis. Initially, the corresponding metal precursor undergoes rapid hydrolysis

to produce the metal hydroxide solution, followed by immediate condensation which leads to the formation of three-dimensional gels (Rao et al., 2017). Afterward, the gel is subjected to a drying process, and the resulting product is readily converted to Xerogel or Aerogel based on the mode of drying (Rao et al., 2017). Sol–gel processing is also a promising method for the preparation of nano dimensional materials. It is the most commonly used technique for the preparation of bulk nanomaterial of Metal Oxides or semiconductor materials such as TiO_2 (Elbushra et al., 2018) or ZnO (Manikandan et al., 2018).

The reaction product of the sol–gel synthesis is either colloidal powders or films. One of the advantages of this method is the ability to control the microstructure of the final product by controlling chemical reaction parameters. It includes the advancement of systems through the arrangement of colloidal suspension (sol) and gelatin to form a network in a continuous liquid phase (gel) (Esposito, 2019). The precursor for synthesizing these colloids is either inorganic salts or organic compounds known as aloxysilanes and metal alkoxides. The most broadly utilized ones are tetraethoxysilanes (TEOS) and tetramethoxysilane (TMOS) which form silica gels. The sol-gel procedure includes at first a homogeneous solution of one or more selected alkoxides. These are organic precursors for titania, silica, zirconia, alumina among others. In most sol-gel processes, a catalyst is used to start reaction at a controlled pH. Sol-gel formation occurs in four stages that are initially hydrolysis, next condensation, after that growth of particles and lastly agglomeration of particles (Sinkó, 2010). The investigation was done by Adhikari et al. (2011), who has done the study on the morphology between the nanohybrid gel of GO and AuNPs. The formation and characterization of AuNPs within the gel have been established using ultraviolet-visible (UV-vis) absorption spectroscopy, X-Ray Diffraction (XRD), and high-resolution transmission electron microscopy (HR-TEM). The spontaneous reduction of Au^{3+} by using UV-vis absorption spectroscopy has been

investigated. Furthermore, the analysis exhibits the absorption spectra of a mixture (GO + tryptophan + $HAuCl_4$). The presence of a surface plasmon resonance band centered at 530 nm suggests the formation of AuNPs within the hydrogel matrix. Suggestively, that Au^{3+} has been reduced by the tryptophan molecule rather than by GO. This established that the synthesis between them can be achieved by separately stirring an aqueous $HAuCl_4$ solution with GO and tryptophan.

The utilization of porous C particles enhances the transport of reactants by constructing a hierarchically and freestanding porous C that is derived from GO gel via an effective and facile in situ sol-gel method. Besides that, GO does not only act as a special C source but also provides the framework of a 3D gel. Furthermore, the proper acidity via it's intrinsic carboxylic (COOH) groups play an important role in the formation of the whole structure (Wang et al., 2012). However, monodispersed AuNPs are usually difficult to be obtained and the particle size is relatively hard to be controlled under 10 nm, with the unexpected aggregations appearing in time. Despite the substantial progress in the normally adapted sol-gel synthesis, the overall multi-step process tends to be labor-intensive and time-consuming. Thus, a prompt, solventless preparation of bulk the AuNPs with the broadly tunable size is of incredible merit in modern material science and nanotechnology (Li et al., 2014).

2.2.1.1 (d) Hydrothermal

The hydrothermal or Solvothermal route involves chemical reactions of substances in a pressurized (from 1-100 MPa) heated (from 373.15-1273.15 K) sealed supercritical or subcritical organic solvent autoclave reactor (Feng & Li, 2017). The synthesis of GO through hydrothermal means was shown by Tang et al. (2012) using glucose as a sole reagent. The produced GO has a wide range of thickness from 1 nm (monolayer) to 1500 nm. While the lateral sizes of the monolayer and few-layer of GON are about 20 mm and

100 mm, respectively. This method is considered low-cost as well as capable of scaling up for mass production while being facile and environmentally friendly. The detailed steps of preparing GON via hydrothermal is schematically illustrated in Figure 2.4.

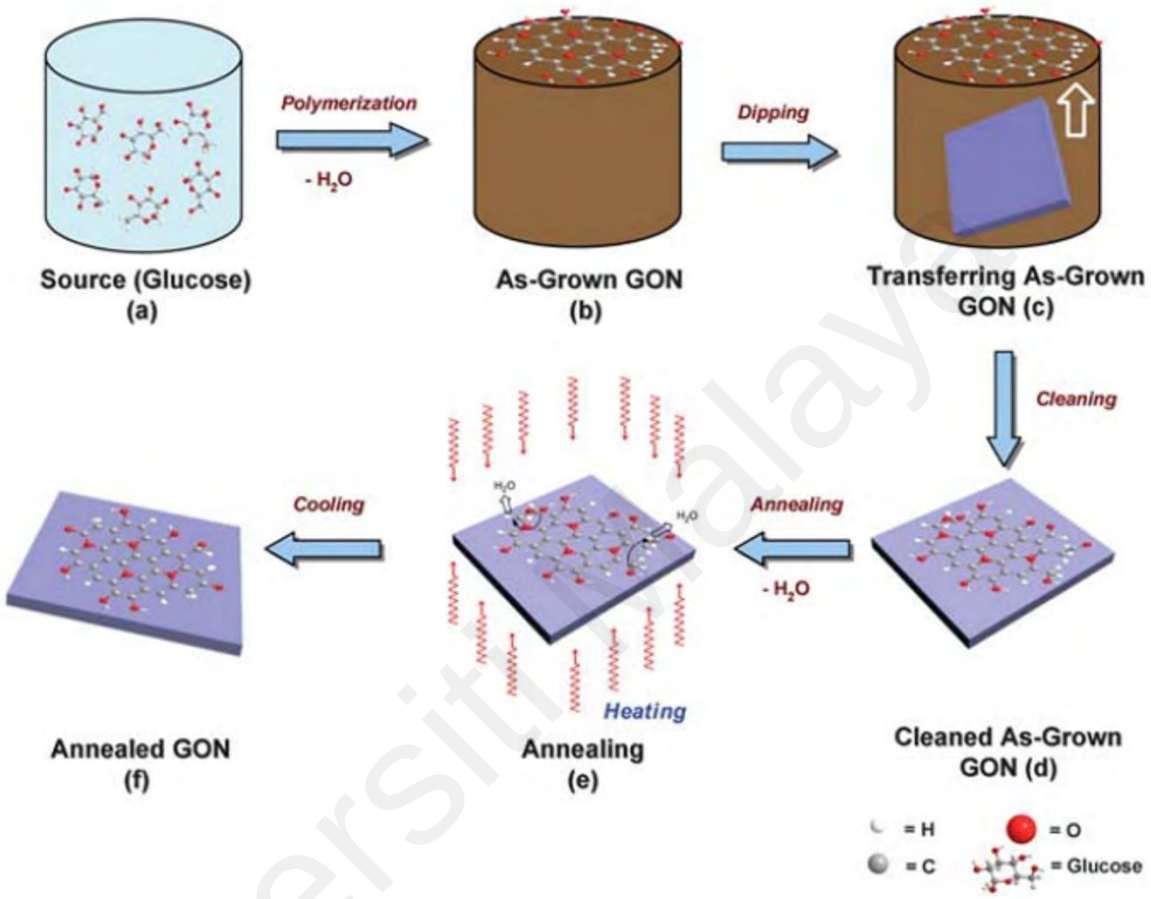

Figure 2.4: The illustration of preparing a GON. (a) Glucose dissolved in DI water to obtain a colourless transparent source solution. (b) Under hydrothermal conditions, polymerization occurs as glucose molecules dehydrate intermolecularly to form a GON which floats onto the surface of the solution due to its hydrophobic property. (c) The as-grown GON can be transferred onto any substrate by dipping and lifting. (d) The transferred GON is rinsed by dipping into DI water to remove the residue. (e) The as-grown GON is annealed at a certain temperature to dehydrate and graphitize for tuning its electrical, optical and structural properties. (f) The annealed GON with the desired thickness and electrical properties (Copyright with permission *(Tang et al., 2012)*).

Generally, some materials have been produced via the hydrothermal route. For instance, the hydrothermal reduction of GO in the presence of urea with a fixed weight ratio of urea and GO (3:1) employed urea as a reducing agent at 463.15 K and 12 hours to produce in situ synthesis procedure using nitrogen-doped GO (NGO). The material

shows an excellent absorption of electromagnetic energy at an X-band of 8 GHz to 12 GHz (Agusu et al., 2018). Also, the synthesis of GO quantum dots (GOQDs) with AuNPs that was immobilized in SiO_2 through the hydrothermal method exhibited a surface area of 64.7 m^2/g and had a good dispersion of GQDs/AuNPs (Yang et al., 2017).

2.2.2 Oxidative properties

Definite clarification of the oxidative properties of AuNPs-GO nanohybrid would help to understand the different roles that can be played in redox and oxidation chemistry. Basically, GO contains a low quantity of COOH and carbonyl functional groups at its edge sites (Figure 2.5). Also, GO is in sheets form with epoxides at its basal plane that stabilize the dispersion of the nanosheets in H_2O and chemical functionalization with O groups such as hydroxyl (OH) (Park et al., 2021). Generally as to oxidative attributes of GO, O-containing functional groups are required for the production of functionalized GO to form composites with organic molecules (Eigler & Hirsch, 2014), metals (Yamamoto et al., 2014) and doping with heteroatoms (Panchakarla et al., 2009) as illustrated in Figure 2.5. GO was discovered to have thermal transport and limited electrical due to the O functionalization on the basal plane surface (Morimoto et al., 2016).

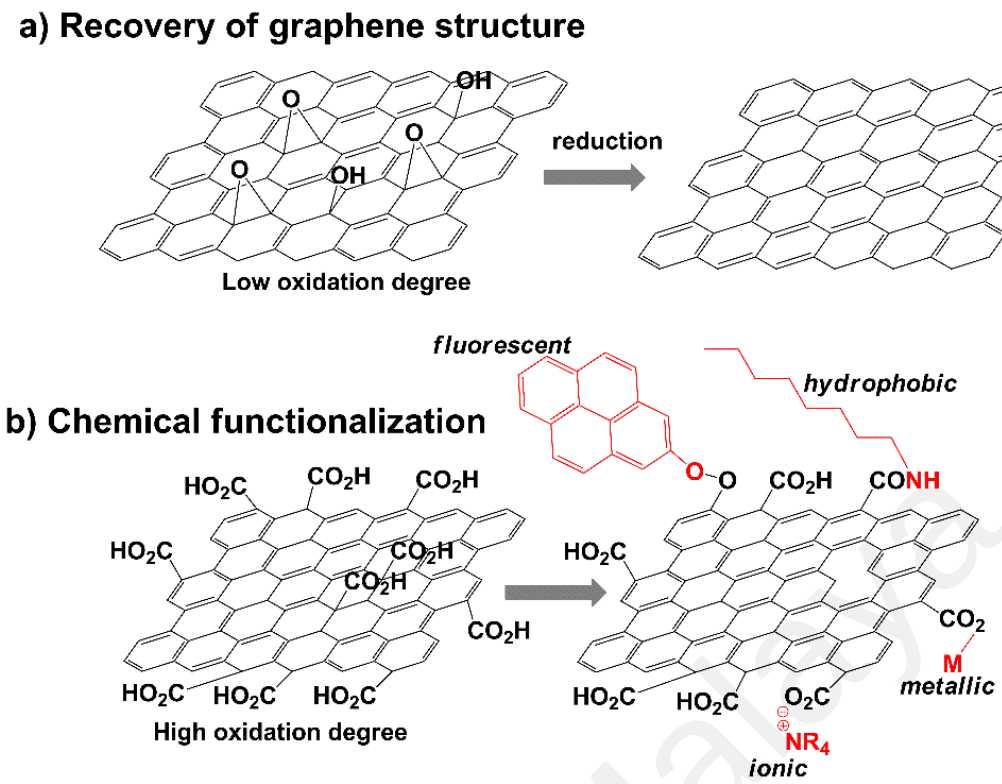

Figure 2.5: Functionalization of GO with different degrees of oxidation (Copyright with permission *(Morimoto et al., 2016)*).

There are several reports showing that Au is a good catalyst that showed importance in improving oxidative properties. Kenny and Venable (2011), indicated that Au has great potential for the development of efficient water and air filters for both household in domestic and industrial area purpose to decrease the number of dioxins, volatile organic compounds, chlorofluorocarbons and carbon monoxide (CO) pollutants in the water and air. Where the use of Au as a catalyst for filters is proven as highly effective, AuNPs with size ~ 2-5 nm showed high oxidative properties that positively influencing photocatalysis activities (Bagheri & Julkapli, 2018; Lohse et al., 2013).

Surface modification of GO surface with AuNPs by Goncalves et al. (2009) justified that the presence of O_2 functionalities within the GO surface provides reactive sites for the nucleation and growth of AuNPs. The AuNPs are effectively grown at functionalized GO surfaces in an aqueous medium using a simple chemical method. The nucleation and

growth mechanism depends on the degree of O-functionalization at the GON while zero AuNPs are obtained at totally rGO surfaces (Goncalves et al., 2009).

Radich and Kamat (2013) deal with the process of photocatalysis and found that the rGO content was oxidized due to the presence of catalytic interaction with AuNPs from two possible reaction pathways. Firstly, the promotion of photolytic OH radical formation via UV photolysis of H_2O_2, thus bringing about higher OH radical concentrations near the AuNP surface. Secondly, the promotion of the interactions between rGO and OH radical aided by changes in the localized oxidation potentials at the AuNP surface. In particular, the catalytic process of the second reaction is facilitated by the fact that AuNPs are bound to the rGO.

2.2.3 Application of gold nanoparticles-graphene oxide nanohybrid in chemical synthesis

2.2.3.1 Hydrogenation reaction

It is proven that GO can take-up H although the elastic energy gain associated with moving atoms out of the GO's plane is high (Elias et al., 2009; Son et al., 2018). When GO interacts with H, buckling deformation caused by the change in orbital geometry possibly from coplanar to tetrahedral results in substantial energy gain to the system. This makes the re-hybridization process energetically unfavorable. However, this singular attribute of GO interacting with H when used as a catalyst support material for hydrogenation could promote the hydrogenation reaction to proceed by the H spillover mechanism (Prins, 2012). This is because C–H bond formation as a result of GO-H interaction induce a certain degree of strain effects (Son et al., 2018). Otherwise, this is considered the "nucleation point" for the hydrogenation to begin (Boukhvalov & Katsnelson, 2009). Therefore, using GO as support material for hydrogenation reaction in general while considering its unique character with the possible spillover

hydrogenation mechanism is still debatable and currently lacks much experimentation (Son et al., 2018).

For the hydrogenation reaction, AuNPs have shown high selectivity on other supporting materials like alumina (Chaiseeda et al., 2017), silica (Wang et al., 2016) and metal oxide (CaO, MgO, TiO_2, ZrO_2) (Alshammari & Kalevaru, 2016). Conventionally these support materials especially silica does not interact with H hence hydrogenation reaction over it proceeds through the non-H spillover mechanism (Halilu et al., 2016). Traditionally silica, as well as other support materials, are prepared with through impregnation (Chen et al., 2008), coprecipitation (Toshima et al., 1981) or deposition-precipitation (Guzman et al., 2005; Haruta & Daté, 2001) methods.

However, GO stands out as a support material for AuNPs that could be used as a catalyst for hydrogenation reaction which favors the H spillover mechanism. Noteworthy, AuNPs are limited with inferior catalytic activity lower temperature for useful applications compared to other noble metals. However, the temperature window of ~ 150 °C is usually required for Au-based catalysts to achieve meaningful magnitudes of reactivity such as in Au-catalyzed alkyne hydrogenation (Shao et al., 2014). Considering Table 2.5, nanohybrid AuNPs-GO achieved 99% selectivity to styrene from hydrogenation of phenylacetylene with a 99% conversion at lower temperatures. There are still challenges to be overcome as to optimizing the hydrogenation process using this kind of nanohybrid catalytic material and to date not much has been done so far. This is going with the fact that the reaction is useful in the industry for the selective production of useful chemicals and materials.

Table 2.5: AuNPs-GO application in hydrogenation reaction.

Catalyst	Reactant	Product	Reaction condition (°C)	Performance		Catalyst Preparation	References
				Conversion (%)	Selectivity (%)		
AuNPs-GO (2 wt%)	Phenylacetylene	Styrene	40	5	99	Impregnation of Au on GO	(Shao et al., 2014)
AuNPs-GO (2 wt%)			60	99	99		
AuNPs-GO (2 wt%)			80	99	99		
AuNPs-GO (2 wt%)			100	99	99		
AuNPs-GO (2 wt%)*			60	60	80		
AuNPs-GO (2 wt%)*			80	70	80		
AuNPs-GO (2 wt%)*			100	90	80		

*= Au supported on GO with prolonged reduction time

2.2.3.2 Selective oxidation reaction

Selective oxidation of alcohols by possibly singlet O is an environmentally friendly and attractive reaction route in the synthesis of intermediates and fine chemicals. Recently, Au supported on most carbonaceous materials have received considerable attention since they exhibit stability and high selectivity for the oxidation of primary alcohol (Pina et al., 2012). The catalytic performance of Au/C catalysts depends largely on the shape and the size of the nature of the supports and the AuNPs used accordingly. The surface chemistry of different C materials is a key factor that determines the catalytic performance. In addition, the amount of surface O-containing functional group has a stable and strong effect on the catalytic activity of Au/C catalysts in selective alcohol oxidation.

The crystalline structure of C supports the control selectivity of Au/C catalysts for selective oxidation of glycerol, plays a significant role in deciding Au/C interaction, and the high crystallinity of C-supports correlates to an increase in activity (Rodriguez-Reinoso, 1998). GO are contains with O functional groups such as carbonyl, OH and COOH groups on the surface, which makes it a good candidate as support for AuNPs in the application of selective oxidation of alcohols (Dreyer et al., 2014). Huo et al. (2017), used three different C materials, including graphite (GRC), active carbon (AC) and rGO as the supports for AuNPs for the process of catalytic performance in the aerobic oxidation of benzyl alcohol (BA) (Figure 2.6). The results showed that Au/rGO catalyst poses much higher activity than Au/GC and Au/AC in the liquid phase aerobic oxidation of benzyl alcohol (Yu et al., 2013). The superior catalytic activity of Au/rGO was suggested to be related to the moderate graphitic character of rGO supports and the presence of surface O-containing functional groups. However, it is hard to compare directly the support effect by using different C materials since they differ largely in the

structure including surface area, electronic structure, surface functional groups, and volume size distribution or others (Huo et al., 2017).

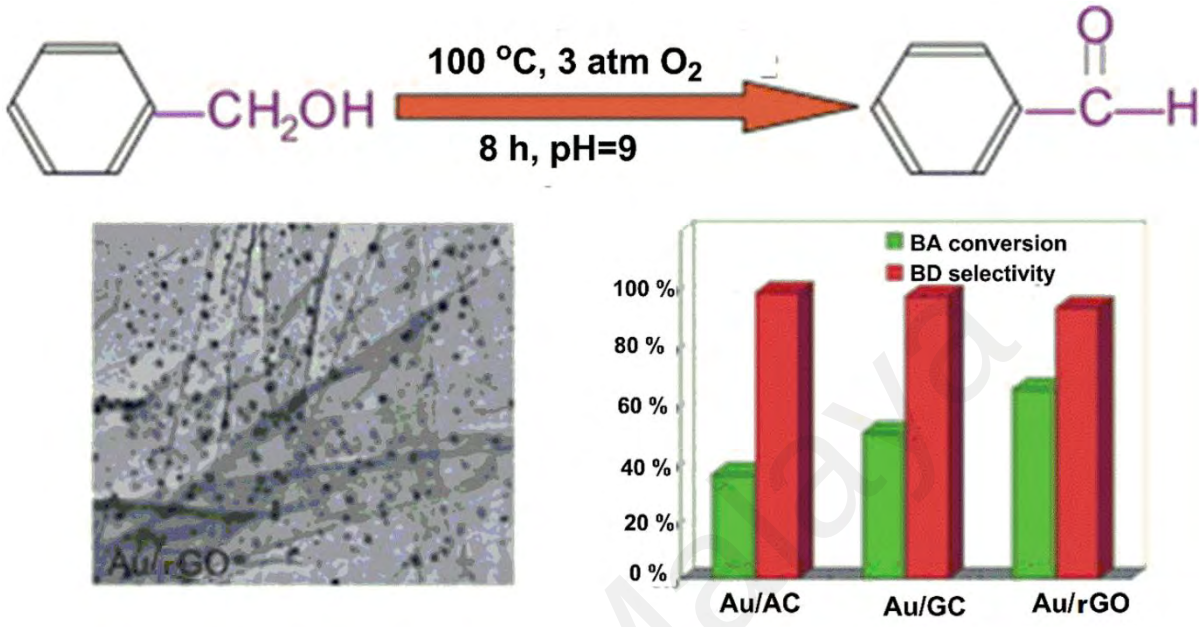

Figure 2.6: Catalytic performance of Au/AC, Au/GC and Au/rGO catalysts in the liquid phase aerobic oxidation of BA conversion and BD selectivity (Copyright with permission *(Yu et al., 2013)*).

Meanwhile, Table 2.6 shows the catalytic performance by Au/rGO related to the moderate graphitic character and the presence of specific surface O-containing functional groups (Yu et al., 2013). The chemical and thermal treatments have a large influence on the crystalline structure of GO supports and the presence of surface oxygenated groups. A strong support effect was observed on the catalytic activity of Au/rGO catalysts for aerobic oxidation of benzyl alcohol (Huo et al., 2017).

Table 2.6: Au/rGO applications in oxidation reactions.

Catalyst	Reactant	Product	Reaction condition (°C)	Performance		Catalyst Preparation	References
				Conversion (%)	Selectivity (%)		
Au/rGO	Benzyl alcohol	Benzaldehyde	100	65	93	Sol-immobilization method	(Yu et al., 2013)
Au/rGO	Ethyl benzenes	Ketones including propyl benzene	70	100	95	Reducing Au(III) chloride using sodium citrate on rGO	(Pocklanova et al., 2016)
AuNPs@SIL-g-G (bifunctional)	Primary & secondary aliphatic and aromatic alcohol	Aldehyde and ketone derivatives	25	>99	>99	AuNPs supported on supramolecular ionic liquid grafted G	(Mahyari et al., 2013)

AuNPs@SIL-g-G = AuNPs in supramolecular ionic liquids grafted on graphene

2.3 Perspective and Conclusion

Increased research proliferation works on G derivatives have resulted in the production of different nanohybrids such as Au/GO for added chemical synthesis applications. Such implementations are mostly in the field of industrially scalable reaction techniques. These presents GO as a good catalytic support product. The circumstances also indicate that GO is an effective carbon-based catalyst, the conditions of which are to be prepared. G-based nanohybrids are structured either by layering G with composite or by functionalizing G with bundles on its edge plane. Through focusing on recent studies on the use of AuNPs-GO in chemical synthesis, the synopsis of the specific synthesis process of AuNPs-GO was addressed in this review and the application of nanohybrid was clarified focusing on hydrogenation and oxidation reactions. It is therefore evident that AuNPs-GO nanohybrid can be used as a catalyst for chemical synthesis. It is envisaged that this review would enable further studies using AuNPs-GO nanohybrid to synthesize specific value-added chemicals.

CHAPTER 3: MATERIALS AND METHODOLOGY

3.1 Introduction

This chapter highlights five workflow processes: from sample preparation into the analysis of hydrosilylation reaction. The first process (**Process 1**) is the graphene oxide (GO) synthesis. Then, the prepared GO and synthesized catalyst from Process 2 was characterized using Raman spectroscopy, Fourier transform infrared (FTIR) spectroscopy, X-Ray photoelectron spectroscopy (XPS), X-Ray diffraction (XRD), Thermal gravimetric analysis (TGA), Field emission scanning electron microscopy (FESEM) + Energy dispersive spectrometer (EDS), High-resolution transmission electron microscopy (HR-TEM) and Ultraviolet-visible (UV-Vis) Spectroscopy. The second process (**Process 2**) is the preparation of AuNPs supported on GO (AuNPs/GO). Furthermore, the prepared AuNPs/GO catalyst was differentiated by molar ratio of Au used on GO surface, different catalyst weight and temperature under solventless reaction in Process 3. The third process (**Process 3**) is the catalytic reaction of dehydrogenative silylation with aldehyde and hydrosilane substrate as first observation by solvent reaction using the synthesized catalyst from Process 2. In addition, overall reaction quantitative and qualitative analysis was observed under Gas chromatography - Flame ionization detection (GC-FID), Gas chromatography - Mass spectroscopy (GC-MS) and Nuclear magnetic resonance (NMR). While the solvent and solventless liquid viscosities had been analyzed using Rheometer instrument. Afterwards overall proceed the observation under solventless reaction. The reaction was further optimized by doing comparison of the catalyst with sodium borohydride ($NaBH_4$) reducing agent that synthesized similar procedure by trisodium citrate ($Na_3C_6H_5O_7$) and each catalyst was further investigated with 12 hours reaction and its reusability (five times) under solventless reaction. The fourth process (**Process 4**) is the characterization of the optimized AuNPs/rGO(C) and

AuNPs/rGO(B) catalysts using FESEM + EDS, FTIR, and XRD analyses. The fifth process (**Process 5**) is the calculation of the conversion, selectivity and kinetic study of all optimized catalyst in dehydrogenative silylation mostly studies the reaction under solventless reaction. Besides that, the reaction also observes the presence of H_2 after reaction through Gas chromatography (GC) coupled with Thermal conductivity detector (GC-TCD) analysis.

3.2 Materials/Chemicals

The chemicals required in this work was benzaldehyde (C_7H_6O) (purity ≥98%), toluene (C_7H_8) (purity ≥99% (GC)) and n-dodecane ($CH_3(CH_2)_{10}CH_3$) (purity ≥99% (GC)) used was manufactured from Nacalai Tesque. While DMPS ($C_8H_{12}Si$) (purity ≥97%) was obtained from Tokyo Chemical Industry; chloroauric acid ($HAuCl_4.4H_2O$) (purity ≥99%), $Na_3C_6H_5O_7$ (purity ≥99%), $NaBH_4$ (powder, ≥98.0%) and graphite (GRC) powder (<20μm) was purchased from Sigma Aldrich. All other chemicals were of analytical reagent grade and used as received, unless otherwise stated. Distilled water was used for all preparations. All reagents was used as received without further purification or modification, unless otherwise stated.

3.3 Experimental Methods

3.3.1 Process 1: GO Synthesis

Based on previous report (Marcano et al., 2010), the synthesis of GO using "improved Hummer's" method. Based on actual Hummer's method, GRC flakes (Sigma Aldrich, 20 μm) was oxidized with the additional of $KMnO_4$. In this work, the procedure used is following the flow diagram in Figure 3.1, a ratio about 9:1 mixture by concentrated H_2SO_4:H_3PO_4 (360 mL:45 mL) was added to a mixture of GRC flakes (3 g) and $KMnO_4$ (18 g that added slowly in portions to keep the reaction temperature below 20 °C), producing a black dark thick paste and slight exotherm to 35-40 °C. The mixture was then

heated to 50 °C and stirred for about 12 hours. The mixture was cooled to room temperature and poured onto ice (around 400 mL). The cool solution was then added with 30% H_2O_2 (around 3 mL) dropwise. For a workup, the mixture was further by washing with DI water, 30% HCl and ethanol continuously to kept maintaining in neutral pH. The mixture was centrifuged at 4000 rpm for 4 hours and for the initial step of washing by centrifuge with 200 mL of DI water the supernatant was separated whereas residue/precipitate was decanted away. For the next washing, the residue or precipitate was taken, and the supernatant was decanted away as well. That remaining solid material (residue/precipitate) was then sonicated in few minutes and washed in succession with 200 mL of DI water, 200 mL of 30% HCl, and 200 mL of ethanol (2 times); for each wash. The solid material was stored in a cellulose bag and was put into a dialysate solution of DI water for 12 hours. The solid was obtained after the process of dialysis and was oven-dried overnight at room temperature or using freeze-drying process for obtaining around 5 to 6 g of GO powder product.

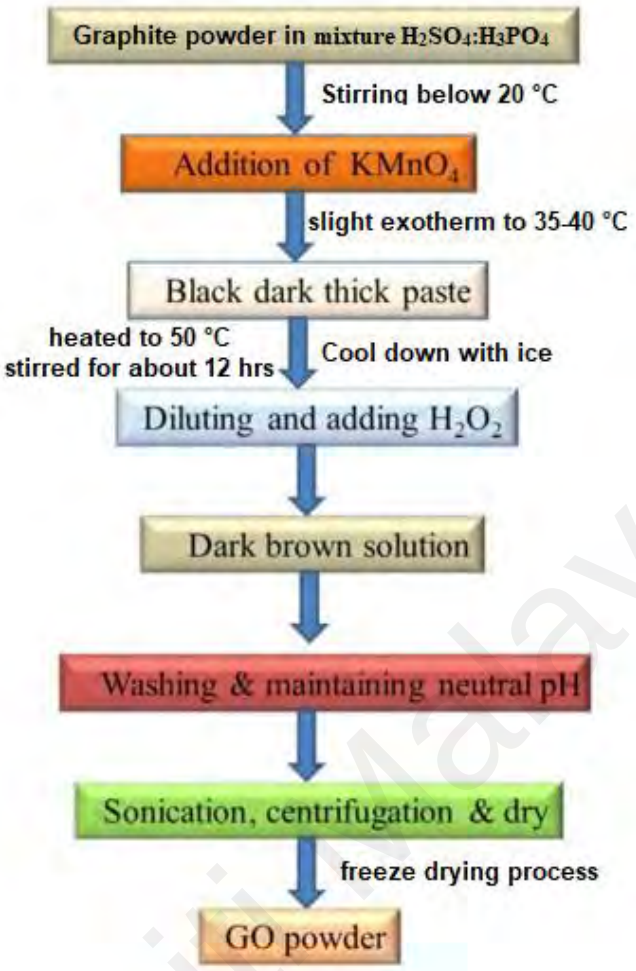

Figure 3.1: Flow diagram of GO synthesis.

3.3.2 Process 2: Au Nanoparticles Synthesis by Supporting on GO (Synthesis of AuNPs/GO)

AuNPs/GO catalyst was synthesized by following the method reported from previous study (Chuang et al., 2014; Zhang et al., 2011). First, an aqueous solution (DI water) of GO (0.275 mg mL^{-1}, 3 mL) was added to a solution of $HAuCl_4$ (0.047 mg mL^{-1}, 10 mL) based on calculation concentration of Au in millimolar (mM) using the formula: Molarity (mM) equal to the amount (in milimoles) divided by the volume of solution (in liters, L) for five different prepared concentration that are 0.2 mM, 0.4 mM, 0.6 mM, 0.8 mM and 1.0 mM. Then the mixture would be ageing for 30 min to promote the interaction of Au ions onto the GO surfaces. The solution was heated at 80 °C before a solution of $Na_3C_6H_5O_7$, depicted as C ($Na_3C_6H_5O_7$ – C) (about 0.085 mol dm^{-3} in 188 mL of the

amount used), which has worked as both reducing and capping agent, was added. The same procedure was used in other catalyst that was prepared with different reducing agent that was $NaBH_4$, depicted as B ($NaBH_4$ - B). This $NaBH_4$ reducing agent-based catalyst would be later compared with citrate reducing agent-based catalyst. The mixture was then kept at 80 °C with continuous stirring for 4 h. Next, the solution was cooled to room temperature before centrifuging at 6000 rpm and washed three times with DI water to remove any free Au ions (Au^{3+}). Lastly, the prepared catalyst was dried through normal or freeze-drying process. The synthesis would be repeated with different quantity of citrate and molar ratio of Au for catalyst optimization in hydrosilylation reaction. This work also can be based on flow diagram in Figure 3.2 below.

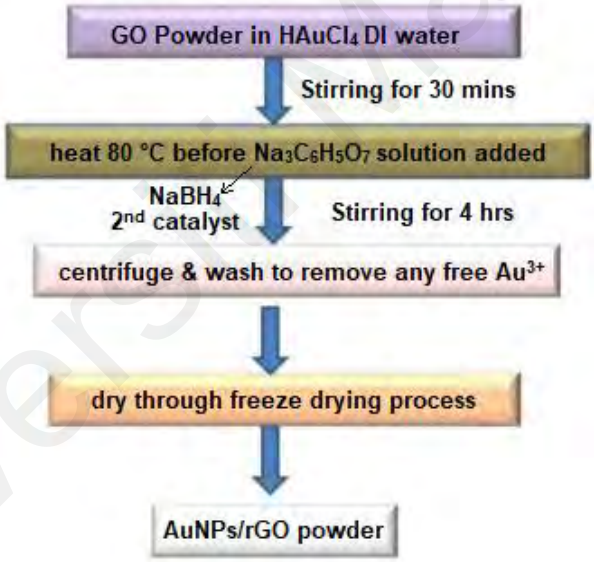

Figure 3.2: Flow diagram of AuNPs/rGO synthesis.

3.3.3 Process 3: General Catalytic Procedure for the Dehydrogenative Silylation with Aldehyde and Hydrosilane

The benzaldehyde (10 mmol) is used in solvent reaction and DMPS substrate together or alone (5 mmol) used for solventless reaction were added together with the AuNps/GO prior to sonication for about 30 mins. The corresponding catalyst of AuNPs/GO (about 0.06 mmol% of metal respect to substrate) and substrate were then charged in a conical flask in reflux set-up as shown in Figure 3.3.

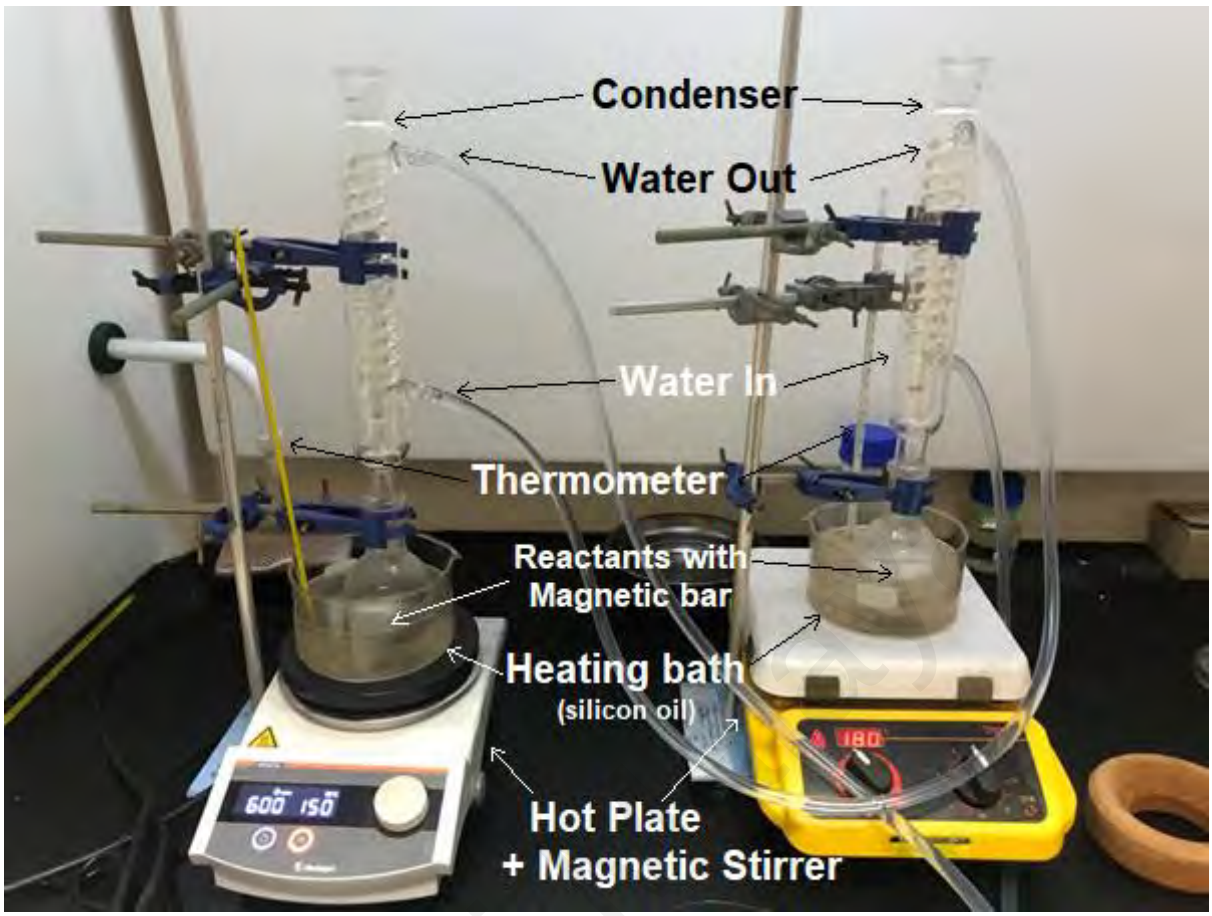

Figure 3.3: Setup for synthesis of disiloxane.

Then dodecane as internal standard was added to the solution. The reaction mixture was magnetically stirred at 120 °C in an oil bath. At the end of the reaction, the reaction mixture has been cooled to room temperature and an aliquot of 0.1 mL is diluted with anhydrous toluene (0.5 mL), filtered, and injected into GC to determine the conversion and product yields based on the dodecane used as internal standard as shown in Figure 3.4. The reactant and final product had been confirmed before and after the reaction is in colourless form. The reaction without the presence of benzaldehyde as a solvent was performed and compared with the reaction in solventless. The reaction optimization and catalyst reproducibility were also investigated. As it is expected, catalytic activity in solvent reaction is higher than solventless reaction. The solvent reaction is illustrated in Figure 3.5.

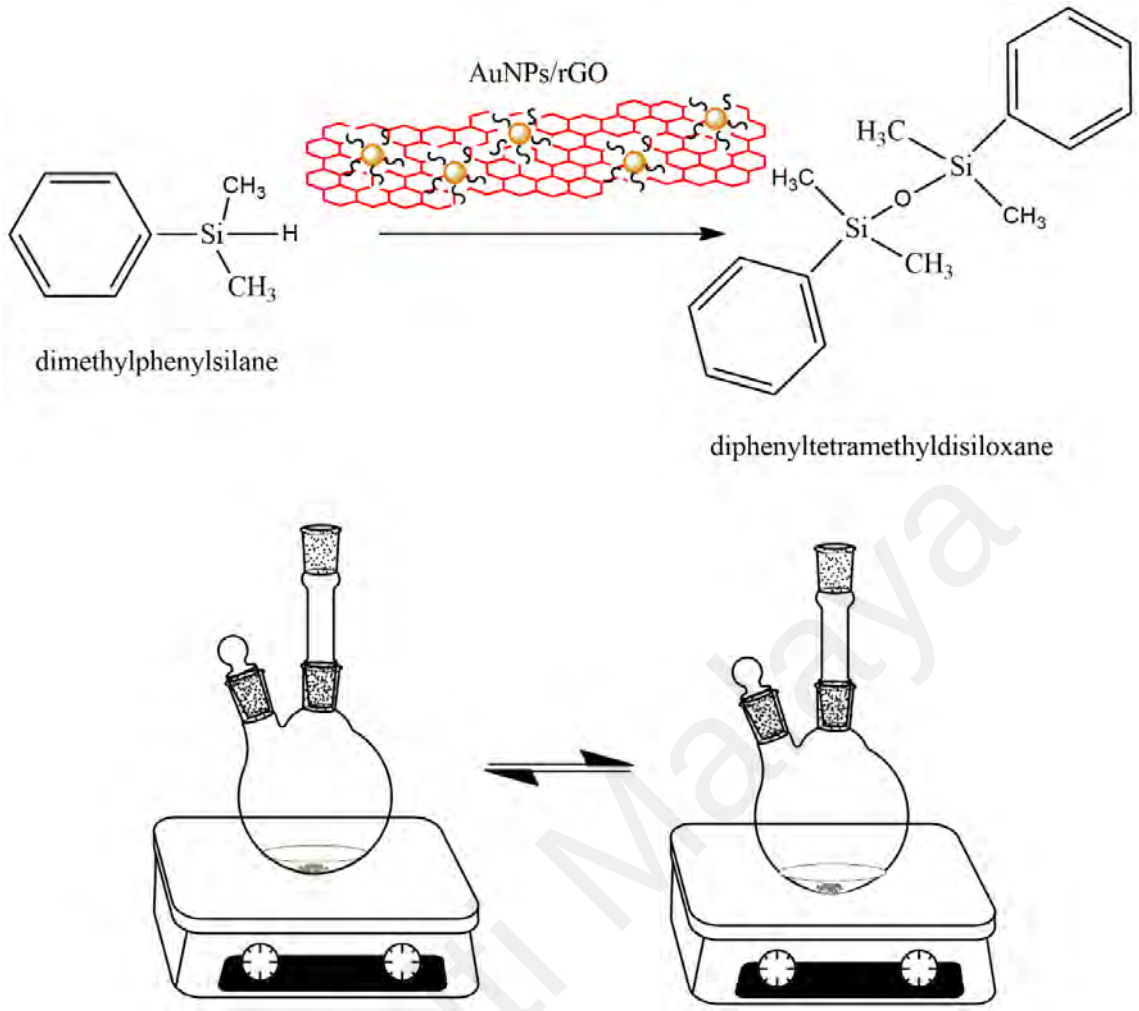

Figure 3.4: Schematic diagram of the reaction - dehydrogenative coupling of DMPS into 1,3-diphenyltetramethyldisiloxane with AuNPs/rGO.

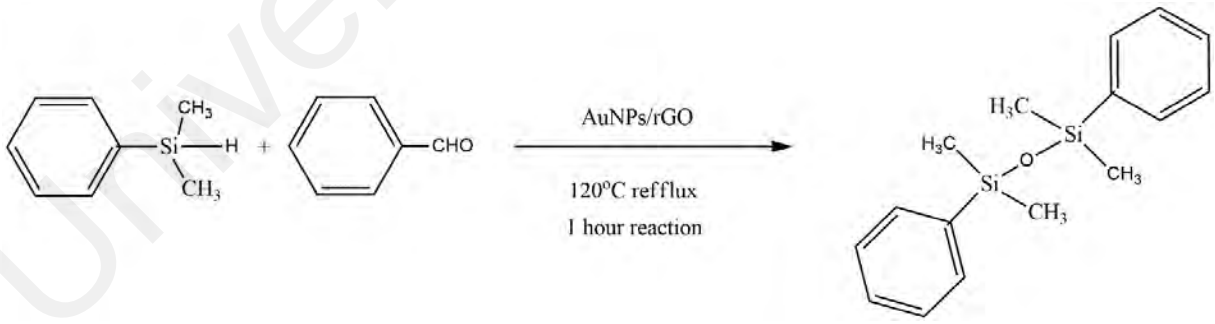

Figure 3.5: Dehydrogenative coupling process of DMPS into 1,3-diphenyltetramethyldisiloxane catalysed AuNPs/rGO under solvent reaction at temperature of 120 °C was completed within 1 hour.

3.3.4 Process 4: Catalyst Characterization

The AuNPs/GO catalysts was characterized using thermal analysis (TGA), textural properties and characterisation (FESEM+EDS and TEM), surface chemical state (XPS) and functional characterisation (FTIR, Raman, UV-Vis). To confirm its catalytic performances, products identification and molecular structure of the samples and final product after process of reaction was analysed under GC-FID, GC-MS, GC-TCD and NMR, respectively.

3.3.4.1 Ultraviolet-Visible (UV-Vis)

The UV-Vis absorption spectra of catalyst samples were recorded in the region of 200 – 800 nm in distilled (DI) water solution at a fast scan rate measurement. The spectra were measured at room temperature using a Shimadzu UV-2600 UV-Vis Spectrophotometer in a 1.0 cm of quartz cuvette. All results are presented in terms of Absorbance (A) versus wavelength (λ, nm) units.

3.3.4.1 Thermal Gravimetric Analyzer (TGA)

TGA is a technique that measures the change in the weight of the sample when it is heated, cooled, or held at constant temperature(s). In this study, the calcination temperature for the as-synthesized AuNPs/rGO was examined using the TGA method. The samples (4 mg – 5 mg) was examined using the TGA (Mettler Toledo, TGA/SDTA - 851^{e}) by placing it into a 100 µl open alumina crucible. The experimental temperature was set from the ambient to 800 °C, at a heating rate of 10 °C min^{-1} ramping under nitrogen gas at a flow rate of 50 ml min^{-1}. It was then cooled to room temperature. This technique was used to identify the composition ratio based on 5 different samples of AuNPs/rGO to ensure that comparison of AuNPs that attached on the surface of rGO is obtained prior to different molar concentration used.

3.3.4.2 X-Ray Diffraction (XRD)

XRD is one of the non-destructive test methods for characterizing crystalline materials. AuNPs/rGO was determined by using Cu Kα radiation (XRD, λ= 1.5406 Å, Bruker AXS - D8 Advance diffractometer). It provides information on structures, phase, preferred orientations and other structural parameters such as average grain size, crystallinity, strain and crystal defects. The sample (1 g) was weighed and placed into the sample holder. Prior to beginning the test, the step size was set at 0.02 °, at a 0.02 °/s scanning rate between 2° - 80° diffraction angle (2θ). From the obtained results, the crystallite size can be determined using the Scherrer equation based on Equation (3.1). The X'Pert Highscore Plus V3.0.4 program interpreted the phase composition and all correlated information pertaining towards all AuNPs/rGO prepared samples.

$$\tau = \frac{K\lambda}{\beta cos\theta} \tag{3.1}$$

where: -

τ = mean size of the crystalline domains.

K = a dimensionless shape factor, with a value close to unity. It has a typical value about 0.9 but varies with the actual shape of crystallite.

λ = X-Ray wavelength.

β = line broadening at half the maximum intensity (FWHM).

θ = the Bragg angle.

3.3.4.3 Raman Spectroscopy

Raman Spectroscopy (Renishaw in Via Reflux with high performance CCD camera and LEILA microscope) was used in this study. It is one of the spectroscopic techniques used to study the vibrational, rotational, and other low frequency transitions in molecules. It was used to determine the substance (phase) from the characteristic spectral patterns,

and quantitatively or semi-quantitatively, the amount of substance in AuNPs/rGO catalyst with high lateral resolution. The sample about 0.05 g was placed into the sample holder and subsequently inserted into the Raman spectroscope. Sample degradation and fluorescence might occur during testing. It significantly impacts upon highly sensitive materials of TiO_2 nanoparticles. Hence, 1% of 0.2 mV laser power at a 180 s exposure time was selected to analyze AuNPs/rGO. The argon gas laser (514 nm) was selected in this work, due to its 1800 mm^{-1} spectral resolution being sufficient to plot excellent spectra. Focusing the laser beam via ×50 objective lens helps collect the scattered radiation, and the laser spot on the sample was approximately 0.836 μm at 514 nm excitation.

3.3.4.4 Fourier Transform Infrared Spectroscopy (FTIR)

The FTIR spectra (Perkin-Elmer 100 spectrophotometer) provide the molecular absorption and transmission (specific frequency of energy), which is useful in analyzing the AuNPs/rGO catalyst functional group, while others are attached to the molecule's functional group together with its linking the catalysts sample. The sample holder was cleaned before using acetone. About 0.3 mg of catalyst sample was mixed with 4 mg of KBr and molded to form a pellet. The pellet was placed in the FTIR sample holder and bombarded with IR radiation. Some of the IR radiation was absorbed by sample, while others passed through via transmission. The resolution of the FTIR was set to 4 cm^{-1}, with 16 scans in the wavelength range 400 cm^{-1} to 4000 cm^{-1}. The FTIR spectra was collected, with its peaks labeled.

3.3.4.5 High Resolution Transmission Electron Microscope (HR-TEM)

HR-TEM analysis was conducted using the JEM-2100F instrument at an accelerating voltage of 200 kV. It has become a major support in the list of characterization techniques for materials scientists, due to its capability in generating image and diffraction

information from the samples. Furthermore, the specified sample which is AuNPs/rGO could be characterized via radiation produced by beams of accelerated electrons. It offers high magnification up to 1.6 times, allowing us to observe extremely small and tiny lattice-fringe spacing. Prior to the HR-TEM characterization, the AuNPs/rGO was prepared by titrating the dispersed samples on 300 mesh copper grids. The samples were prepared and left overnight to dry. The samples was then placed into the HR-TEM sample holder prior to being inserted into the HR-TEM. Images of AuNPs/rGO was selected and taken at 50,000, 100,000, and 500,000 × magnification. The size and lattice-fringe spacing was measured using image-J. The particle size distribution was plotted after 20 particles of AuNPs/rGO was measured, and the lattice-fringe spacing was used to support the results from XRD analysis.

3.3.4.6 Field Emission Scanning Electron Microscopy (FESEM) + Energy Dispersive Spectrometer (EDS)

The morphology of AuNPs/rGO was investigated using Scanning Electron Microscope (JSM - 7500F Jeol). First, the AuNPs/rGO was sprayed with Platinum (Pt) prior to loading into the instrumentation sample stage. After that, the prepared samples was then mounted onto the sample holder using double-sided electrically conducting using adhesive tapes of carbon to prevent surface charge on the specimens when exposed to the electron beam. The fracture surfaces of the catalyst sample on the glass substrate was sputtered with Pt prior to morphological observation to prevent charging during imaging. However, for AuNPs/rGO was not necessary to undergo such process, just proceed to next step and Pt step. The SEM micrographs was obtained under conventional secondary electron imaging conditions at an acceleration voltage of 5 kV.

The elemental analysis of the AuNPs/rGO was determined using EDS, equipped in the FESEM. EDS is an analytical technique used for elemental analysis or chemical

characterization. The energy of the beam is typically in the range of 10 to 20 keV. The accumulation of the energy counts (intensity) creates a spectrum, representing the chemical analysis of the sample. The higher a peak is in the EDS spectrum, the more concentrated the element present in the sample. This allows us to obtain the atomic percentages + weight. To confirm the presence of the Watt content located at the bottom of the prepared catalysts, the cross-section of the EDS analysis was conducted. The area scanned in the EDS analysis was conducted by taking the atomic percentages + weight from single spots along the prepared catalysts.

3.3.4.7 X-Ray Photoelectron Spectroscopy (XPS)

XPS is a quantitative spectroscopic technique that measures the chemical and electronic state, empirical formula and elemental composition of the outer 10 nm or less of any solid surface. XPS is the mainstay of almost all surface analysis labs worldwide due to the higher sensitivity (concentrations down to 0.1 atomic%) could be detected from the outer solid surface. For this study, photoelectron spectra was obtained using XPS (JEOL JPS-1000SX) with a dual X-Ray source, in which an Al-K_α (30 kV) anode and a hemispherical energy analyzer was used. The background pressure during data acquisition was maintained at 7.0×10^{-9} Torr. The spectra was calibrated by setting the C1s peak of adventitious carbon at 284.8 eV as a charge reference. The XPS spectra was further deconvoluted via Gaussian-Lorentzian curve fitting technique using the software of Multi Pak 9.0. The XPS spectra are obtained by irradiating a material with a beam of X-Rays while simultaneously measuring the number of electrons and kinetic energy that escape from material under ultra-high vacuum condition.

XPS derives the information by directing an energetic photon beam (X-Rays) to induce the emission of core-level electrons. Photoelectron production in its simplest form describes a single step process in which an electron initially bound to an atom/ion is

ejected by a photon. Since photons are a massless (zero rest mass), chargeless package of energy, these are annihilated during photon-electron interaction with complete energy transfer occurring. If this energy is sufficient, it will result in the emission of the electron from the ion/atom as well as the solid. The energy of the electron emissions is then measured since this provides insight into the specific type of ions/atoms the electrons emanated from the elements. The kinetic energy that remains on the emitted electron is the quantity measured.

3.3.4.8 Nuclear Magnetic Resonance (NMR)

NMR is a spectroscopic technique based on the magnetic properties of certain non-zero nuclear spin atomic nuclei. It is an absorption spectroscopy, the basis of which lies in the abdertion of energy (radio frequency) by a magnetically active nucleus (nonzero spin) that is located within a magnetic field and which due to the absorption of this radiofrequency undergoes a reorientation of the magnetic moment of the nuclear spin in that field. The fundamental parts of an NMR spectrometer are an electromagman,a radio frequency oscillator that supplies the energy needed to change the orientation of nucleares spines, a detector coil that receives signals, and a computerized system that governs the entire device and includes an amplification and recording system. The most common nuclei in organic compounds based on this research study that are magnetically active include proton (^{1}H), carbon (^{13}C), silicon (^{29}Si). The most common spectra are representationsof absorption intensity versus resonance frequency (usually representing the magnitude of the chemical shifter, δ) and present signals whose position, shape and size are intimately related to the molecular structure. Detailed analysis of these spectra provides valuable structural and stereochemical information. Two-dimensional (2D) spectra allow relationships between different cores or different magnitudes of the same nucleus. The equipment used to carry out this research study has been in FT-NMR AVANCE III 400 MHz (AVN 400) and Lambda JEOL 400 FT-NMR spectrometer.

The samples were prepared by dissolving about 3 mg of the product or mixture from which the spectrum was desired in 0.7 mL of deuterate chloroform ($CDCl_3$) solvent. The deuterated chloroform solvent was used to perform NMR based on its subunits and structure through 2D Cosy, HSQC, ^{1}H-13C and ^{29}Si correlations to calculate the selectivity of the reactions to the desired product.

3.3.4.9 Rheological Measurement

Viscosities are measured using a Brand Alpha Analytical model MCR301 of Anton Paar Physica Modular Compact Rheometer at various temperatures (from 20 to 90 °C). Sample holder and rotator was cleaned with acetone firstly to ensure the purity and accurate result. Nearly 5 ml of the DMPS of that reactant solution was poured into the sample holder until the holder was filled up to the upper surface of the rotator. After each measurement, the parts was washed with water and acetone repeatedly.

3.3.4.10 GC-FID, GC-MS & GC-TCD

GC-FID is a technique to identify compounds based on retention time that convert into system-independent constants commonly known as Retention index. The retention indices of each chemicals compound are calculated based on its retention time standardized to the retention times of nearby eluting n-alkanes (e.g., heptanes, octane or hexane). Retention times differ with the individual chromatographic system as it depends on the length and type of the column, velocity, film thickness, time consumed, diameter and pressure of carrier gas in the analysis. The derived retention indices are relatively independent of these parameters and allow comparing values measured by different analytical laboratories under varying conditions. Retention indices could help in identification of components by comparing experimentally established retention indices with identified values. Despite the use of linear retention indices and extensive studies, it needs to be aware when using such indices in an absolute sense. Usually, data from one

laboratory to another will commonly not be accurately reproduced, though by combining with mass spectral results, retention data does still provide a good guide to discover the identities of components.

(GC-MS) is a combination of GC is highly efficient separation column that attach with selective or specific detectors (MS). Thus, makes GC a more favorable technique. The GC-MS also known as hyphenated analysis technique whereas; the combination of spectroscopic detection methods or can used other detection techniques to get better separation of the quality of data or components from an analysis. GC function as describe before is to separate the elements of a mixture while mass spectroscopy characterizes each of the elements individually thus, a solution that containing several chemicals can be qualitatively and quantitatively evaluated claimed that this method can be used to analyze mixtures of chemicals including essential oils. While the MS is a technique of analysis that engages generating charged particles (ions) from molecules of the analytes. The generated ions are analyzed to supply information about the chemical and molecular weight of the present compound structure. There are three main separate regions in mass spectrometers include the ionizer or ion source, ion itself or mass analyzer, and most important part is the detector.

GC-TCD is typically used in packed-column. Helium (He) was used as the carrier gas for analysis of gas samples. The sensitivity of TCD detection was enhanced based on large difference in thermal conductivity between He gas and other gases. Usually, it will produce a linear response. Nonetheless, there are some problems related with analysis of hydrogen (H_2) using He as a carrier gas. Although the thermal conductivity of H_2 is more prominent than that of He, the thermal conductivity of the H_2-He binary mixture is not a simple monotonic increasing function of H_2 concentration. Instead of thermal

conductivity goes through a local minimum at low concentrations of H_2 before increasing to the pure H_2 value (Cowper & Derose, 2013).

In this experiment, GC-FID was used quantitatively to check the performance of the catalyst whereas GC-MS was used to identify qualitatively the final product for the reaction. Generally, GC-FID separates the analyte in the sample. The analyte was evaporated in the injector port and eluted by nitrogen gas into the capillary column. The analyte is separated in the column depending on the polarity and oven temperature profile. Then the separated analyte will be ionized by the flame of flame ionization detector (FID). The ions are impelled by electric potential towards electrodes producing a minute current on the order of picoamps. From the current the detector creates a chromatogram which we can analyze the compound in our sample. The carrier gas used was nitrogen gas and purified air with the system pressure of 35.4 kPa. The programming of oven temperature as shown in Table 3.1. This work used split injection mode with split ratio 50:1 with injection temperature of 250 °C. The temperature of detector used was 300°C. The nitrogen gas flow was set up to 1mL/min. The total run time was 33.2 minutes. This work used gas chromatography from Shimadzu model GC-2010.

Table 3.1: Method Used for GC-FID Analysis.

	Rate (°C/min)	Oven Temperature (°C)	Hold Time (min)	Run Time (min)
Initial	0	60	4	4
Ramp	5	150	3	25
Ramp	25	280	3	33.2

Furthermore, GC-MS sample device detector is used in this experiment to identify the product formed at the end of the reaction and the method used to set up the GC-MS analysis also almost like GC-FID analysis. This gas chromatography was equipped with mass spectrometry as the detector. The eluted sample was detected by the mass spectrometry to determine the qualitative analysis of the sample to confirm the

compounds in the sample. The column used was a non-polar column (ZB-5MS) with the length of 30.0 m, diameter of 0.25 mm and thickness of 0.25 mm. Helium gas was used as carrier set at 1 mL/min. Initially the oven of the GC was set at 60 °C and increased up to 300 °C at the increment rate of 25 °C per minute. The final temperature at 300 °C was held for 5 minutes. The mass spectrometer was operated in the electron ionization mode. Mass spectrometer data was recorded between 4.5 - 12 minutes. For GC-MS, the sample is injected amount about 0.2 µL. While the injection temperature was 300 °C and the injection mode used was split mode with ratio of 70:1. The oven temperature programming is shown in Table 3.2. The total runtime for this method was 30.5 minutes. The overall sample analysis used Shimadzu GC-MS instrument model name Shimadzu GCMS-QP 2010 Plus.

Table 3.2: Oven temperature programming for GC-MS.

	Rate (°C/min)	**Oven Temperature (°C)**	**Hold Time (min)**	**Run Time (min)**
Initial	0	60	4	3
Ramp 1	5	150	3	22
Ramp 2	10	300	5	30.5

The H_2 gas was analyzed using an GC-TCD instrument manufacture Agilent Technologies 6890N system on with filament that equipped with a Agilent 19095P-MS6 of HP Plot MS & Plot Q capillary column (60.0 m × 530 μm, 25 μm nominal). The column temperature was programmed to 60.0 °C only and held for 10 minutes at 230 °C. Helium was used as the carrier gas at a flow rate of 10 mL per minute with a split ratio of 10 : 1. The gas sample was collected in a gas sampling bag that was connected with reflux set-up. After reaction completed, the gas forms the sampling bag was withdrawn manually usually gas injector syringe and injected to the inlet port. The injector port temperature was set to 150 °C and detector to 250 °C.

3.3.5 Process 5: Conversion, selectivity and kinetic study of dehydrogenative silylation of solventless reaction

The corresponding catalyst of AuNPs/rGO (about 0.25 mol% of metal respect to substrate) about 5 mg is introduced in a conical flask that has been reflux by stirring. The conversion rate of 1,3-diphenyltetramethyldisiloxane with different molarity of AuNPs/rGO catalyst was calculated based on the analysis from GC-FID results. The Equation (3.2 to 3.4) below to calculate the conversion, selectivity and yield, respectively. Each equation is quantification about the rate of DMPS to disiloxane:

$$X = \frac{pA_{(\text{sub})t=0} - pA_{(sub)t=h}}{pA_{(\text{sub})t=0}} \times 100\% \quad (3.2)$$

$$S = \frac{pA_{(\text{main product})t=h}}{pA_{(\text{product})t=h} + pA_{(+\text{product})t=h}} \times 100\% \quad (3.3)$$

$$Y = X.S \quad (3.4)$$

where: -

X = conversion (%)

S = selectivity (%)

Y = yield (%)

$pA_{(sub)t=0}$ = peak area of substrate at initial reaction.

$pA_{(sub)t=1h}$ = peak area of substrate at final reaction.

$pA_{(product)t=h}$ = peak area of seleted product at final reaction.

$pA_{(+product)t=h}$ = peak area of other product at final reaction.

CHAPTER 4: RESULTS AND DISCUSSION

4.1 Catalyst Characterizations

AuNPs/rGO catalyst with Au concentration of 0.2,0.4,0.6,0.8 and 1.0 mM were characterized using XRD, SEM, RAMAN, UV-vis, FT-IR and TGA instruments. The 0.4 mM AuNP/rGO catalyst was further characterized using HR-TEM and XPS instruments.

4.1.1 Integrated XRD FESEM Analysis of AuNPs/rGO

XRD was used to identify the structure of cellular units, known as d-spacing to investigate AuNPs/rGO morphology and structure. First, the radiation with wavelength, λ of 1.54060 Å was used in the diffractometer. The GO alone shows a peak exactly at 2Θ = 10°, which contains d-spacing of 8.9 Å specific to (011) plane (Figure 4.1). For further observation confirmed that the smooth area between 12 to 25 of 2Θ indicates the rGO in the AuNPs/rGO (Saquib & Halder, 2018). Besides that, the sample shows the purity and that AuNPs effectively prevented the restacking of rGO layers (Naeimi & Farahnak Zarabi, 2018). From Figure 4.1, there are 4 peaks which indicated the presence of AuNPs (2Θ = 38.1, 44.4, 64.6, 77.6 and 81.7) All peaks have a standard Bragg reflection of (111), (200), (220), (311) and (222). The most extreme diffraction at a peak of 38.1 shows that zero valent Au chosen growth orientation is set in (111) direction.

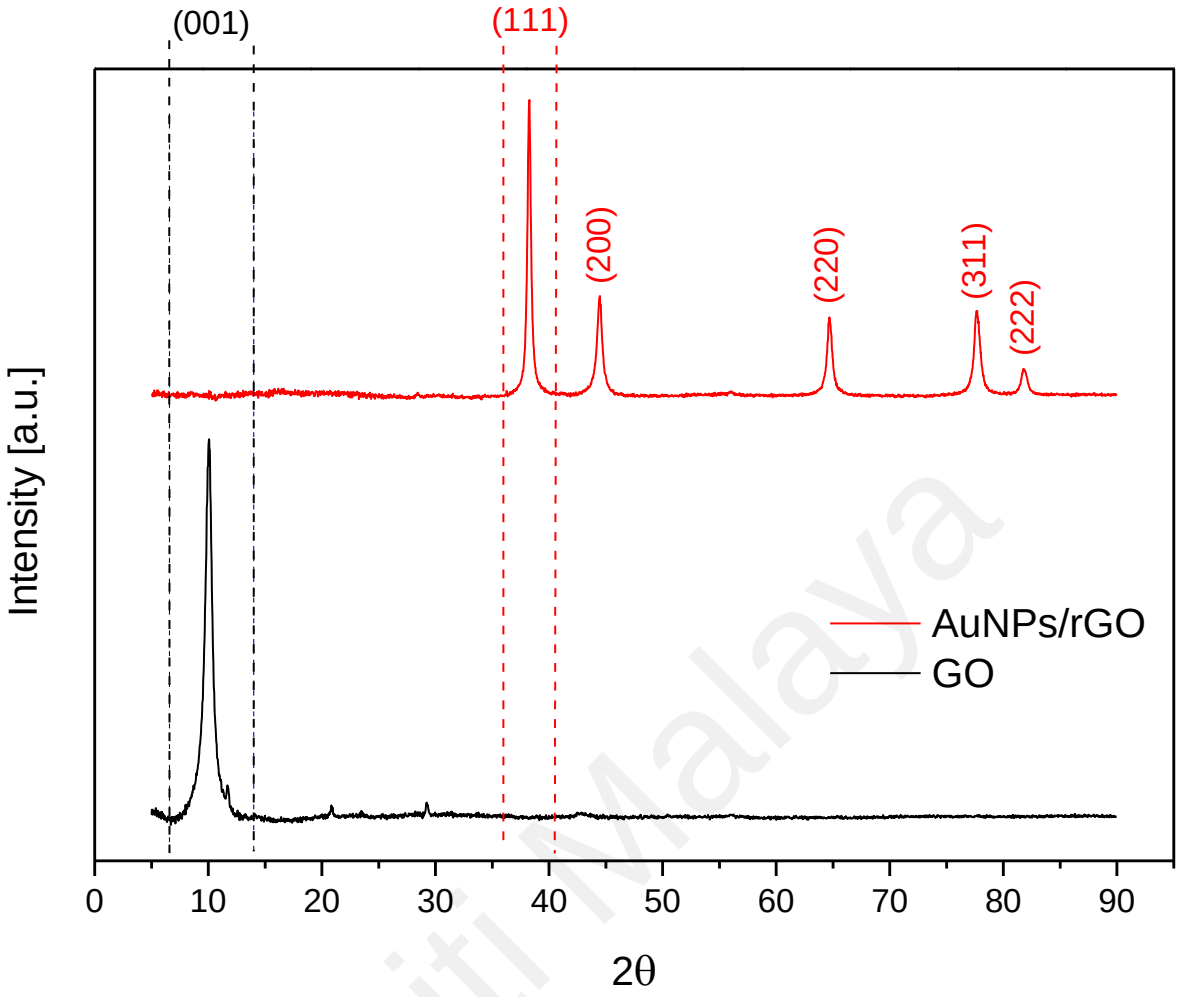

Figure 4.1: XRD patterns of 4mM AuNPs/rGO and GO.

It refers to molecular solids formed with a repeated 3D pattern of atoms or molecules identical to each portion (Krishnamurthy et al., 2014). The XRD diffractogram with different Au concentrations are compared with FESEM images in Figure 4.2. It is observed that Au crystallinity peaks are reduced with the increasing of Au composition after 0.4mm AuNP/rGO in Figure 4.2. Each diffractogram shows that the surface images of FESEM have a clear difference in morphology. Small bright dots in FESEM images in Figure 4.2 suggested AuNPs presence and this was further verified using EDS analysis in Table 4.2 (García et al., 2013). The abundance of AuNPs is seen at high molarity compared to less molarity of AuNPs/rGO. The number of bright dots is increasing proportionally with the composition of Au in AuNPs/rGO. Nevetheless, Au crystallinity

and calculated crystallite size from XRD diffractogram is disproportional to the composition of Au in EDS after 0.4 mM Au in AuNPs/rGO.

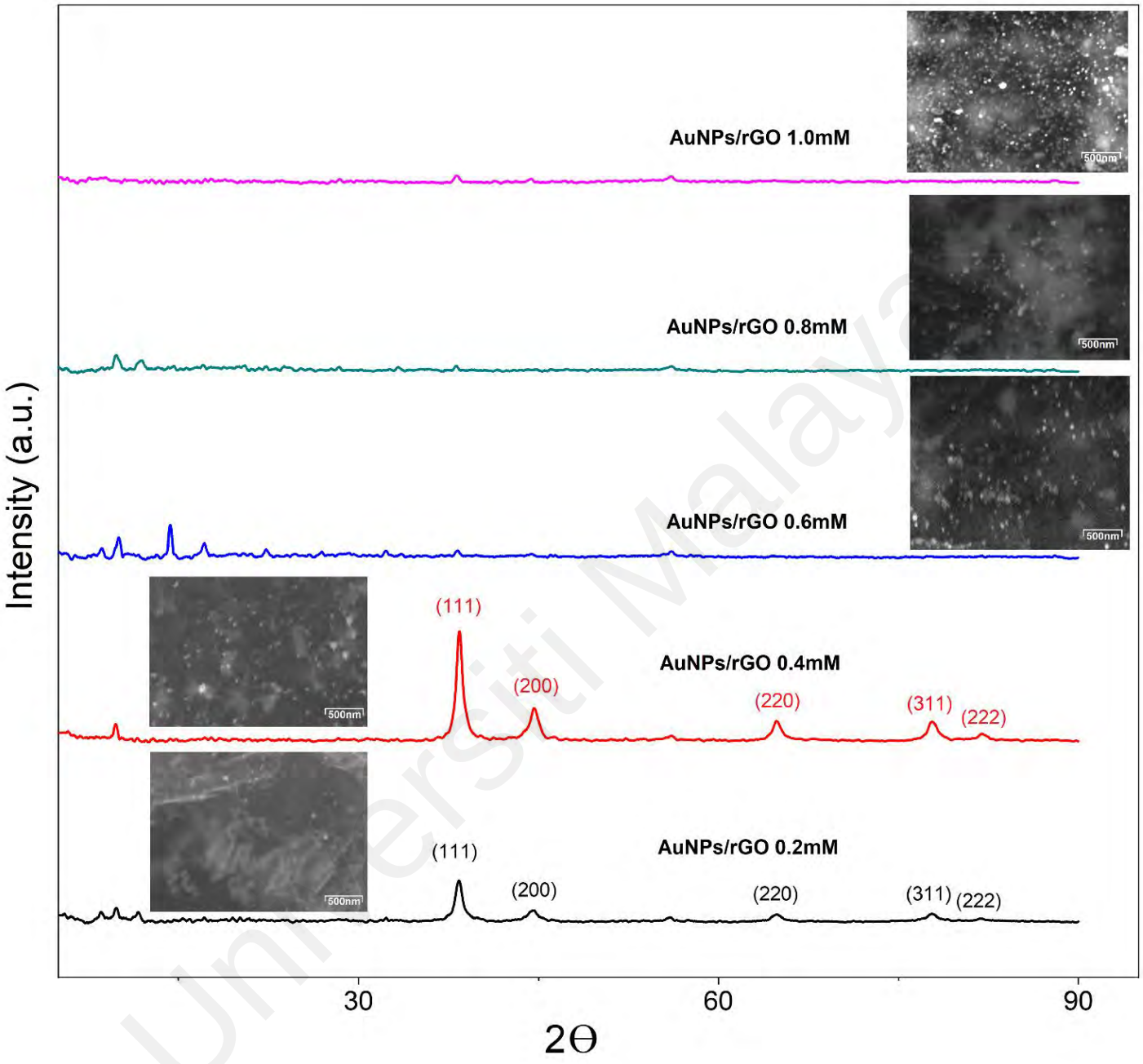

Figure 4.2: Powder XRD spectra combine with FESEM micrographs of AuNPs/rGO with different molarity of 0.2 mM, 0.4 mM, 0.6 mM, 0.8 mM and 1.0 mM.

Table 4.1: The crystallite size of AuNPs/rGO catalyst with different molarity.

AuNPs/rGO (mM)	Crystallite size (nm)
0.2	8.23
0.4	11.27
0.6	2.13
0.8	2.07
1.0	2.12

Therefore, it is assumed Au particle size from 0.6 to 1.0 mM are amorphous based on the XRD diffractogram in Figure 4.2. Based on Table 4.1, the crystallite size is increasing from 0.2 to 0.4 mM Au in AuNPs/rGO catalyst. However, the crystallite size for 0.6 to 1.0 mM Au catalysts is constant around 2.10 nm and in agreement with the amorphous phase in XRD diffractogram. The explanation could be related by synthesis process that is difficult to get uniform small size of AuNPs. There are several justifications of trials to attach the AuNPs into the rGO layers. Where the study done by Zabetakis et al. (2012), explain that in using higher Au salt concentrations and higher in citrate to Au ratios contribute to the increasing in polydispersity indices. This incident is most probably due to the increase in ionic strength which contributes to a higher propensity of the AuNPs for agglomeration (Zabetakis et al., 2012). However, the graphene restacking and to avoid of agglomeration from AuNPs, which cause a less usage of AuNPs that are still remain unresolved problems so far (Lazar et al., 2020). Other than that, the GO is not properly reduced during the synthesis using citrate as reducing agent. The calculation of crystallite size of 0.4 mM optimized AuNPs/rGO catalyst was then verified afterward with TEM analysis in Figure 4.7.

4.1.2 TGA analysis for AuNPs/rGO

Functionalization on the carbonaceous nanocomposite and AuNPs surface was examined using TGA. Figure 4.3 shows TGA curves under nitrogen gas flow for GO that was synthesized after freeze-drying in comparison with different molarity synthesis of AuNPs/rGO under the same freeze-drying process. Functionalization of these materials between GO and AuNPs/rGO shows multi-stages decomposition patterns. GO thermal degradation can be classified into 3 stages, the first weight loss of about 20% occurred at temperature around 190 °C or below, attributed to the evaporation of citrate precursor on the AuNPs/rGO (Obireddy & Lai, 2021). The second weight loss to 50% occurred at temperature up to 300 °C, related to the removal of oxygen (O) - functional groups such as CO_2 gases, CO and H_2O (Liu & Speranza, 2021). A sharp decrease in weight, ~50%, appears between 400 and 560 °C. As obvious seen only one peak based on 0.6 mM sample, it can be concluded that there is only one material that decomposes, namely, the rGO at 560 °C attribute to the stable oxygenated functional groups (Tene et al., 2020). The remain mass amount about 40%, typically and it could represent the amount of AuNPs, as the maximum heating at 900 °C temperature of the analysis is lower than the melting point of Au usually under 1064 °C (Bonvicini et al., 2022).

The decomposition behavior of AuNPs/rGO with different molarity of AuNPs attached with constant amount of GO was compared using TGA in Figure 4.3. There is a different pattern of decomposition between highest to lowest molarity of AuNPs/rGO catalyst. The lowest molarity of 0.2 mM shows the highest and fastest decomposition when further by increasing the temperature followed by 0.4 mM > 0.6 mM > 0.8 mM > 1.0 mM of AuNPs/rGO catalyst. Overall, high amount of AuNPs on the rGO surface shows the least amount and slow to undergo the decomposition process. The pattern shows slow in decomposition process when used high loading of AuNPs due to the abundant amount of Au attached on rGO surface. It was possibly due to the layered of

AuNPs on the surface of rGO when used high concentration of Au solution (Yang et al., 2022). The thermal properties confirmed on the composition of the catalyst correlate well with other characterization results such as FTIR, Raman and XRD.

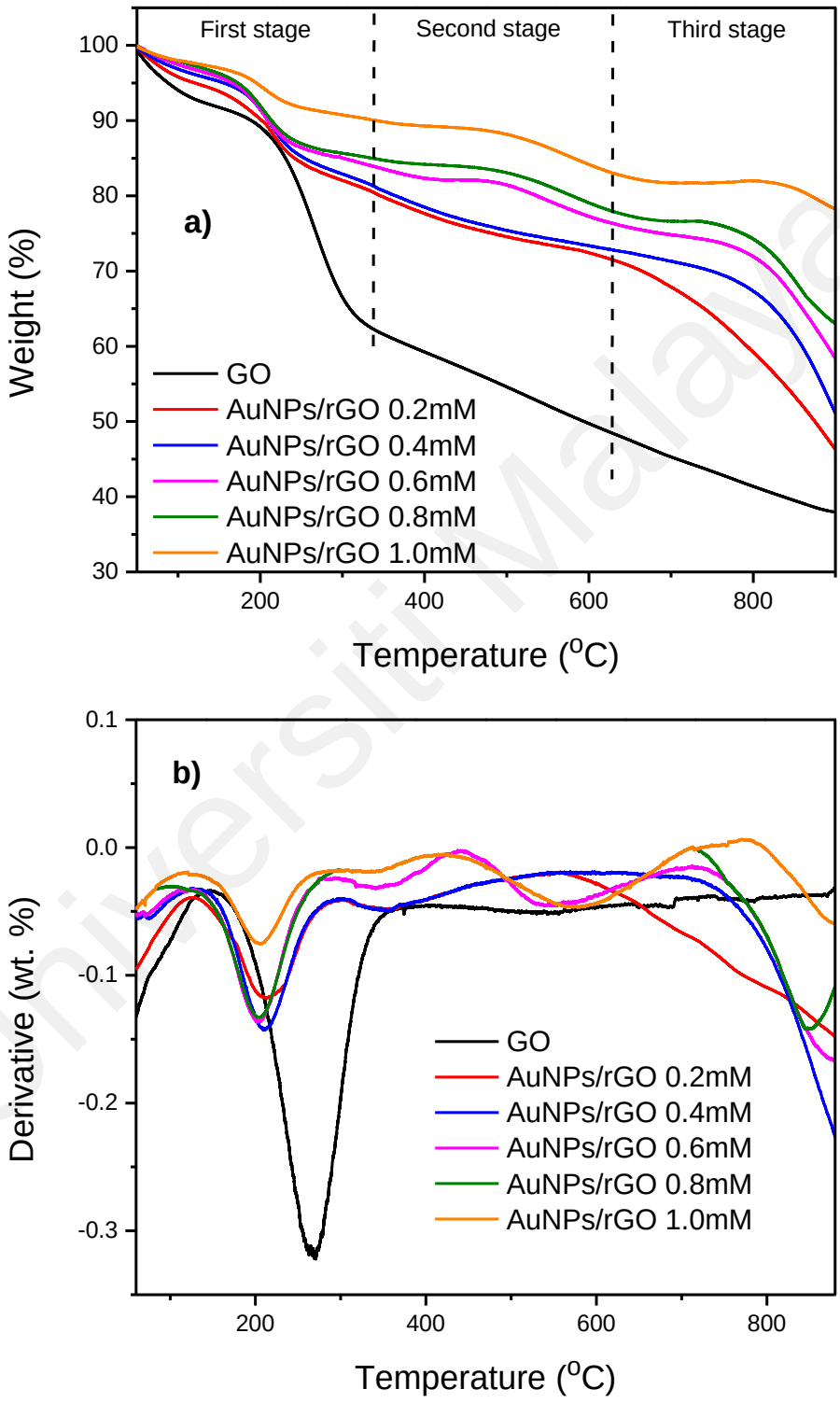

Figure 4.3: (a) TGA and (b) DTG curves for GO in comparison with different molarity of AuNPs/rGO.

4.1.3 EDS analysis for AuNP/rGO

By observation from EDS analysis, its elucidates the presence of nanoparticles is well established with elements identification for all 5 samples. As expected, overall EDS analysis only shows 3 observable peaks for 3 elements of C, O and Au, respectively. The higher the amount of Au content, the higher the diffraction angle of EDS. For 1.0 mM of AuNPs/GO catalyst shows highest weight percent (wt%) with a total of 17.06% (C: 7.71%; O: 4.77%; Au: 4.58%) compared to the rest of the AuNPs/rGO.

This proved that higher Au loading will be resulted in more diffraction angle (Shang et al., 2014). From Table 4.2, the result shows the amount of wt% for AuNPs/rGO catalyst with different molarity from 0.2 until 1.0 mM. Figure 4.4 shows the EDS results for different precious metal loading of AuNPs on the rGO to confirm the presence of Au, C and O in the AuNPs/rGO catalyst.

Table 4.2: Amount of weight percent (%) for AuNPs/rGO catalyst with 1.0mM, 0.8 mM, 0.6 mM, 0.4 mM and 0.2 mM.

AuNPs/rGO catalyst (mM)	Weight percent (wt%)		
	C	O	Au
0.2	0.86	0.50	0.76
0.4	1.07	0.58	1.18
0.6	7.90	4.22	2.08
0.8	8.02	3.67	3.75
1.0	7.71	4.77	4.58

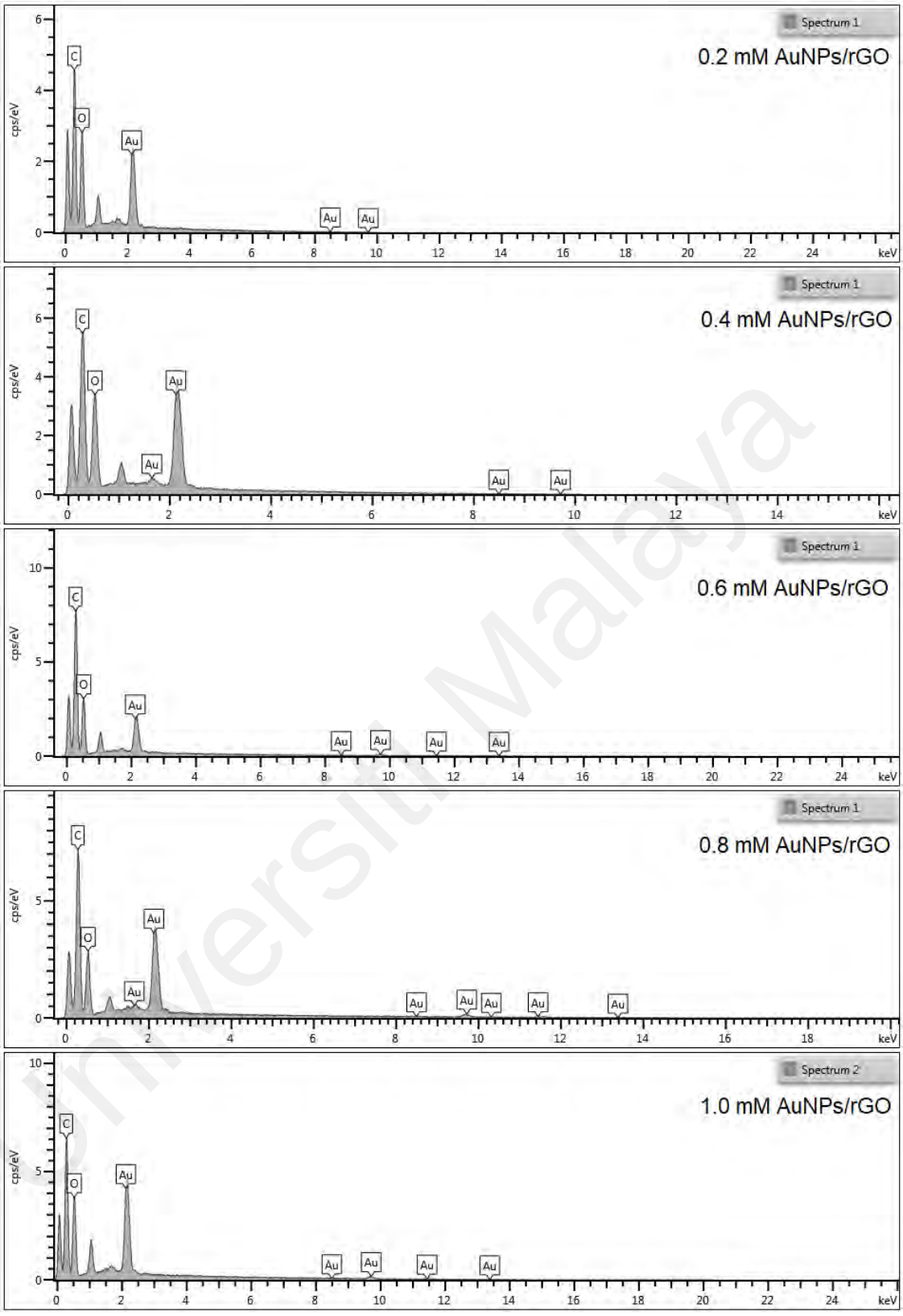

Figure 4.4: EDS images of AuNPs/rGO catalyst of 1.0mM, 0.8 mM, 0.6 mM, 0.4 mM and 0.2 mM.

4.1.4 UV-Vis Analysis for AuNPs/rGO

The GO peak is usually observed around 230 to 300 nm due to the π- π transition of aromatic C-C bonds (Zhang et al., 2011). However, the main interest for the study is to observe the absorbance peaks from different concentrations of Au content on the surface rGO composites. This is because AuNPs have a distinct optical characteristic known as localized surface plasmon equilibrium (LSPR), such as the mutual oscillation of electrons in the conduction band of AuNPs in equilibrium with incident energy light wavelength. LSPR of AuNPs resulted strong absorbance in 500-600 nm, which known as visible region. The wavelength of peak absorbance increases with AuNPs amount and its distribution on rGO surface. The peak for AuNPs was observed at around 521 to 525 nm (Biradar & Asefa, 2012). From Figure 4.5, it is clearly observed that peak for 1.0 mM AuNPs/rGO were slightly more blue-shifted compared with other different molarity. The trend of AuNPs/rGO was followed as 1.0mM > 0.8mM > 0.6mM > 0.4mM >0.2mM. This can be suggested that the particles distribution or aggregation of 1.0mM AuNPs/rGO was the more abundance due to high concentration of AuNPs content. Meanwhile, there is less significant changes in absorbance intensity has been observed in the 0.2mM AuNPs/rGO. This is due to the amount of AuNPs content which consequently contribute to the less absorption peak observed. Figure 4.5 shows the characteristic absorption spectra related to the surface plasmon resonance (SPR) of different particle size AuNPs for the same single AuNPs concentration (Zuber et al., 2016).

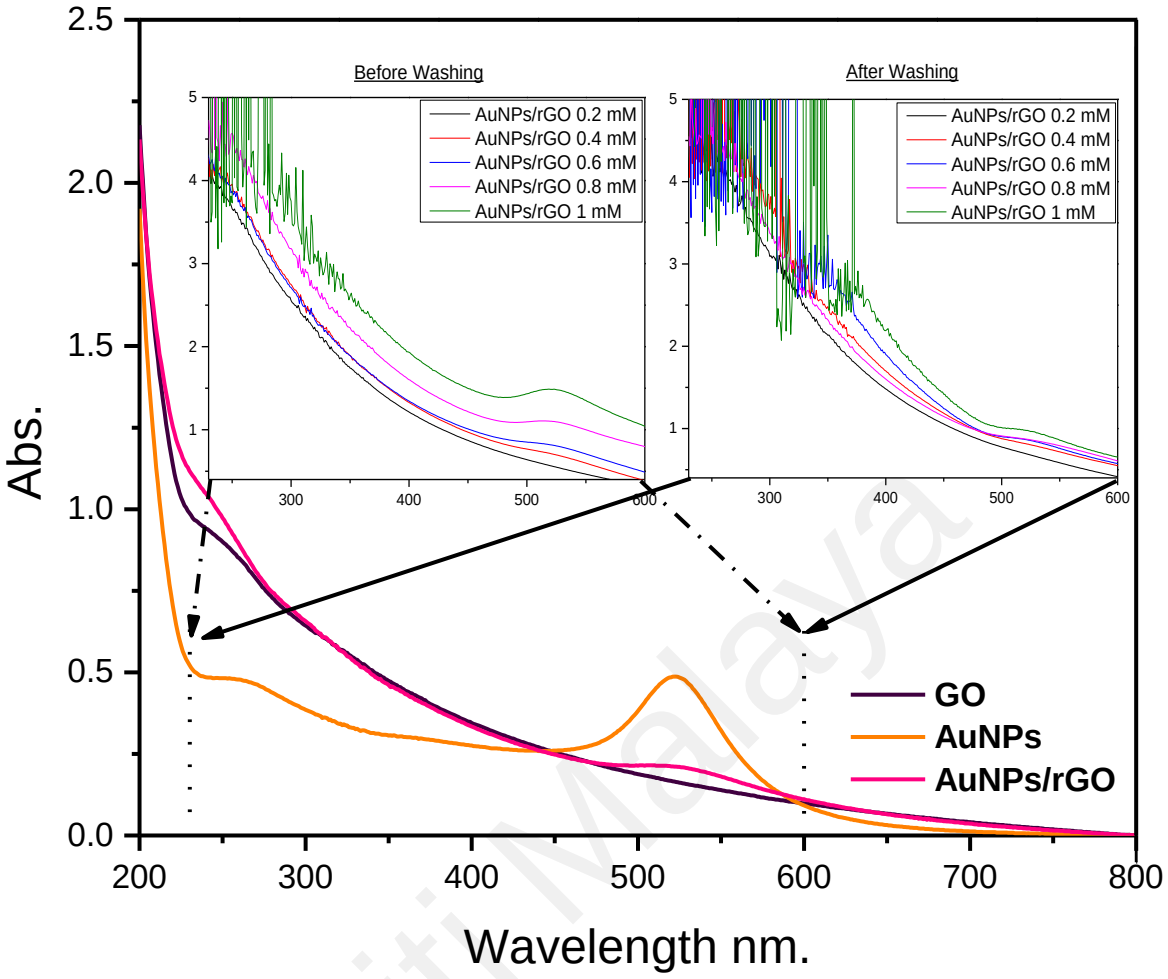

Figure 4.5: Absorption spectra of GO, AuNPs and AuNPs/rGO with different molarity of AuNPs/rGO (comparison between before and after washing).

4.1.5 Raman Spectroscopy Analysis of AuNPs/rGO

Raman spectroscopy results for all different molarity of AuNPs/rGO along with GO are as shown in Figure 4.6. The ratio of D band and G band (ID/IG) commonly used to measure the extent disorder of both samples (Guo et al., 2010). The Raman spectra of all the AuNPs/GO catalyst at different concentrations show strong G band at around 1650 cm^{-1} and a weak D band around 1350 cm^{-1} and D band overtone at around 2680 cm^{-1} (Zhang et al., 2011). The AuNPs/rGO also showed similar kind of peaks but the intensity ratio of ID to IG increased gradually as molarity increased. This increase in the ID/IG indicates the concentration of AuNPs on GO sheets. The intensity ratio of D and G band may affect by the number of defections within the G sheets and the plane crystallite size

(Lazar et al., 2020). The intensity of D band increased with higher AuNPs/GO composite as well as ID/IG ratio. According to Figure 4.6, the amount of AuNPs in the catalyst have strong influence to the ratio as nucleation of metal on the surface of rGO caused additional defect into the structure (Marinoiu et al., 2020). Intensity is proportionate to the degree of defection of D band and G band of rGO, thus increasing the ID/IG ratio. It is suggested that this is possibly caused by G defected in the catalyst. Therefore, 1.0 mM of AuNPs/rGO catalyst showed the highest intensity among the other sample because of higher Au content. Increased ID/IG ratio is expected as the reduction of GO into rGO. Based on the band originates from the carbon stretching vibrations and sp3 phase, which explains the relationship between the degree of reduction the ID/IG ratio from GO (Lee et al., 2021).

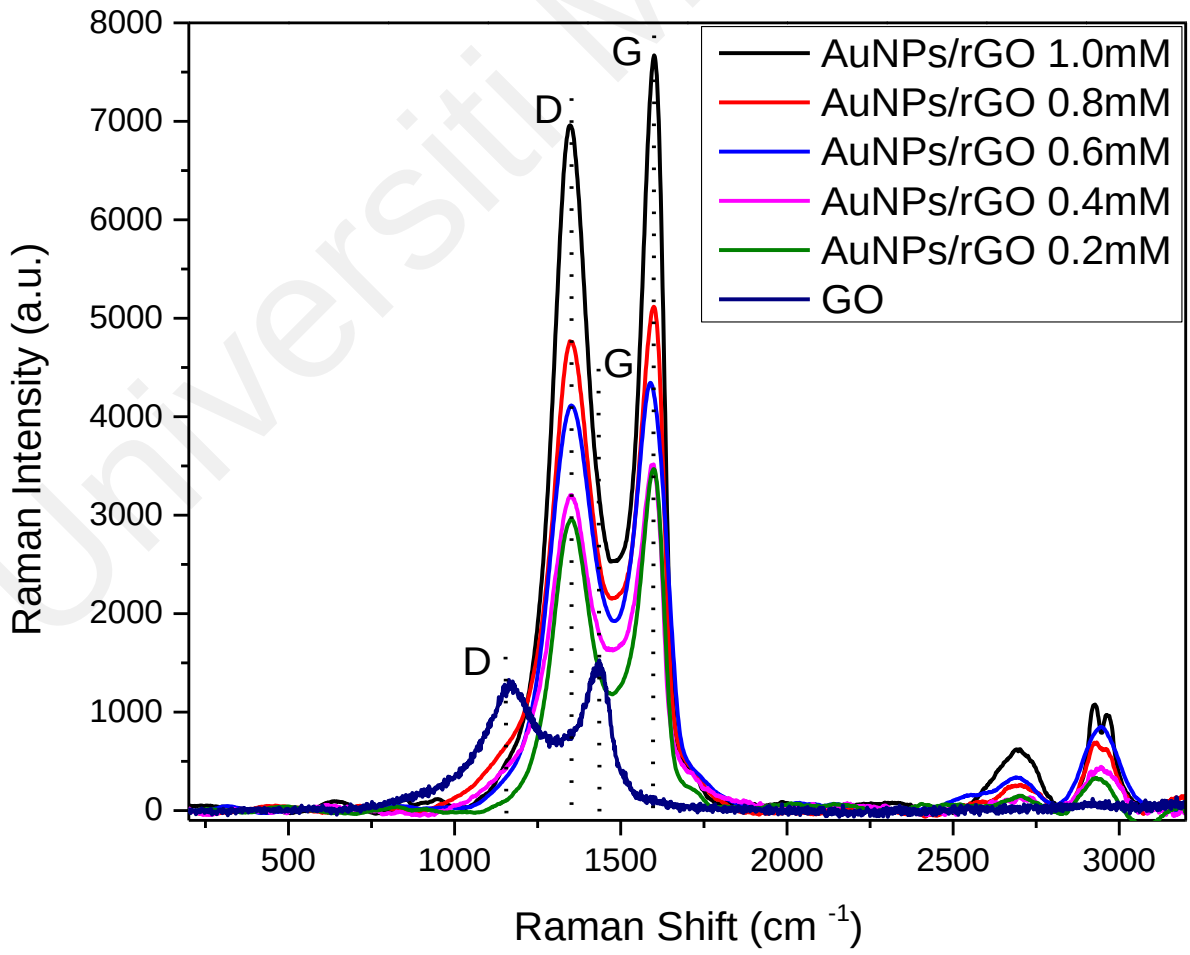

Figure 4.6: Raman spectra for GO and different molarity of AuNPs/rGO samples.

4.1.6 HR-TEM Analysis of AuNPs/rGO

0.4mM AuNPs/rGO catalyst was analyzed using HR-TEM. Figure 4.7 shows HR-TEM micrographs from 0.4 mM AuNPs/rGO catalyst. Upon increasing the resolution to the nano-regime of 100 nm the dark spots only become more visible. The results confirmed that 100 nm and 0.2μm resolution are not sufficient to confirm the presence of single atom AuNPs doped on rGO. As shown in Figure 4.7 (a), the nanostructures are surrounded by rGO to support AuNPs. In addition, it shows the AuNPs uniformly distributed over the surface of rGO. It was observed deep into 100 nm from Figure 4.7 (b) that the AuNPs were uniformly distributed over the surface of rGO support. In general, a homogenous dispersion and uniform particle features based on histogram plotted with the particle size ranged from 7 to 17 nm obtained.

The particle sizes of sample determined from the HR-TEM images are in good agreement with the crystallite size values determined based from XRD analysis. The estimated average particle size using statistical analysis of HR-TEM images was 11 nm. The interplanar distances for AuNPs was measured with the algorithm Fast Fourier transformation (FFT) in different areas of the HR-TEM micrographs. Based on Figure 4.7 (c), the interplanar distance of 0.215 nm for AuNPs corresponds to the crystal plane (111), which is in good agreement with XRD results. AuNPs have greatly increased surface-to-volume ratio of course due to their smaller in size. This strongly increases the specific catalytic activity from the reaction because the surface of the particle contributes into the chemical reactions. Therefore, the faster the reaction time is based on the availability from the larger surface area (Moore, 2019). Overall, the micrographs of this analysis show a good arrangement between rGO and AuNPs. Overall, the micrographs of this analysis show a good arrangement between rGO and Au. The grain boundary separating single AuNPs and rGO mostly through Au-O-C linkage can be seen in Figure 4.7(c) was further evaluated in XPS analysis.

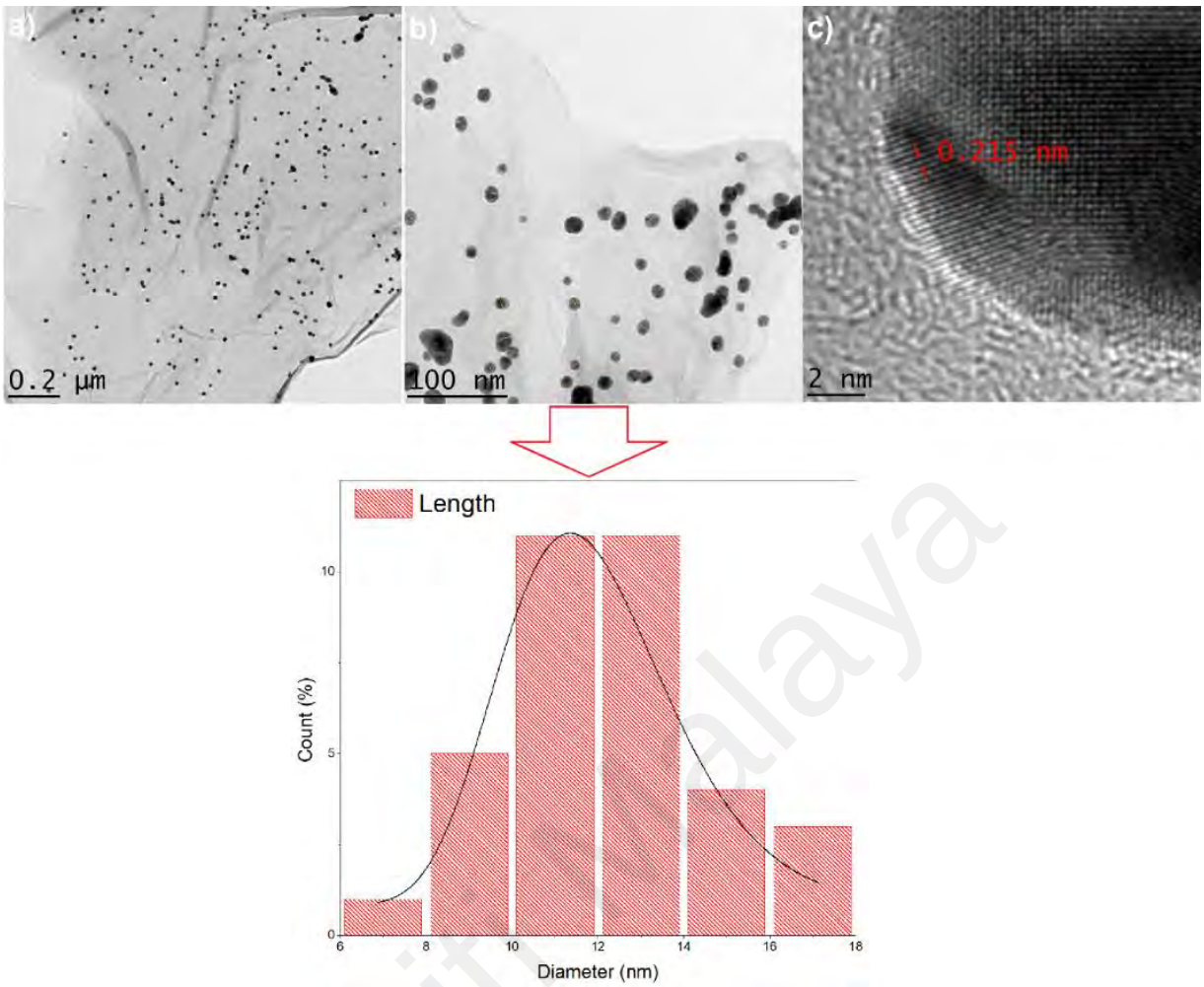

Figure 4.7: (a) HR-TEM micrograph of 0.4 mM AuNPs/rGO at 0.2 µm. (b) HR-TEM micrograph more deep at 100 nm that show the arrangement of AuNPs/rGO together with particle size measurements of AuNPs and (c) interplanar distance of 0.215 nm associated to lattice (111) of AuNPs.

4.1.7 XPS Surface Chemical State of AuNPs/rGO

The XPS technique becomes useful to further investigate the structural evolution of the synthesized 0.4 mM AuNP/rGO nanohybrid selected as optimized catalyst. Survey-scan XPS spectra obtained from optimized sample AuNPs/rGO is shown in Figure 4.8. Due to the deposition of a thin layer of the materials on the Si substrate and the takeoff angles used for XPS analysis, the signature of silicon (Si) signal arising from the Si-substrate underneath can be detected in the survey scans of both samples. It is evident from full scan XPS spectra in Figure 4.8 (a) that composed of C, O and Au. Deconvoluted O1s core lines in Figure 4.8 (b) exhibit distinct peaks of Au-O, C=O, C-O, -OH, and O-C=O bonds with binding energies of 531, 532, 533, 534, and 536 eV. These findings

confirmed oxygenates on the surface of rGO and that during the covalent functionalization at 531 eV binding energy, Au establishes a connection with one of these oxygenates (Hareesh et al., 2017; Kar et al., 2016). The Au 4f5 (87.66 eV) and Au 4f7 (83.99 eV) spin-orbit doublets were seen in Figure 4.8 (c) high-resolution Au4f spectra taken from an Au-rGO sample. The chemical makeup of Au in Au-rGO has been attributed to metallic Au in this study (Au^0). There is also Au^{3+}, a suitable linkage to allow the production of Au-O-C bonds that is also suggested as grain boundary in TEM analysis. This adds another chemical component to the deconvolution of Au4f7/2 spectra (Hareesh et al., 2017; Marinoiu et al., 2020). A substantial interaction between Au and the rGO framework is indicated by the observed modest negative shift (0.4 eV) in the location of the Au4f spin-orbit doublet relative to the usual reference positions of metallic-Au. It is possible to divide the high-resolution C1s spectra of rGO and Au-rGO into four Gaussian components. Peaks centred at binding energies of 284.63 eV (sp2 -C=C), 285.13 eV (sp^3; -C-C, C-H), 286.80 eV (epoxy and/or hydroxyl -C-O/C-OH), and 288.00 eV (carbonyl and/or carboxyl -C=O/O-C=O). Furthermore, in Figure 4.8 (d), the success of the peak fitting protocol used to separate the C1s profiles into their components is indicated by the excellent agreement between the experimentally measured C1s profile (represented by a solid black line) and the resultant fit profile (represented by green coloured hollow circles).

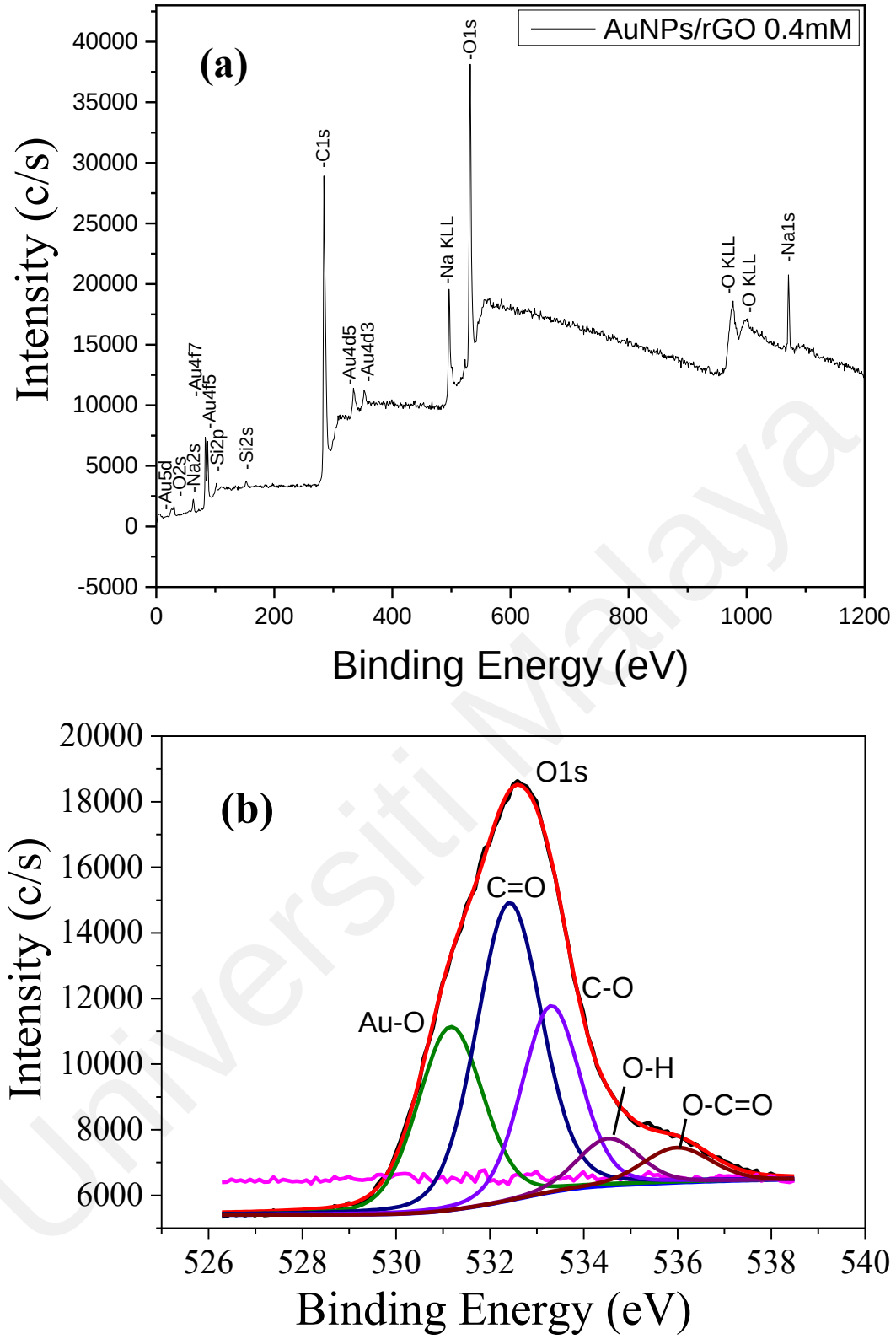

Figure 4.8: (a) Full XPS spectrum of AuNPs/rGO and high-resolution XPS spectra of (b) Core-level of O1s.

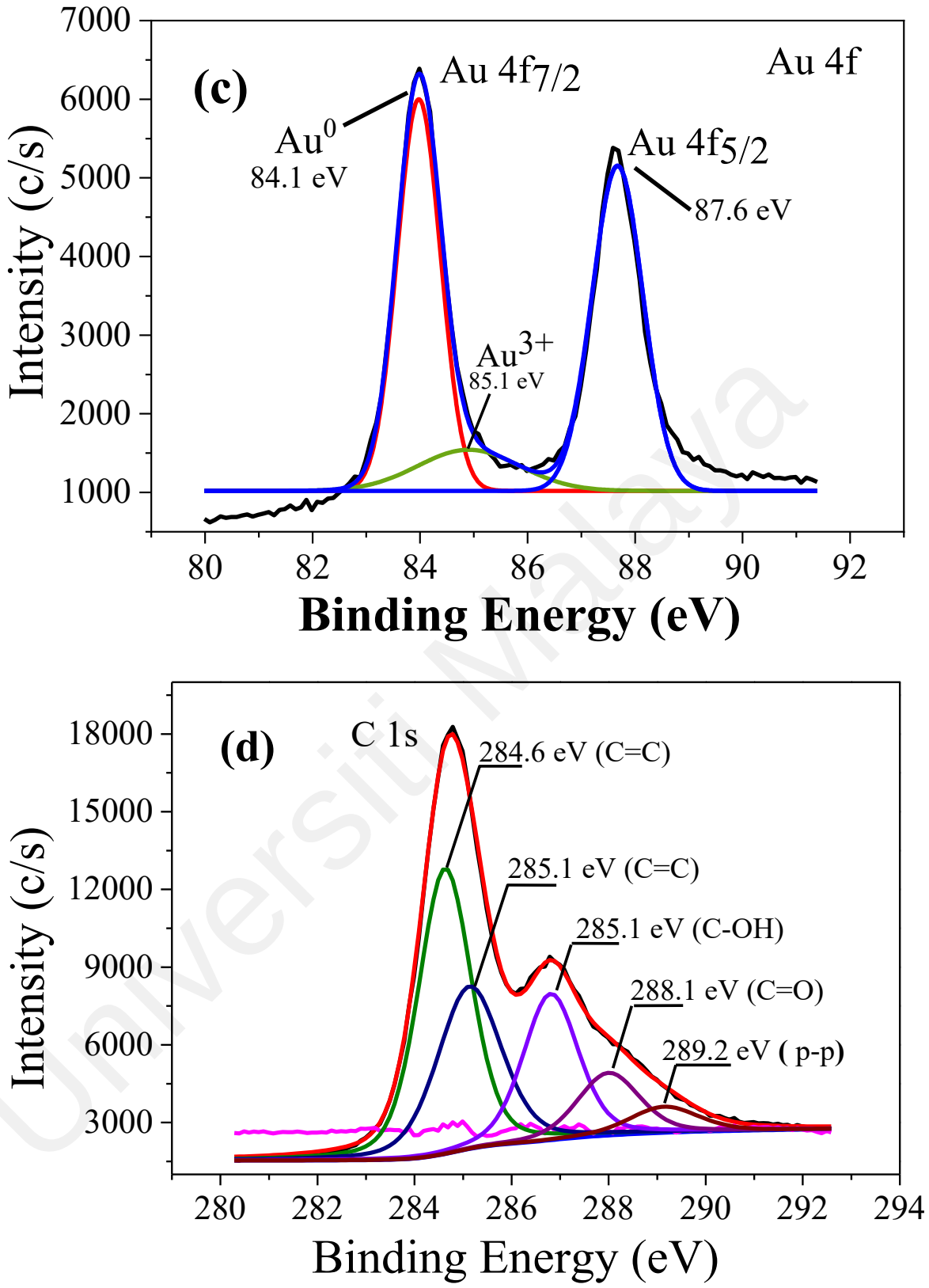

Figure 4.8 (cont.): (c) Au 4f core levels, and (d) C 1s core level. Deconvoluted spectra are in multiple colour lines while the experimental spectra are thick single-colour continuous lines.

4.1.8 FTIR Analysis of AuNPs/rGO

The functional groups on surface which brought to the formation of AuNPs on rGO surface was studied using FTIR analysis. FTIR spectra in the Figure 4.9 (in the range of 500–4000 cm^{-1}) shows the spectra of 0.4 mM AuNPs/rGO (optimized catalyst), GO synthesis by freeze dryer process and GRC that was used to synthesis the GO. The reduction of GO was depicted based on the several peaks of C–O vibrations (1060 cm^{-1}) and C–OH stretched or O–H deformation of alcohol groups observed between 1273 – 1390 cm^{-1}. While the peak of C=C stretches from unoxidized graphitic domain (1623 cm^{-1}), C=O (carboxyl group vibration – 1720 cm^{-1}) and C–H (aliphatic – 2805 cm^{-1}) are arrange accordingly. Lastly, the obvious broad peaks of –OH (hydroxyl) stretching bond vibrations or/and COOH functional group is observed at 3350 cm^{-1} (Emiru & Ayele, 2017). In the case of the functionalized GRC and AuNPs/rGO, the intensity of that sample peaks decreased dramatically or even disappeared after synthesis and reduction process, respectively. Conversely, the characteristic absorption peaks of –OH, –C=O in the AuNPs/rGO composite decrease dramatically, indicating the transformation from GO to rGO (Amanulla et al., 2017).

Figure 4.9 below shows the peaks corresponding to the O containing functionalities of AuNPs/rGO was decreased obviously as compared to the intensities of GO peaks and even some disappeared. This result suggested the reduction of GO by $Na_3C_6H_5O_7$ used and in agreement with the result shown in Raman spectroscopy analysis. However, some peaks at from 1060 to 1390 cm^{-1} are not disappeared which seems to indicate that GO was not completely reduced by in citrate as reducing agent thus indicating the presence of some GO functional groups (Emiru & Ayele, 2017).

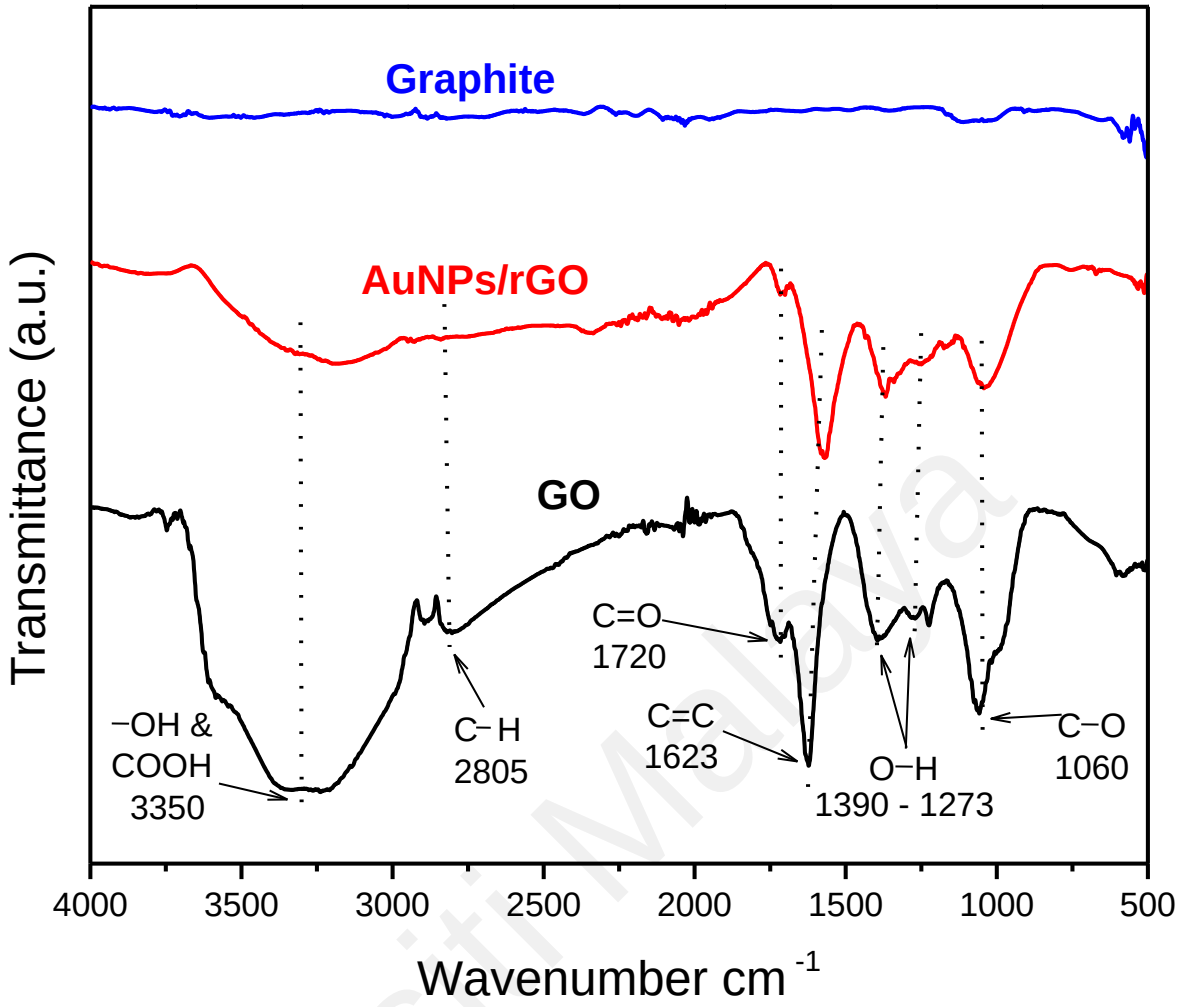

Figure 4.9: FTIR spectra of graphite, 1.0 mM of AuNPs/rGO and GO.

Based on Figure 4.10, FTIR analysis confirmed the presence of the citrate ligand on the surface of AuNPs/rGO catalyst for all catalysts. These results was also compared together with FTIR spectra of sodium citrate and Au/citrate from previous study done by Mohan et al. (2013). The peak intensity of 1.0 mM AuNPs/rGO shows the highest stretching vibration of C=O at 1580 cm^{-1} compared to catalyst series. This peak intensity is reduced with the reduction of Au composition in AuNPs/rGO. The group of the carboxyl and -OH from $Na_3C_6H_5O_7$ have formed strong H bonds with residual O functionalities on the rGO surfaces seen at 3350 cm^{-1}. Moreover, the surface-bound from $Na_3C_6H_5O_7$ can be found at the intensity of the O–H deformation vibration peak at 1380 cm^{-1} (Figure 4.10). The $Na_3C_6H_5O_7$ vibrations are relatively small for 0.2 and 0.4 mM AuNPs/rGO whereas the vibrations intensity is increased at 0.6 and 0.8 mM AuNPs/rGO.

The highest $Na_3C_6H_5O_7$ vibrations are observed for 1.0 mM AuNPs/rGO. This result shows the increase of citrate anionic ligand with the addition of Au composition in the catalyst. Together, these findings clearly confirm that the used of $Na_3C_6H_5O_7$ moieties role as capping reagent is strongly attached to the surface of rGO (Zhang et al., 2011). Tran et al. (2018) suggested that the citrate anionic ligand used as adsorbate can possibly inhibit the active site of AuNPs. Therefore, these catalysts would be tested in hydrosilylation reaction for a production of disiloxane to check the effect of citrate inhibition on catalyst surface. Lastly, the used of AuNPs/rGO to give better catalytic performance may be associated with the presence of the moderate graphitic character and specific surface O-containing functional groups (Yu et al., 2013).

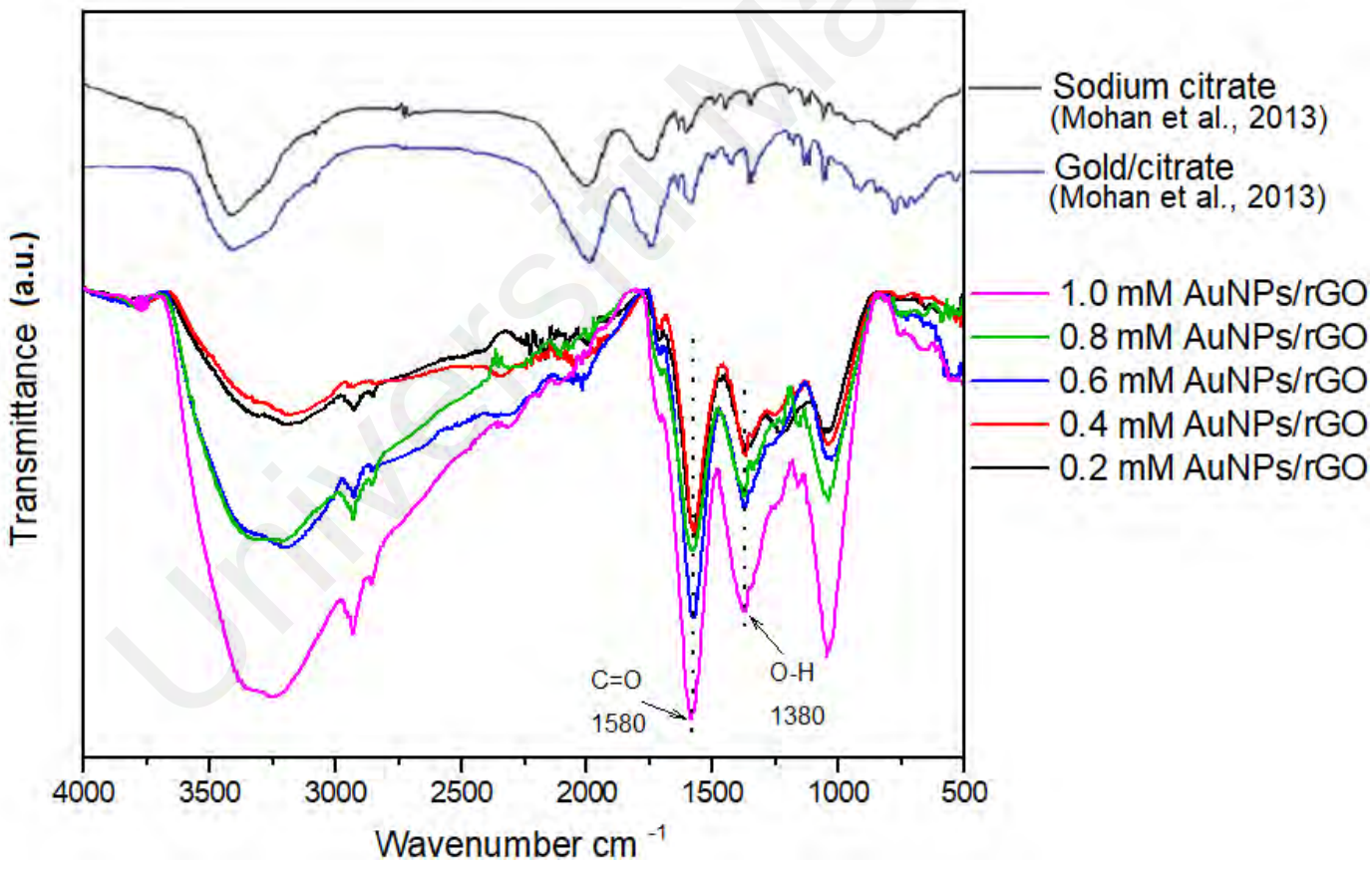

Figure 4.10: FTIR spectra of different molarity of AuNPs/rGO comparison together with spectra of sodium citrate and Au/citrate from *Mohan et al. (2013)*.

4.2 Catalytic activity of disiloxane using AuNP/rGO

In the initial experiments of the reaction, 0.4 mM AuNPs/rGO catalyst was tested in dehydrogenative coupling of hydrosilane for solvent and solventless reaction to produce disiloxane . Figure 4.11 shows the comparison of hydrosilylation reaction by benzaldehyde solvent and solventless at 120 °C within three hours using 5 mg catalyst.

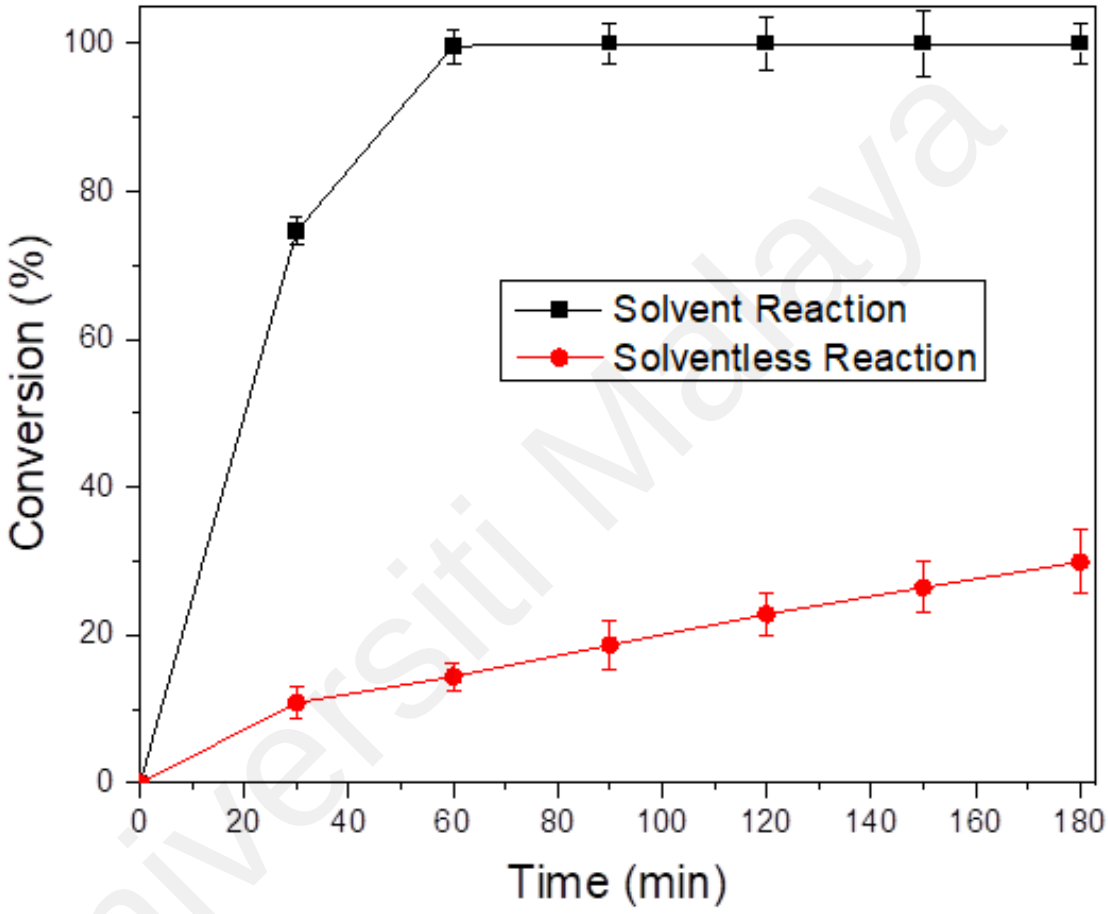

Figure 4.11: The dehydrogenative coupling of DMPS with benzaldehyde into 1,3-diphenyltetramethyldisiloxane catalysed by AuNPs/rGO for a comparison between solvent and solventless reaction.

Even though the solvent reaction showed faster reaction, the side products are observed from GCMS analysis which are consisting of benzyl alcohol, phenol 4-ethyl-2-methoxy, benzyl benzoate and 1,1,3,3,5,5-hexamethyl-1,5-diphenyl-trisiloxane as shown in Figure 4.12. After one hour of reaction, the reaction showed 83.86% selectivity.

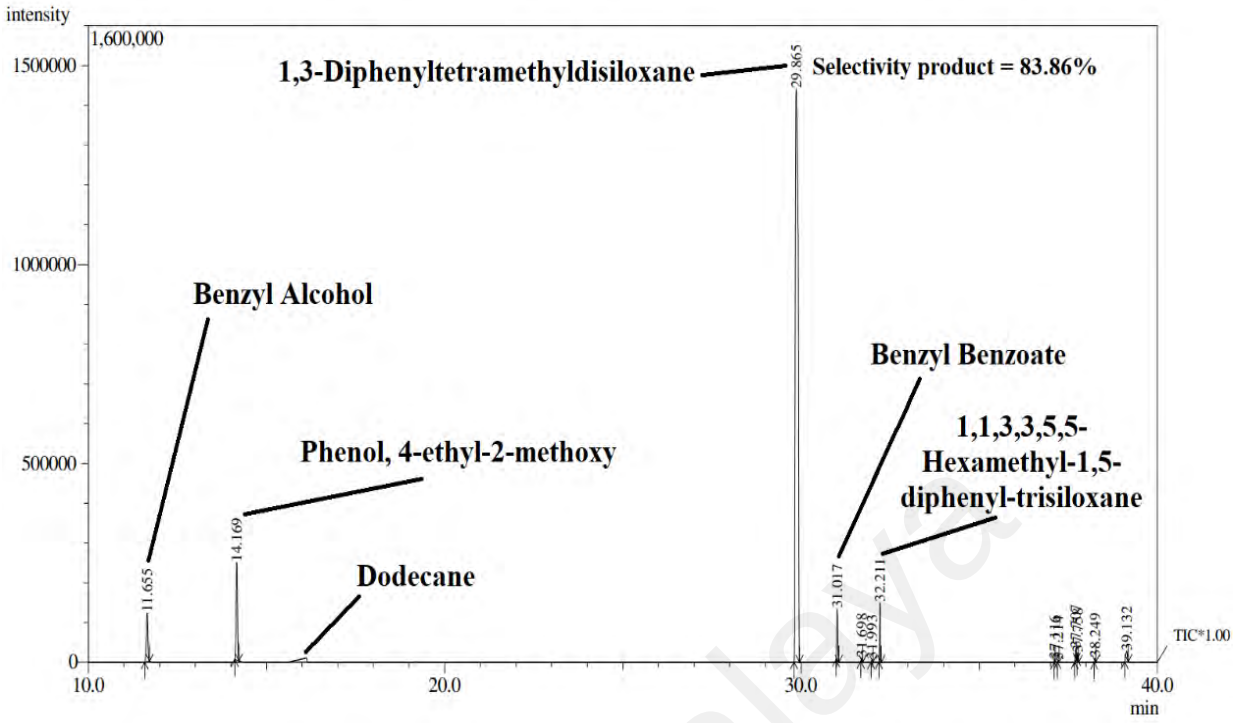

Figure 4.12: GC-MS analysis of catalysed AuNPs/rGO under solvent reaction at temperature of 120 °C for 3 hours.

Whereas the solventless reaction has demonstrated low conversion showed 100% selectivity of disiloxane in Figure 4.13. GCMS analysis in Figure 4.13 was analysed in solventless reaction after 12 hours reaction with 70% conversion was achieved. The sole product from solventless reaction was then confirmed with GCMS, ^{1}H NMR and ^{13}C NMR analyses. It was noticeable to mention that this reaction was a slow reaction due to diffusion limitation of substrate during reaction.

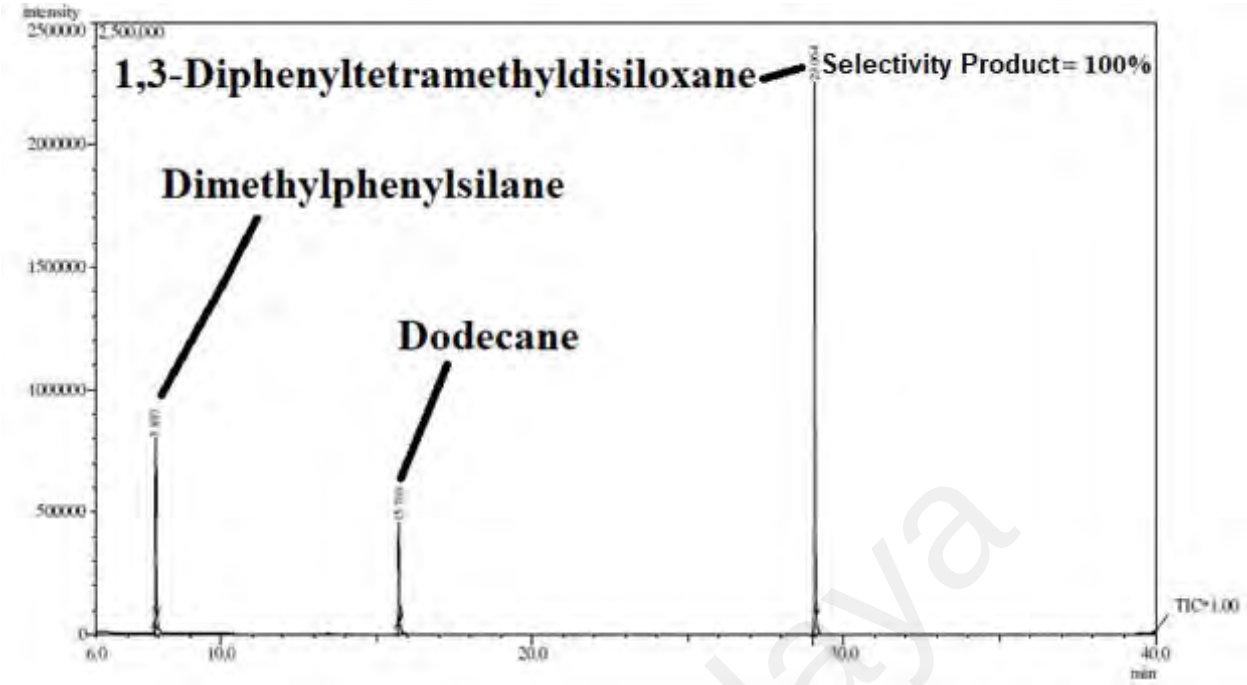

Figure 4.13: GC-MS analysis of catalysed AuNPs/rGO under solventless reaction at temperature of 120 °C for 12 hours.

Rheology is the study of the flow and deformation of materials. Usually, the characterization is useful to observe the interactions between the different components within a material. In this analysis, the study has been focused only on 1 material of DMPS used as the reactant substrate for the reaction. The results indicated that the viscosities were dependent on the shear rate behaving like of non-Newtonian fluids, suggesting the shear-thinning properties of the DMPS in Figure 4.14 (a) shows the viscosity versus the shear rate has viscosity around 0.55 Pa·s. Besides that, the relationship between shear stress and shear rate of the DMPS also is shown in Figure 4.14 (b). This indicates that the substrate of DMPS use is almost to pseudoplastics or shear thinning fluids by dilatant materials that display the opposite properties. This show as more stress is applied to pseudoplastics the viscosity decreases. DMPS has a high viscosity which is around 0.55 Pa·s while DMPS in benzaldehye during reaction has a low viscosity of 0.0036 Pa·s. Therefore, high viscosity in solventless caused diffusion limitation in the reaction thus reducing the catalytic acitivity. This postulate would be further evaluated in the apparent activation energy study.

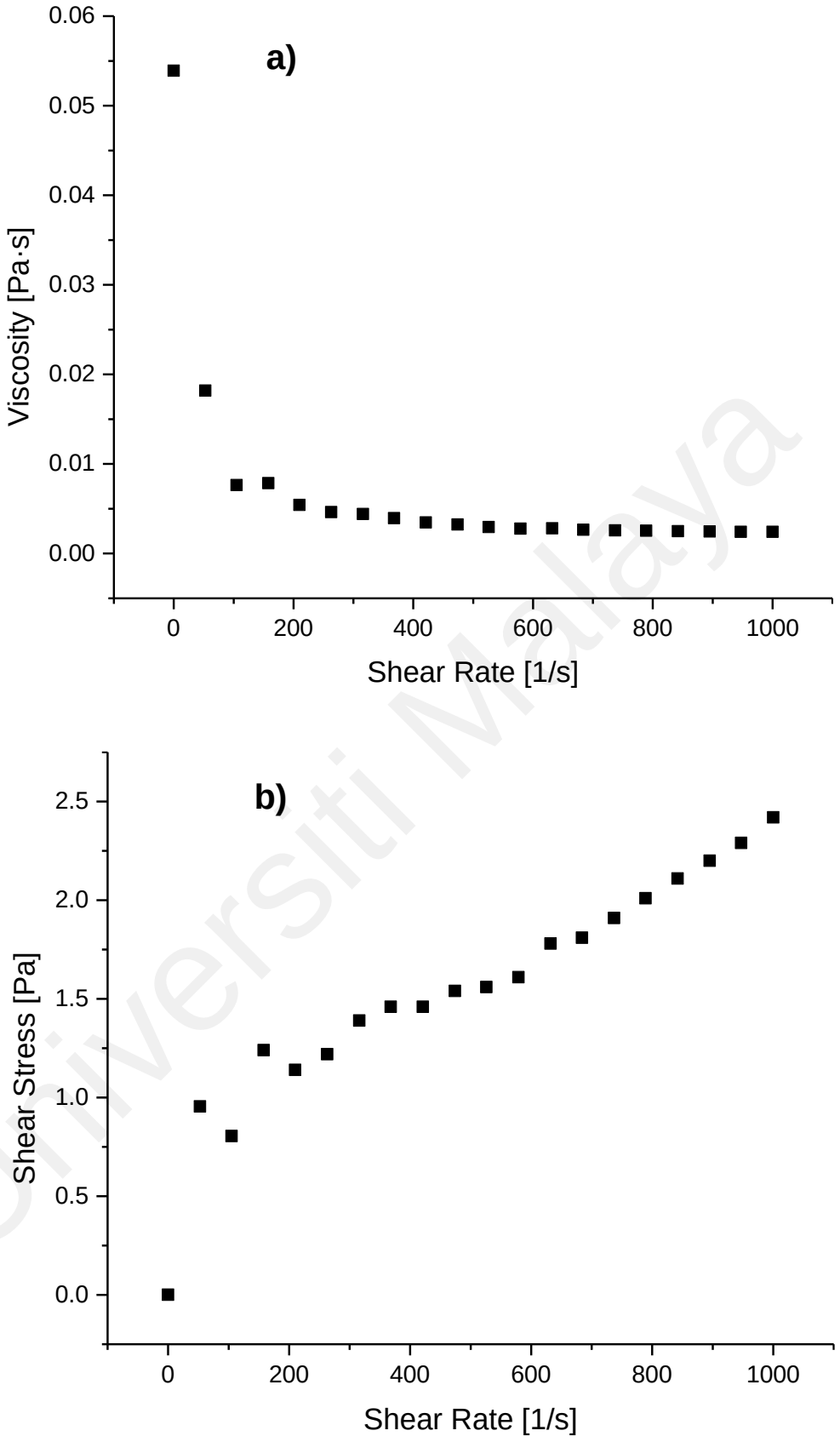

Figure 4.14: Viscosity versus shear rate (a) and relathionship ploting between shear stress and shear rate (b) for dimethyphenylsilane.

Nevertheless, it is of interest to study hydrosilylation reaction in solventless condition. Furthermore, the solventless reaction has many advantages including low costs, simplicity in process to handle (especially important in industry), high selectivity and of course it can reduce pollution (Tanaka & Toda, 2000). Based on our knowledge, there is no study that has been reported for solventless hydrosilylation reaction catalyzed using AuNPs that attach with rGO based materials. Even though the solventless reaction shows lower catalytic activity compared to solvent reaction, this study would be a major advantage for chemical industry in producing disiloxane as the cost for the solvent is not applicable and the separation between product and solvent is eliminated. In addition, solventless is most preferable when the reactions that proceed moderately in the absence of solvent or in a water suspension (Loupy, 1999; Tanaka & Toda, 2000). Therefore, it can minimize the overall production cost of disiloxane.

Specifically, the compound of 1,3-diphenyltetramethyldisiloxane (Figure 4.15) is the final product was yielded through synthesis disiloxane by dehydrogenative coupling of DMPS catalysed using AuNPs/rGO under solventless condition. The synthesis was involved two reaction pathways possible to produce disiloxane which is classify as organosiloxane product. The spectroscopic feature of final product in ^{1}H NMR can be differentiated from the appearance of peak region either upfield or downfield region. In compound 1,3-diphenyltetramethyldisiloxane, the presence of symmetrical benzene ring was indicated by the abundance of multiplet peaks at the region of 7.0 to 8.0 ppm as shown in Figure 4.16. The formation of high intensity singlet peak at 0.35 pm was attributed to four methyl groups contained in 1,3-diphenyltetramethyldisiloxane (Stein et al., 1994). Moreover, ^{13}C NMR of 1,3-diphenyltetramethyldisiloxane in Figure 4.17 confirmed the proposed structure due to the most deshielded C of benzene ring appeared at region 120 to 140 ppm. The C peak at 1.70 ppm indicated the presence of four terminal

methyl groups in the structure. The spectral data showed good agreement with published data by (Sawama et al., 2016) and Fleming et al. (1998).

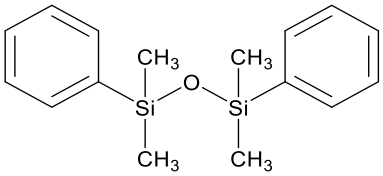

Figure 4.15: The structure of 1,3-diphenyltetramethyldisiloxane.

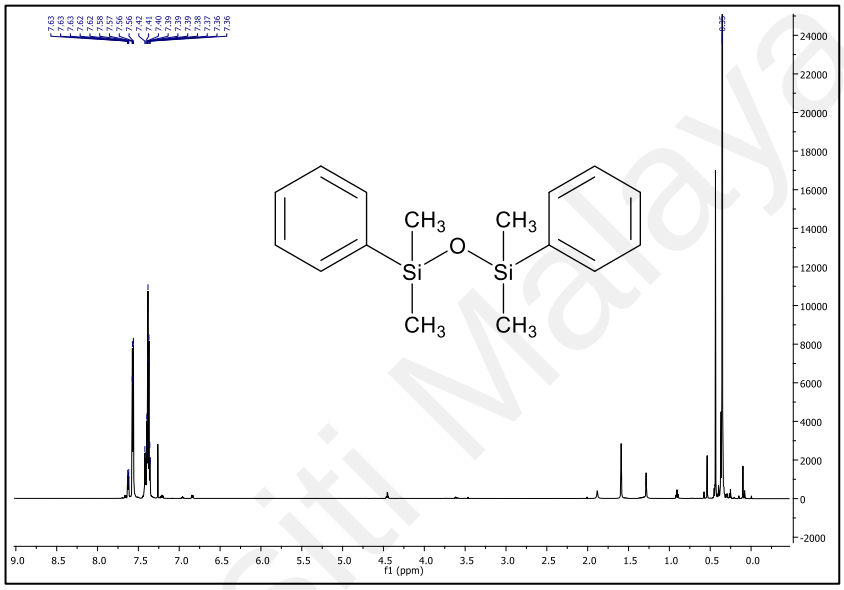

Figure 4.16: The ^{1}H NMR spectrum of 1,3-diphenyltetramethyldisiloxane.

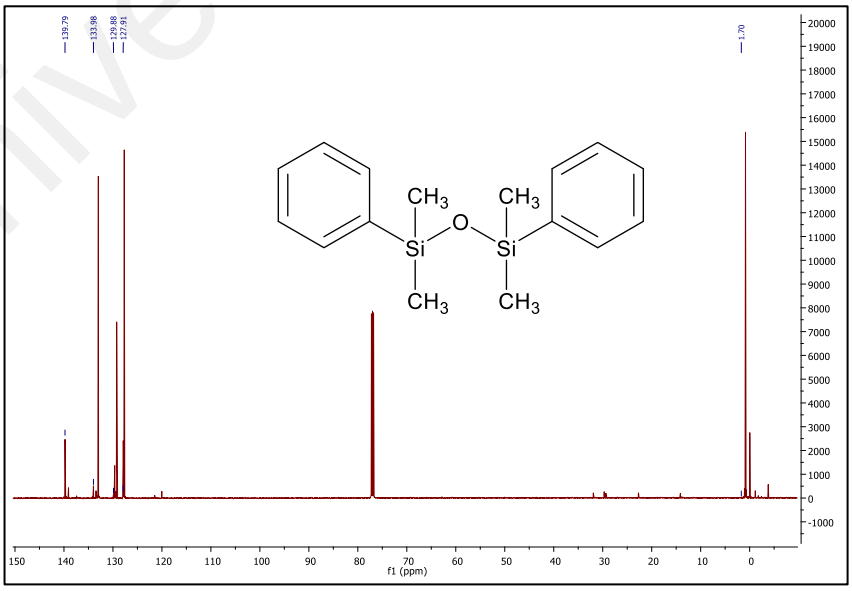

Figure 4.17: The ^{13}C NMR spectrum of 1,3-diphenyltetramethyldisiloxane.

Figure 4.18 shows the dehydrogenative coupling of DMPS into 1,3-diphenyltetramethyldisiloxane catalyzed by AuNPs/rGO using different concentration of Au in AuNPs catalyst series. The right-side Y-axis is the conversion in percentage whereas the left Y-axis is the concentration of reactant in mmol/L. The conversion is kept increased by using 0.2 mM to 0.4 mM of AuNPs/rGO. It was determined that the most optimized catalyst used is 0.4 mM AuNPs/rGO that produces 30% conversion with 4.47 mmol concentration of substrate remaining after 3 hours reaction.

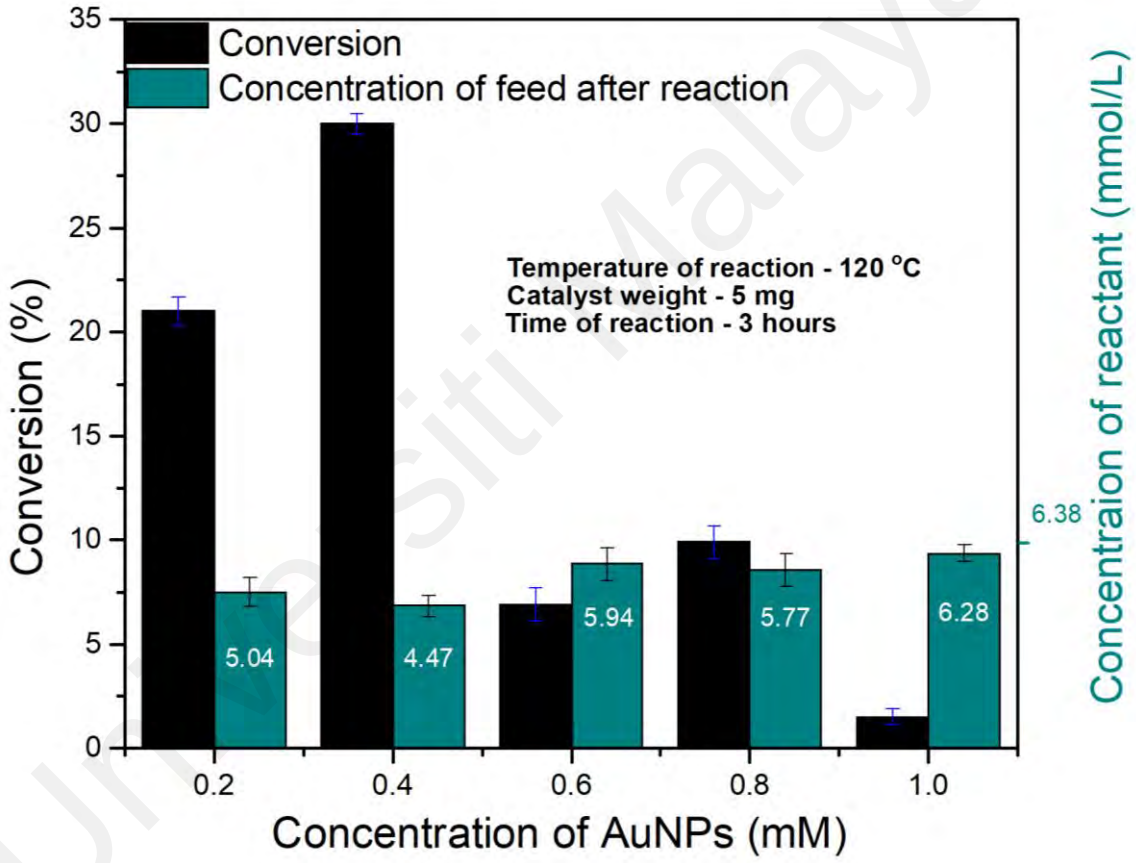

Figure 4.18: The dehydrogenative coupling of DMPS into 1,3-diphenyltetramethyldisiloxane catalysed by AuNPs/rGO with different concentration of Au.

The reaction shows 0.6 dan 0.8 mM of AuNPs/rGO at 10% and 8% conversion, respectively whereas catalyst with 1.0 mM Au demonstrates the lowest catalytic activity at 2% conversion. The hydrosilylation conversion is low due to citrate precursor deposition at high Au concentration of catalyst thus leading to catalyst deactivation. This

finding is in agreement with Tran et al. (2018) as the presence of the citrate precursor inhibited AuNPs active sites. Based on FTIR analysis in Figure 4.10, the concentration at 0.2 dan 0.4 mM of Au in AuNPs/rGO shows small citrate vibration thus the citrate percussor did not inhibit AuNPs active sites. Whereas the citrate vibration was significantly higher based on the concentration of Au from 0.6 to 1.0 mM, thus the citrate precursor was blocking the AuNPs active sites especially for 1.0 mM AuNPs/rGO catalyst. Although Au was in nanoparticle size as calculated in Scherrer equation in Table 4.1 from XRD analysis especially for 0.6, 0.8 and 1.0 mM of Au, the high amount of citrate that attach to Au as adsorbate prove it have less active component was involved during reaction especially for Au concentration more than 0.4 mM. Furthermore, it was difficult for the reactant to adsorb on the catalyst surface because citrate precursor blocked the access thus rendering AuNPs as inactive. Thus, the concentration of Au in AuNPs/rGO catalyst and citrate precursor are critical for the optimization of solventless reaction in this catalyst series.

The reaction effect of catalyst loading in the conversion of disiloxane was also done using different dosage by differentiate lower amount (1 mg and 3 mg) and higher amount (7 mg and 10 mg) based on 5 mg standard amount used from previous study. By referring Figure 4.19, the conversion increased with the higher amount of catalyst loading with maximum conversion around 30%. This is due to increase availability and concentration of active sites when higher loading amount is used in the reaction (Ketabchi et al., 2020). In Figure 4.19, the linear increase is shown until a catalyst mass of 5 mg. The addition of catalyst weight beyond 5 mg resulted in a region of external mass transfer diffusion limitation as the conversion for catalyst mass of 7 mg and 10 mg are almost constant. Therefore, 5 mg catalyst would be used in every reaction.

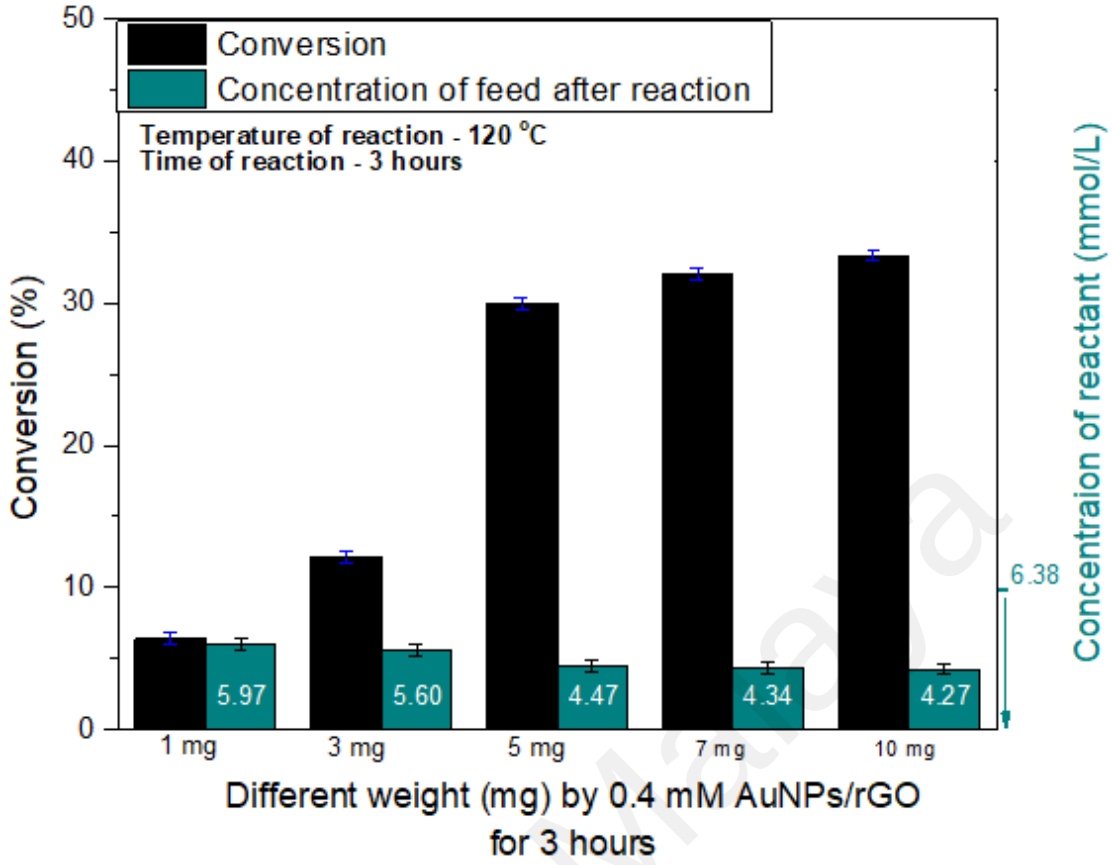

Figure 4.19: Optimize by different dosage with dehydrogenative coupling of DMPS into 1,3-diphenyltetramethyldisiloxane using 0.4mM AuNPs/rGO optimized catalyst.

It was demonstrated that 0.4 mM Au in AuNPs/rGO was the best catalyst from the catalyst series. Therefore, it was of interest to vary reaction variables such as temperature and catalyst weight using the promising catalyst in solventless reaction. Figure 4.20 shows the catalytic activity of 0.4 mM Au in AuNPs/rGO with the right Y-axis depicted as conversion (%) whereas the left Y-axis depicted concentration (mmol) of feed by the reactant after completing the reaction for 3 hours. To investigate the effect of temperature in formation of disiloxane, the reaction was executed with a series of temperature range from 100 °C to 140 °C using same amount of 5 mg catalyst loading, while 140 °C is sufficient to run the reaction and directly to promote lower temperature based on green chemistry approach. From Figure 4.20, the conversion percentage increased from 26% to almost 30% within the temperature range. Based on the conversion it can be concluded that the conversion rate is directly proportional to the reaction temperature. According to

Arrhenius equation, rate constant is directly proportional to the reaction temperature and the reaction order of this reaction is zero order reaction thus the rate of the reaction is only dependent on the rate constant. The same outcome of catalysis reaction has also been reported by Zhang et al. (2020).

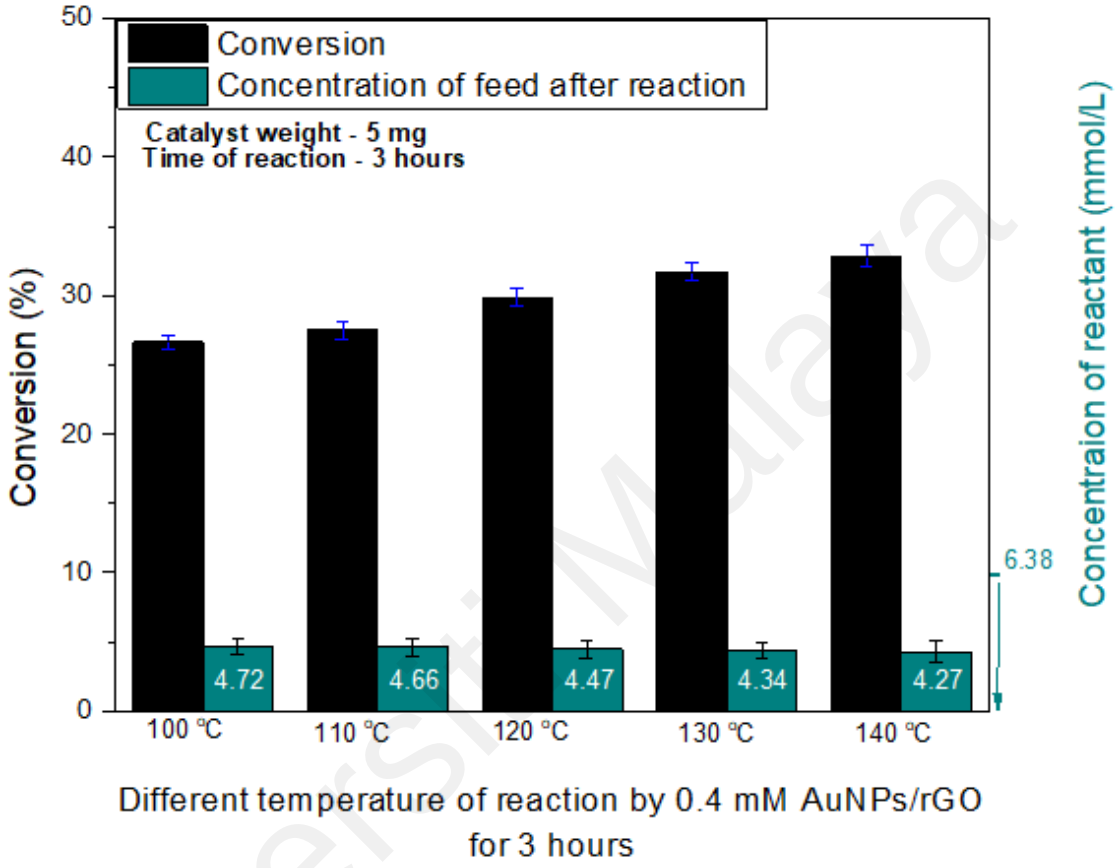

Figure 4.20: Optimize by different temperature with dehydrogenative coupling of DMPS into 1,3-diphenyltetramethyldisiloxane using 0.4mM AuNPs/rGO optimized catalyst.

It was demonstrated that 0.4 mM Au in AuNPs/rGO was the best catalyst from the catalyst series. Therefore, it was of interest to run the reaction with comparison of that catalyst by using two different reducing agent C and B. To determine the catalytic activity of AuNPs/rGO in a long reaction run, 12 hours reaction was conducted using both AuNPs/rGO(B) and AuNPs/rGO(C). To determine the highest catalytic conversion, the reaction was performed for 12 hours reaction (Deraedt et al., 2014; Haider et al., 2016; Luty-Błocho et al., 2011). In this study, for every 2 hours the samples was collected for GC-FID analysis to monitor the catalytic activity and determine the reaction order of

disiloxane reaction. Figure 4.22 shows the catalytic activity from 0 hour to 12 hours for both AuNPs/rGO(B) and AuNPs/rGO(C).

4.2.1 Activation Energy

Figure 4.21 shows the Arrhenius plot from the results of dehydrogenative coupling of DMPS into 1,3-diphenyltetramethyldisiloxane without solvent using 0.4mM, 5 mg of AuNPs/rGO catalyst in ambient pressure and the temperature was varied from 100 °C to 140 °C. From Figure 4.20 above, the result shows the conversion was found to increase with the increasing temperature.

The activation energy shown below is measured to be apparent activation energy since this method is used to represent the energy related with (i) adsorption/desorption of substrates to and from the surface of the catalyst; and (ii) the accumulation of the surface reaction. The reaction is frequently measured free from mass transfer resistance when the activation energy is higher than 25 kJ/mol (Rothenberg, 2017). The apparent activation energy from 10 to 25 kJ/mol is usually meant as mass transfer constraints in the reaction. However, the Figure 4.21 showed the apparent activation energy of 4.3 $kJmol^{-1}$ in the Arrhenius plot.

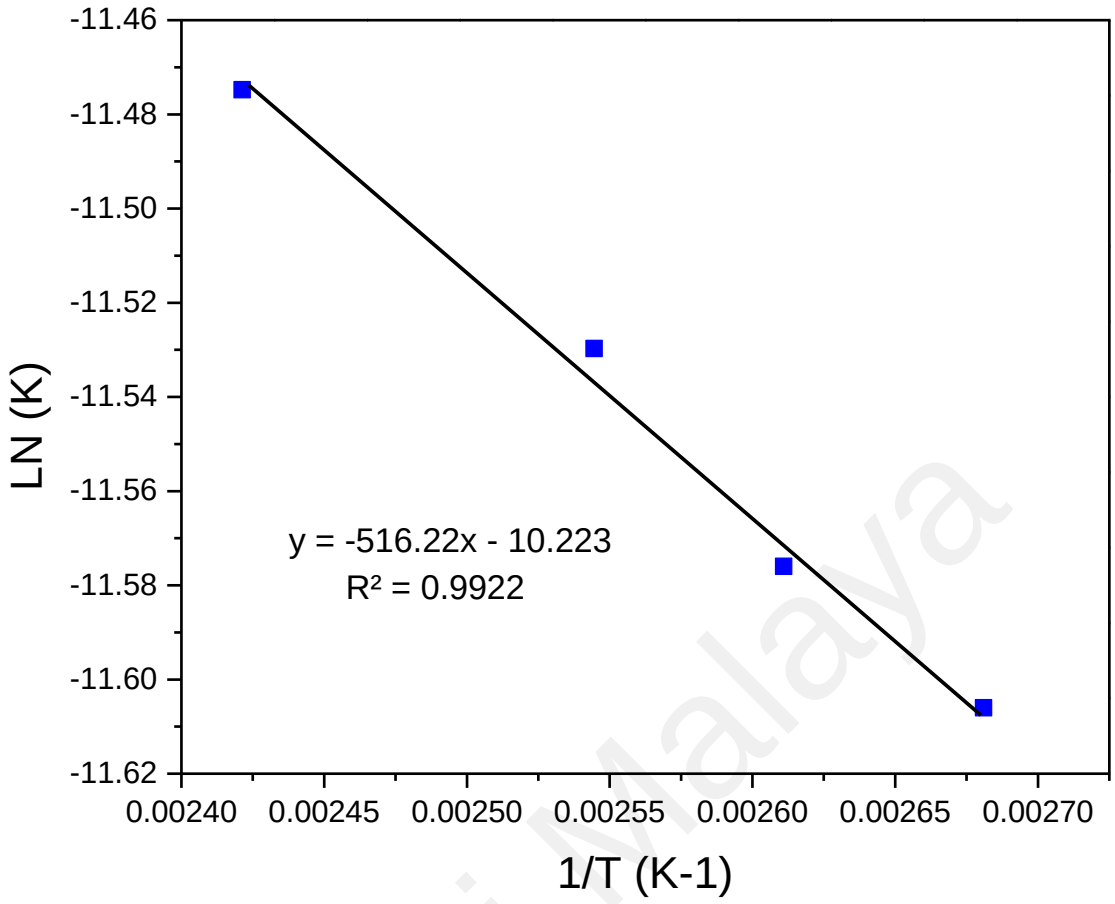

Figure 4.21: An Arrhenius plot for dehydrogenative coupling of DMPS into 1,3-diphenyltetramethyldisiloxane using 0.4mM and 5 mg of AuNPs/rGO catalyst.

Since the apparent activation energy was less than 10 kJ/mol, the reaction without solvent is diffusion-controlled as the reaction is limited by the diffusion of DMPS as the liquid viscosity in the solventless substrate is higher than the solvent substrate. It was also postulated that the diffusion and adsorption of DMPS to the pores and active sites onto the catalyst surface of AuNPs/rGO catalyst was limited due to the diffusion-controlled process during the reaction.

4.2.2 Comparison of Catalysts AuNPs/rGO

The comparison of catalytic activity of both catalysts was shown in Figure 4.22. It is clear that the AuNPs/rGO(B) which was reduced using $NaBH_4$ perform better than the AuNPs/rGO(C) which was reduced using citrate, $Na_3C_6H_5O_7$. The conversion of both AuNPs/rGO(B) and AuNPs/rGO(C) was almost similar in the 4 hours. However, after 12

hours showed AuNPs/rGO(B) and AuNPs/rGO(C) conversion at 85% and 70%, respectively (Deraedt et al., 2014; Haider et al., 2016; Luty-Błocho et al., 2011). It was suggested by Deraedt et al. (2014) that AuNPs synthesis from $NaBH_4$ is stable and not easily degraded. This type of catalyst is also catalytically active because Cl^- and BH_4^- formed strong bonds surrounding the AuNPs core with Na^+ cations covering at the rear. It was also noted that $NaBH_4$ is generally a stronger reduction agent compared to citrate.

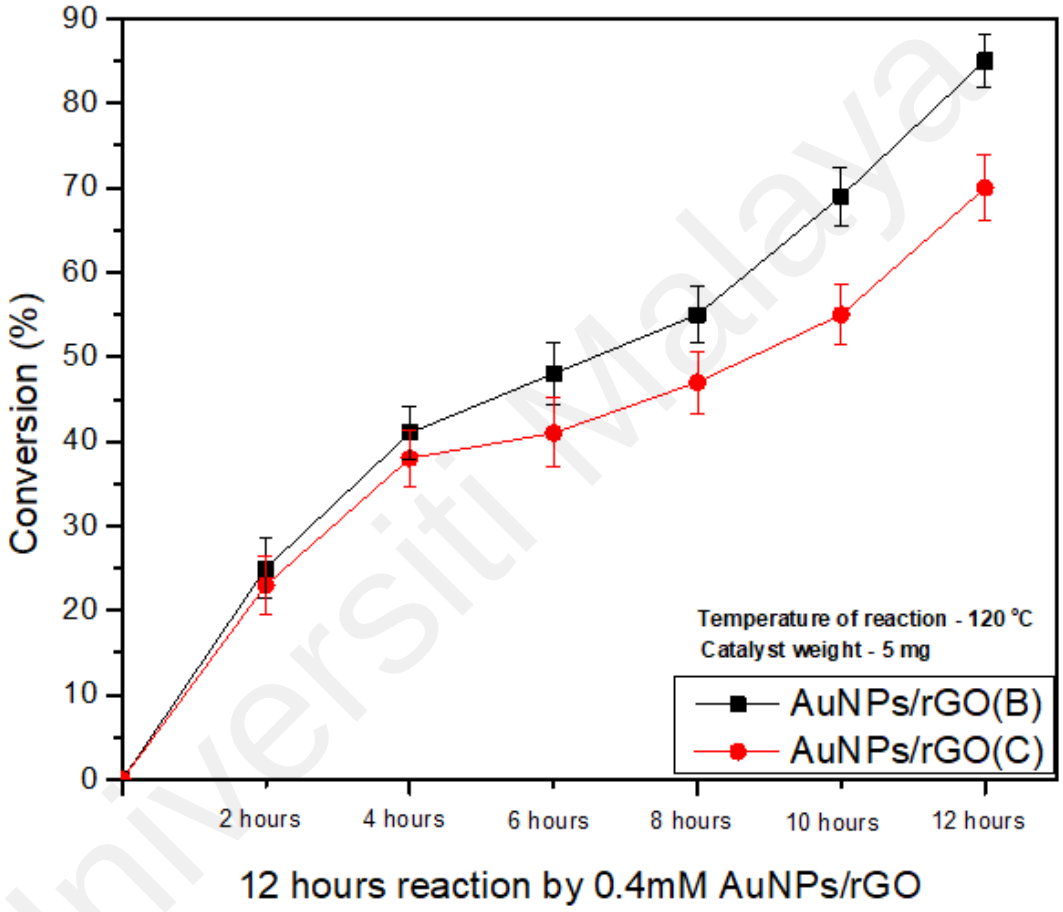

Figure 4.22: Comparative study for conversion of DMPS into 1,3-diphenyltetramethydisiloxane of AuNPs/rGO(B) (black) and AuNPs/rGO(C) (red).

The significant peak based on GC-FID for 1,3-diphenyltetramethyldisiloxane in Figure 4.23 is observed for both reactions after 12 hours. There are some noise peaks in the chromatogram which are possibly due to the contamination of the column or the carrier gas.

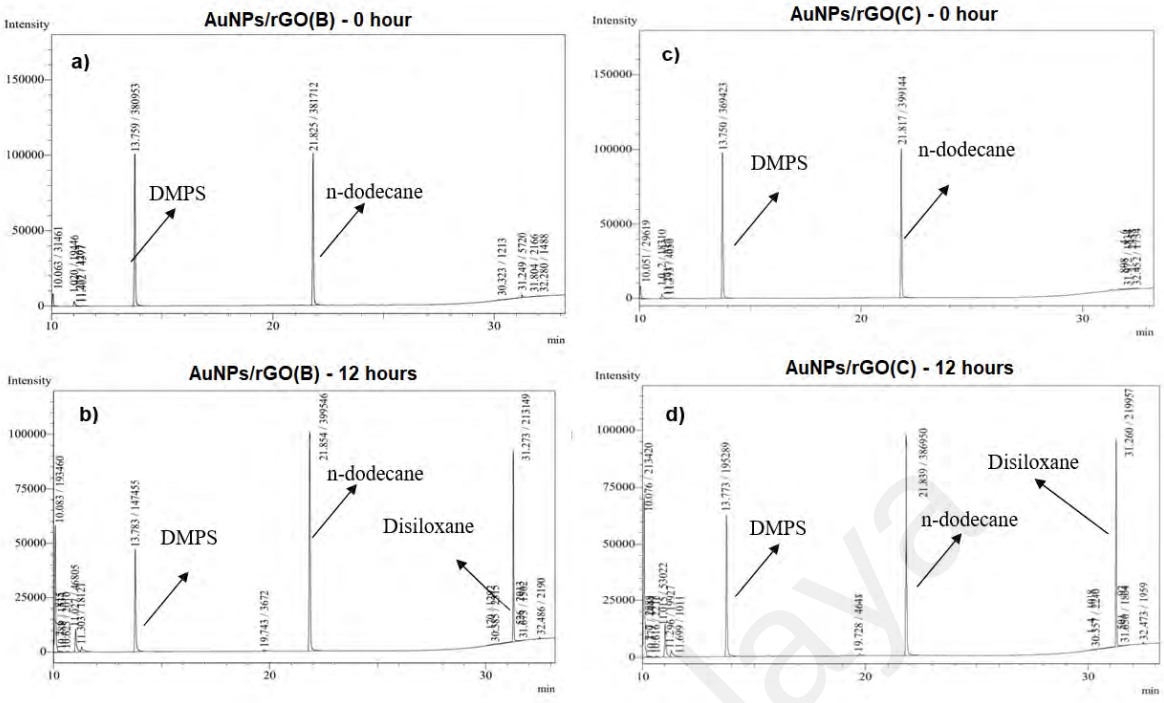

Figure 4.23: GC-FID chromatogram initial and final sample using AuNPs/rGO(B) for (a) 0 hour and (b) 12 hours and AuNPs/rGO(C) for (c) 0 hour and (d) 12 hours.

Then, to determine the selectivity of both catalysts, the sample after a 12 hours reaction was analyzed using GC-MS. By using GC-MS, the product of our reaction can be confirmed qualitatively. Software in GC-MS shows the best match of the chromatogram pattern based on the GCMS library. Figures 4.24 and 4.25 show the GCMS chromatogram of both samples taken from reaction catalysed by AuNPs/rGO(B) and AuNPs/rGO(C), respectively. From the results, it is confirmed that both samples only contain DMPS which is the substrate, n-dodecane the internal standard and 1,3-diphenyltetramethyldisiloxane which is the interest product from the reaction. Hence, it can be confirmed that the selectivity of both catalysts is 100% 1,3-diphenyltetramethyldisiloxane selectivity only.

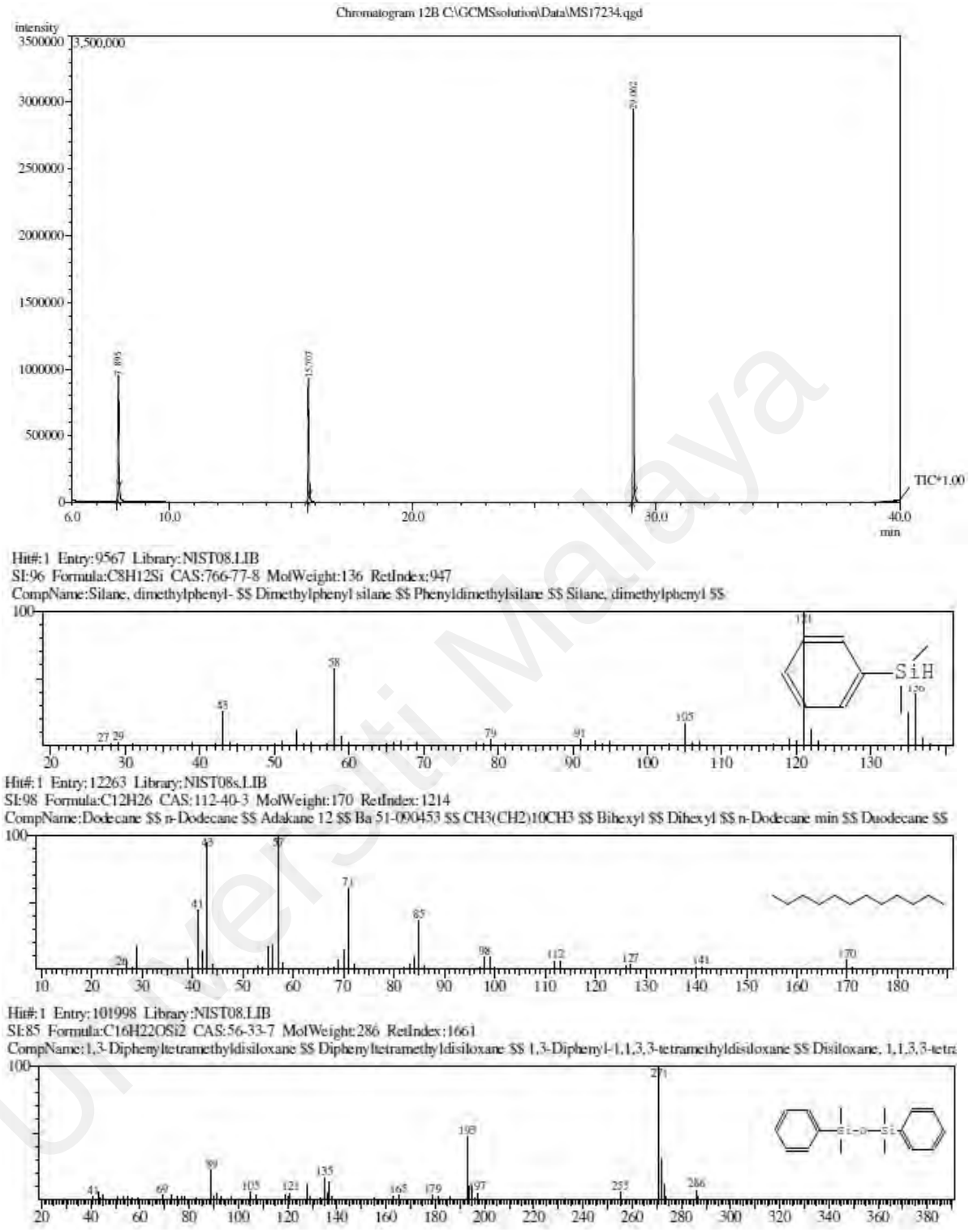

Figure 4.24: The GC-MS chromatogram of sample using AuNPs/rGO(B).

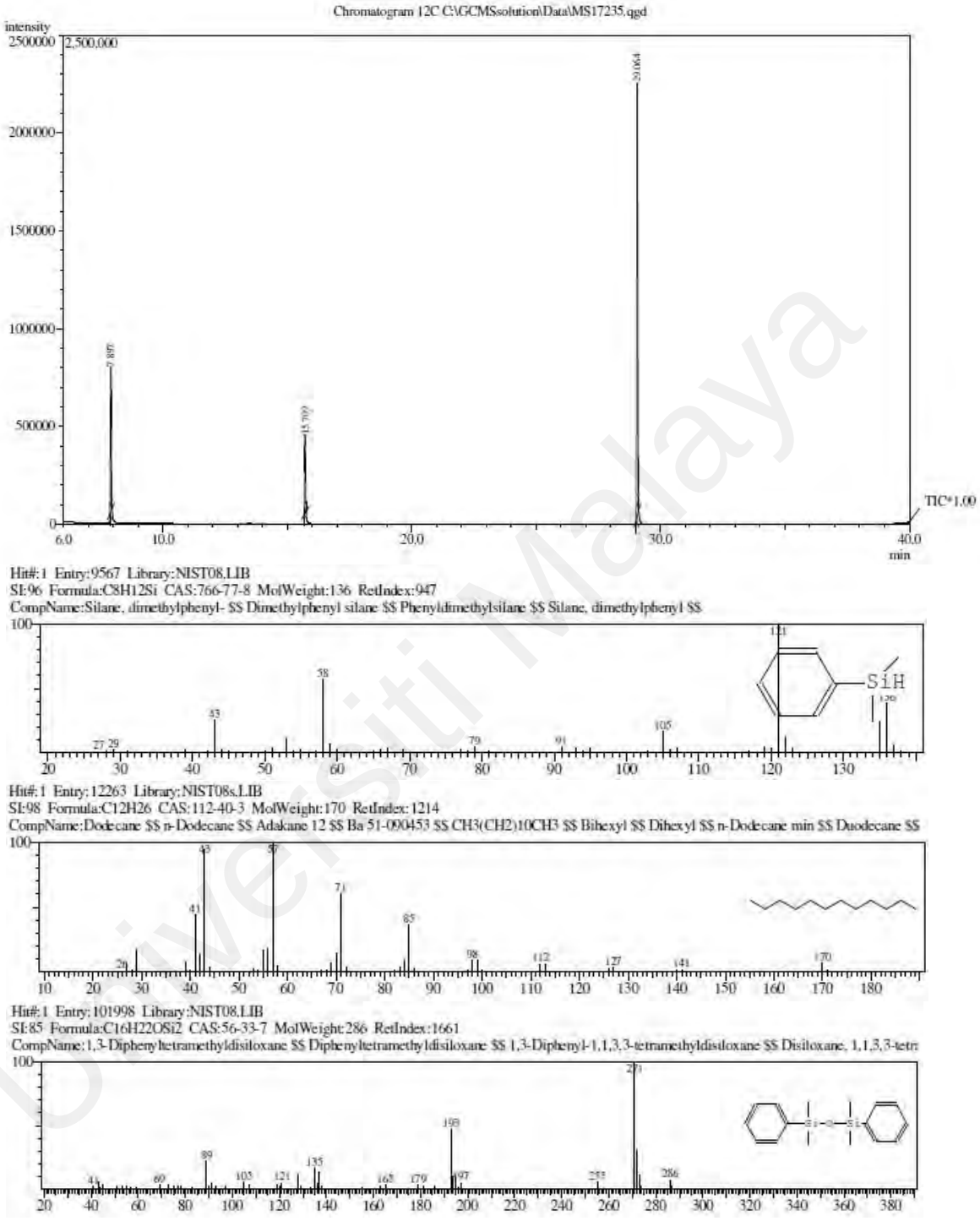

Figure 4.25: The GC-MS chromatogram of sample using AuNPs/rGO(C).

To understand the preliminary kinetics of the DMPS conversion to diphenyltetramethyldisiloxane which follows chemical reaction Equation (4.1) similar to the previous report (Sawama et al., 2016).

$$2C_6H_6Si(CH_3)_2H + H_2O \longrightarrow C_6H_6Si(CH_3)_2OC_6H_6Si(CH_3)_2 + 2H_2 \quad (4.1)$$

The result based on GC-MS analysis already confirm the conversion of DMPS at 70% with 100% selectivity to 1,3-diphenyltetramethyldisiloxane through 12 hours reaction. According to kinetic model fitting as shown in Figure 4.26, the selective DMPS conversion to 1,3-diphenyltetramethyldisiloxane follow zero order kinetics in cognisance to the chemical reaction Equation (4.1). Both reactions in AuNPs/rGO(B) and AuNPs/rGO(C) show zero order integrated rate law with R^2 values in the region of 0.98 as shown in Figure 4.26. The gradient slopes show the zero order rate constant *k* in mol L^{-1} min^{-1}. The reaction rate in zero order is usually preferred for overall reaction rate to represent actual reaction rate of the catalyst.

The rate law for zero order reaction is $\frac{dA_{DMPS}}{t}$ = -k, and the combined rate law and mole balance using Equations of (4.2 to 4.4) as follows: -

$$\frac{dA_{DMPS}}{t} = -k \quad (4.2)$$

Integrating with $A_{DMPS} = A_{DMPS0}$ of both sides, where C is the integration constant:

$$A_{DMPS} = -kt + C \quad (4.3)$$

At the time zero $A_{DMPS} = A_{DMPS0}$, therefore,

$$A_{DMPS} = -kt + A_{DMPS0} \quad (4.4)$$

The reaction with zero order was also observed by Li et al. (2015) that using catalyst with the dehydrogenative coupling of organosilanes under mild conditions with volume

and depth of water about 200 mL and 3.2m, respectively. That study concludes the reaction is independence to the concentration of DMPS.

From the plot, the reaction rate for both AuNPs/rGO(B) and AuNPs/rGO(C) is 0.472 $\frac{\text{mmol/L}}{\text{hour}}$ and 0.3173 $\frac{\text{mmol/L}}{\text{hour}}$, respectively. Thus, the reaction rate for AuNPs/rGO(B) is faster than AuNPs/rGO(C).

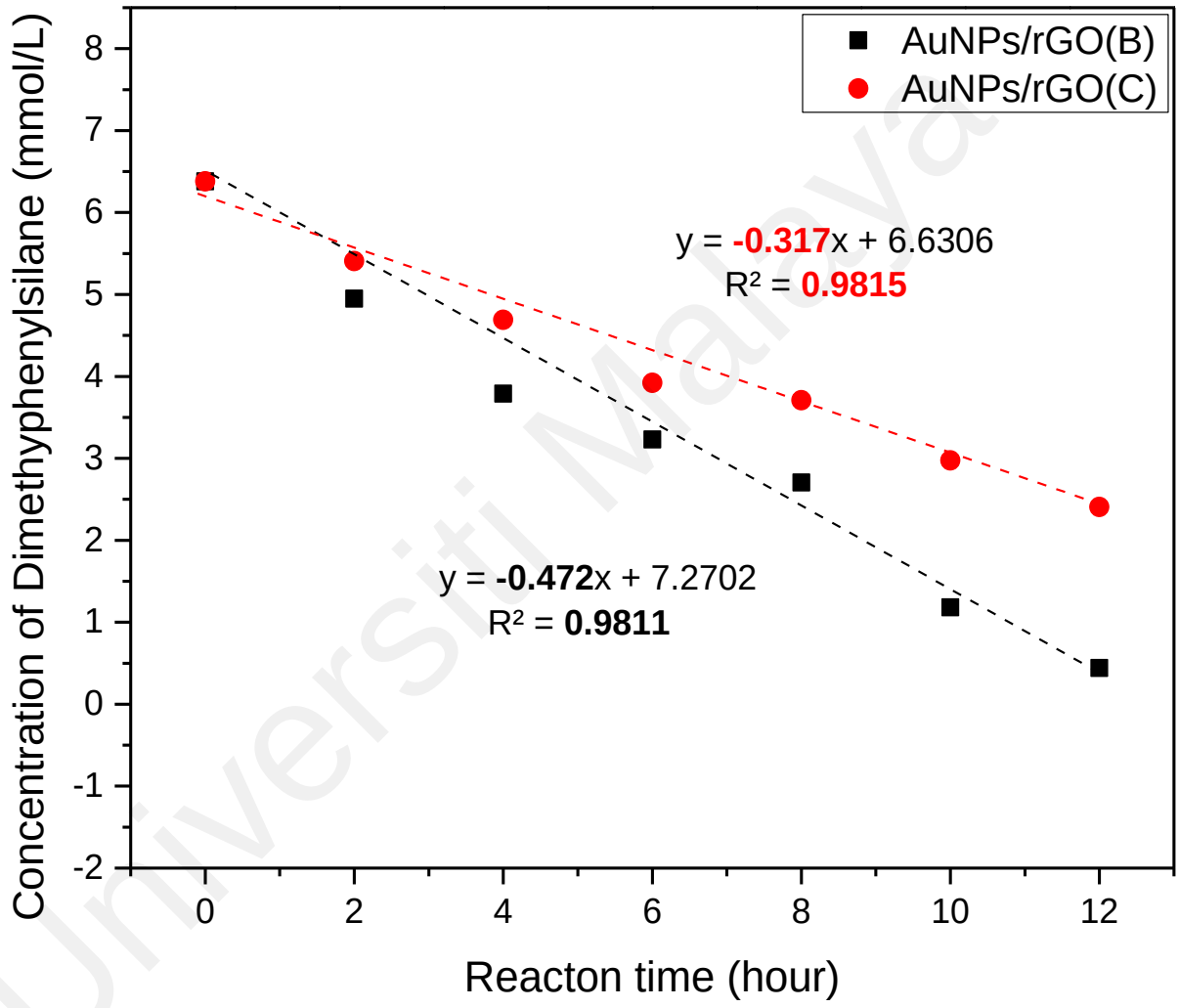

Figure 4.26: Zero order plot for kinetic of DMPS conversion using AuNPs/rGO(B) and AuNPs/rGO(C).

4.2.3 The recyclability of AuNPs/rGO catalyst

The recyclability of both catalysts was performed five times. Tables 4.3 and 4.4 show the conversion of both catalysts for five cycles. It was found that there is no significant loss of activity in both catalyst after 5 runs. Based on Figure 4.27, the conversion of

AuNPs/rGO(B) is higher than AuNPs/rGO(C) due to loss of AuNPs in AuNPs/rGO(C) catalyst since the former reaction has higher catalytic activity due to $NaBH_4$ is a stronger reducing agent compared to $Na_3C_6H_5O_7$ dihydrate (Pal et al., 2015). The particle size of AuNP would be further discussed in XRD discussion in the following sub-section. Hence, it was proved AuNPs/rGO can be recycled for synthesis of 1,3-diphenyltetramethyldisilixane with no significant conversion reduction up to five cycles run.

Table 4.3: Catalytic conversion of AuNPs/rGO(B).

Number of Cycles	Conversion Percentage (%)
1	33.7
2	33.1
3	32.1
4	31.2
5	32.2

Table 4.4: Catalytic conversion of AuNPs/rGO(C).

Number of cycles	Conversion Percentage (%)
1	29.8
2	29.2
3	28.6
4	29.4
5	29.1

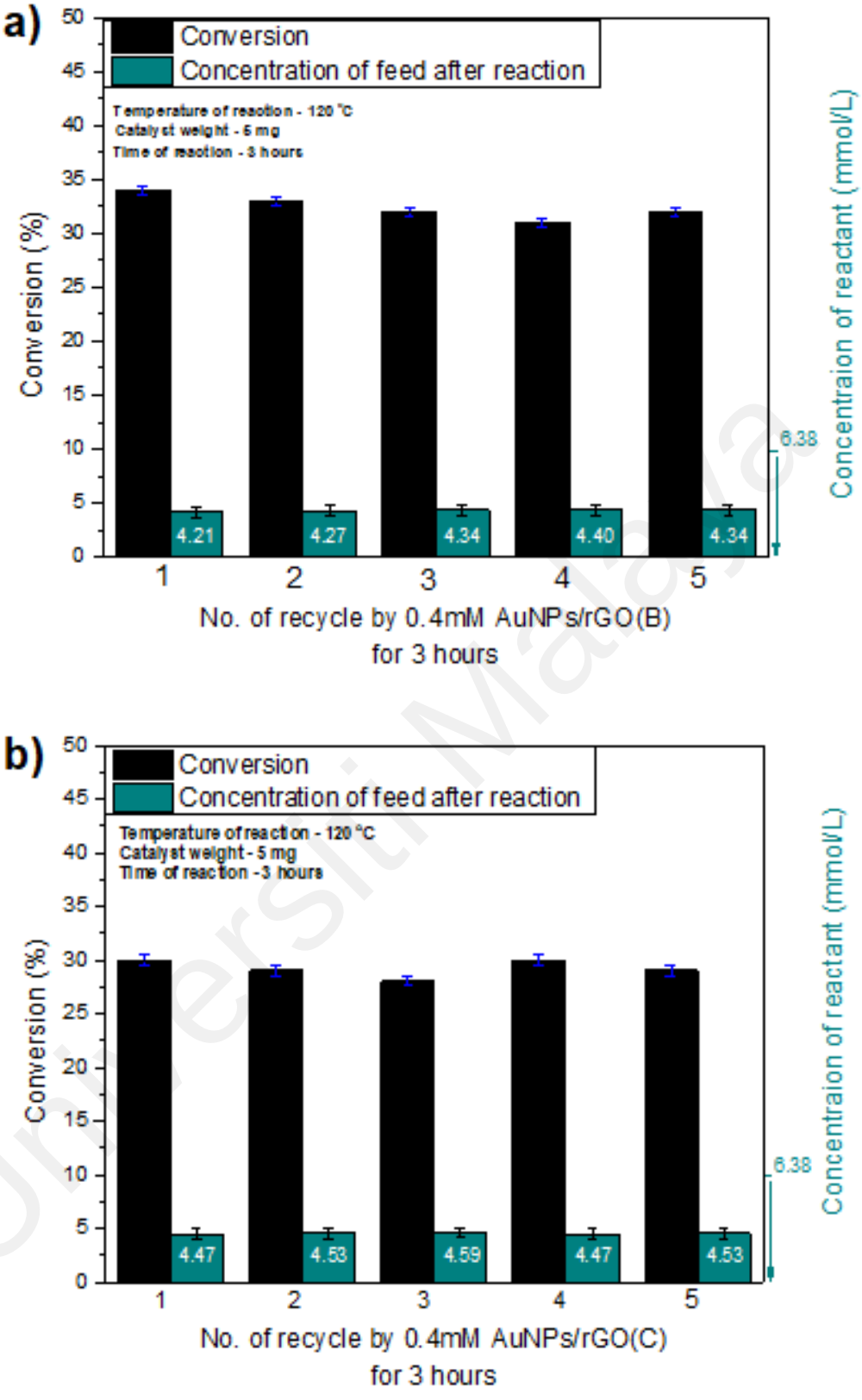

Figure 4.27: The comparison of recyclability test of (a) AuNPs/rGO(B) and (b) AuNPs/rGO(C).

4.3 Characterization After Reaction

4.3.1 FTIR Analysis of Recycled AuNPs/rGO

Figure 4.28 shows the FTIR spectra of AuNPs/rGO(B) before and after recycled together with GO as comparison to show the catalyst is completely reduced. The peak at 3400 cm^{-1} is due to -OH stretching vibration of hydroxyl groups and the peak at 1560 cm^{-1} can be assigned to C-H vibration in the aromatic ring (Vellaichamy et al., 2018). The peak at 1080 cm^{-1} is close to the peak 1070 cm^{-1} reported by (Zhang et al., 2014) which indicates C-O alkoxy stretching. Then the band at 1850 cm^{-1} and 1650 cm^{-1} is the carbonyl group stretching and C=C olefinic compound (Nandiyanto et al., 2019). The peak at 2310 cm^{-1} represents the C=C=C vibration (Lazar et al., 2020). There was no changes in catalyst functionalized group after the reaction as it the AuNP/rGO involved in the catalytic activity.

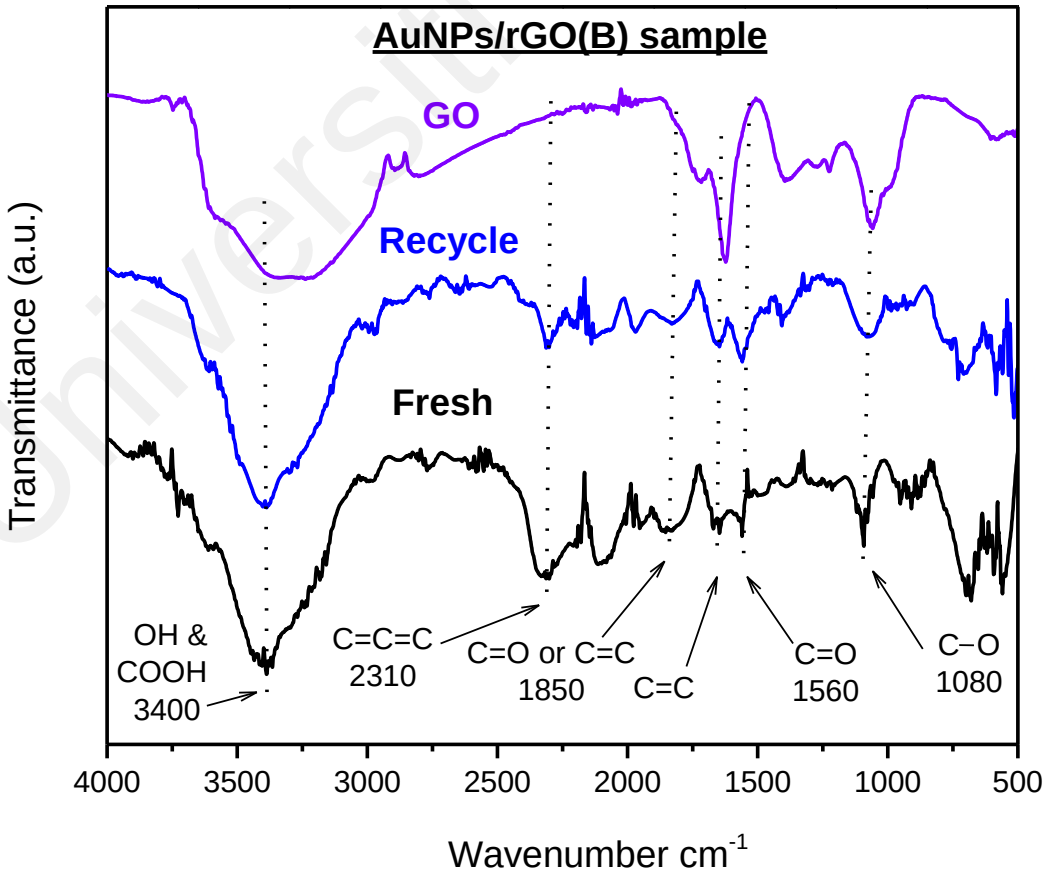

Figure 4.28: FTIR spectra of AuNPs/rGO(B) before and after recycled.

Figure 4.29 shows the FTIR spectra of AuNPs/rGO(C) before and after use. The peak at 3380 cm^{-1} can be assigned to -OH stretching (Yousefimehr et al., 2021). The aromatic C- H bond stretching is identified at 2980 cm^{-1} while the peak at 1270 cm^{-1} is due to C-O-C aromatic ethers stretch (Nandiyanto et al., 2019). The peaks appear at 1570 cm^{-1}, 1385 cm^{-1} and 1060 cm^{-1} shows the C=C stretching, -OH deformation and C-O alkoxy stretching (Vellaichamy et al., 2018; Zhang et al., 2011).

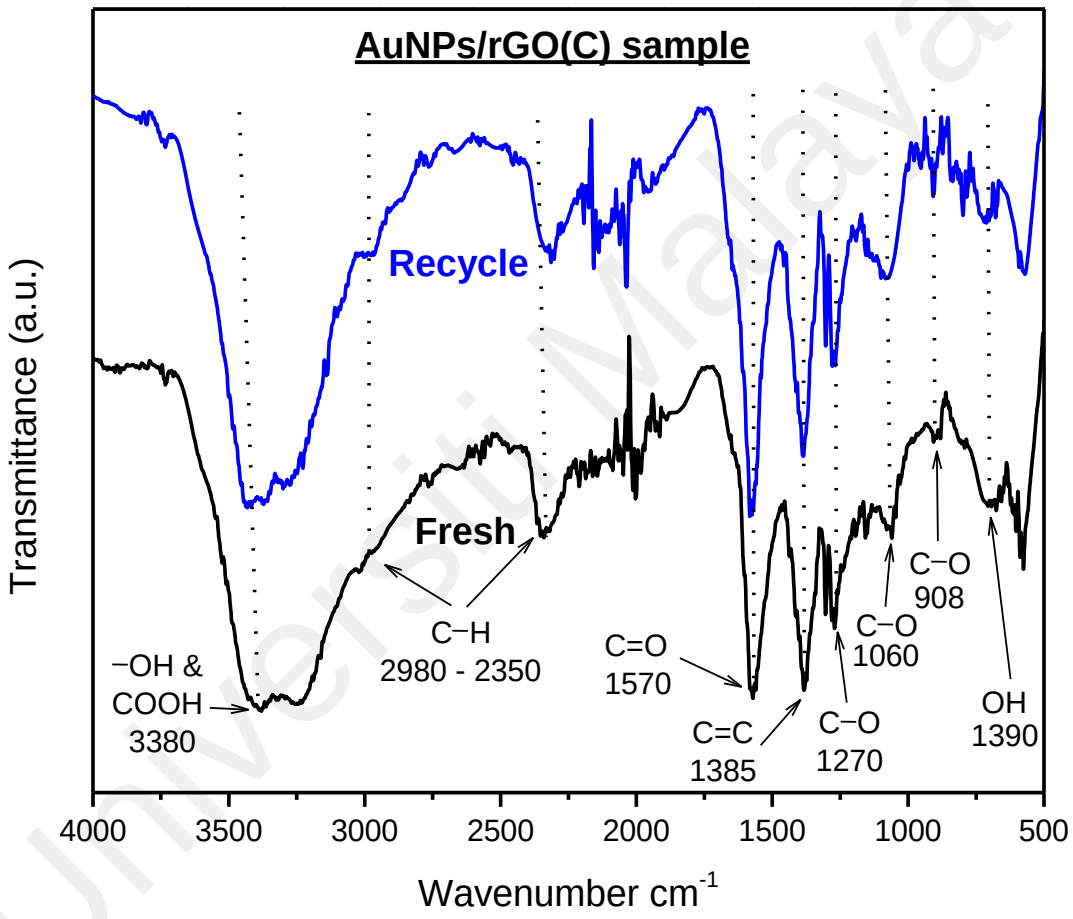

Figure 4.29: FTIR spectra of AuNPs/rGO(C) before and after recycled.

Based on both FTIR spectra, it is observed that the functional group peaks still presence before and after recycling of the catalyst. Thus, it is suggested that the chemical structure of the rGO did not change significantly after recycling. There was not changes in catalyst functionalized group after the reaction with the AuNP/rGO involvement in the catalytic activity and confirm to approved that there was no redox reaction was involved during the reaction.

4.3.2 XRD Analysis of Recycled AuNPs/rGO

From the XRD diffraction pattern in Figure 4.30, both catalysts show similar XRD peaks with different peak intensity. There are 5 peaks which indicate the presence of AuNPs. The sharp peaks are observed at ($2\theta = 38.3°$, 44.7°, 64.9°, 77.8° and 82.3°) which can be attributed to (111), (200), (220), (311), and (222) planes of cubic crystallites which matches the JCPDS card No 004–0784 (Yousefimehr et al., 2021). These peaks suggested the single-phase AuNPs with face-centre cubic structure and high crystalline structure (Dheyab et al., 2021; Vellaichamy et al., 2018). The peaks intensity of AuNPs/rGO(C) is higher than AuNPs/rGO(B) which means the particle size of AuNPs in AuNPs/rGO(C) is higher than AuNPs/rGO(B) and this was also observed in FESEM images.

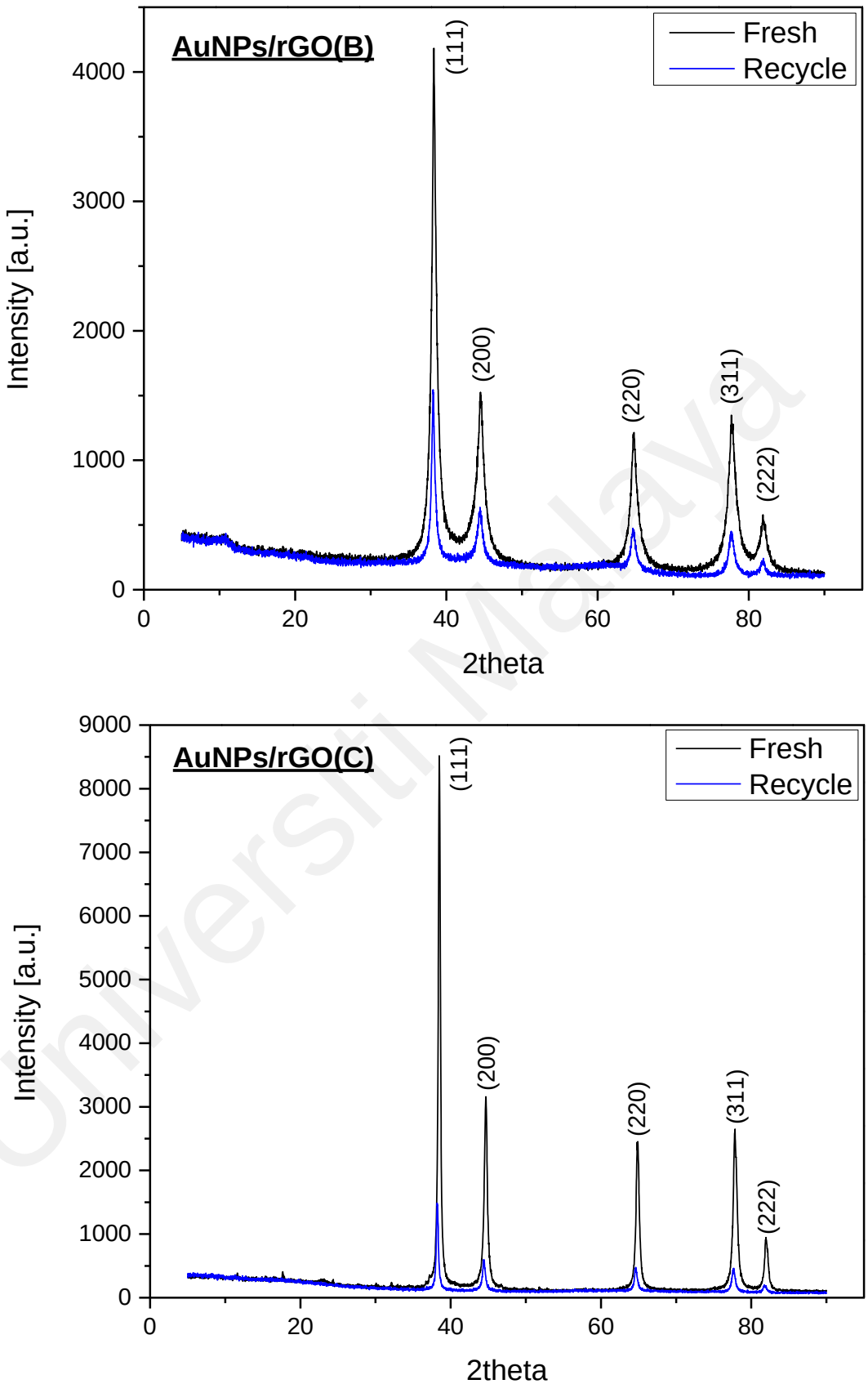

Figure 4.30: X-Ray diffraction spectra for samples AuNPs/rGO(B) and AuNPs/rGO(C).

Table 4.5 shows the average crystallite size of AuNPs/rGO(B) and AuNPs/rGO(C) as comparison between before and after recycling. From the average crystallite size that calculated using Scherrer equation for both catalysts, it can be observed the size increases after the catalysts was recycled which also persist with the SEM images where the particles become larger after recycled for five times. AuNPs/rGO(B) having smaller crystallite size explains the better catalytic activity than AuNPs/rGO(C).

Table 4.5: The average crystallite size of AuNPs/rGO(B) and AuNPs/rGO(C) before and after recycling.

AuNPs/rGO	Average Crystallite Size (nm)
(B)-Fresh	8.28
(B)-Recycled	11.74
(C)-Fresh	12.82
(C)-Recycled	17.69

4.3.3 FESEM+ EDS Analysis of Recycled AuNPs/rGO

Based on FESEM images of both catalysts in Figure 4.31, it is suggested that the AuNPs was immobilized on the rGO surface. The presence of AuNPs represented by the white spots charges that are clearly seen in all the images on Figure 4.31 (a) to (d).

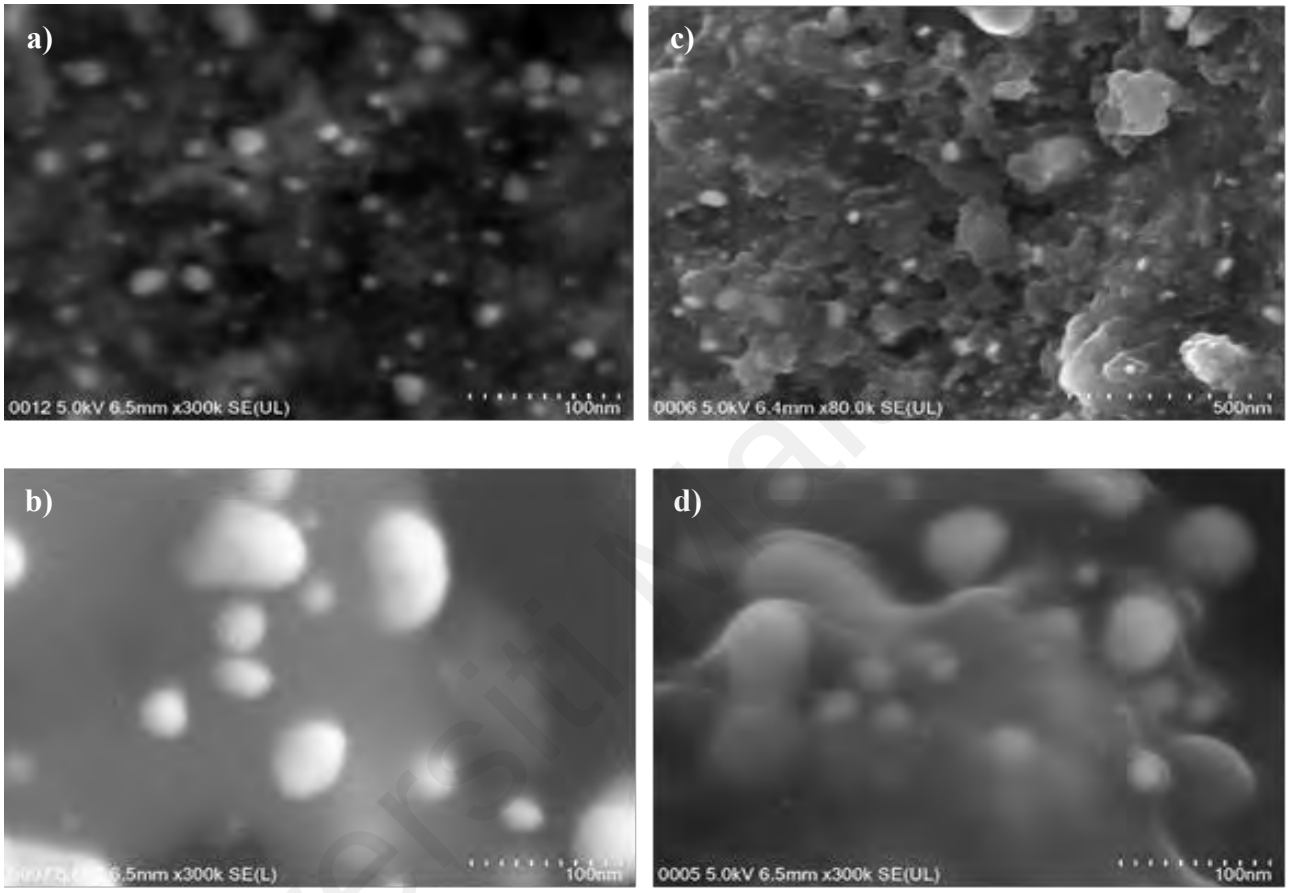

Figure 4.31: FESEM images for AuNPs/rGO(B): (a) fresh catalyst; (b) after recycled and FESEM images for AuNPs/rGO(C): (c) fresh catalyst; (d) after recycled.

The measurement of AuNPs size was measured using FESEM. When compared both AuNPs/rGO(B) and AuNPs/rGO(C) in Figures 4.32 and 4.33, respectively. While the diameter has been measured accordingly with AuNPs in AuNPs/rGO(B) that are smaller (3 nm – 13 nm) in fresh catalyst and (6 nm – 14 nm) after recycled.

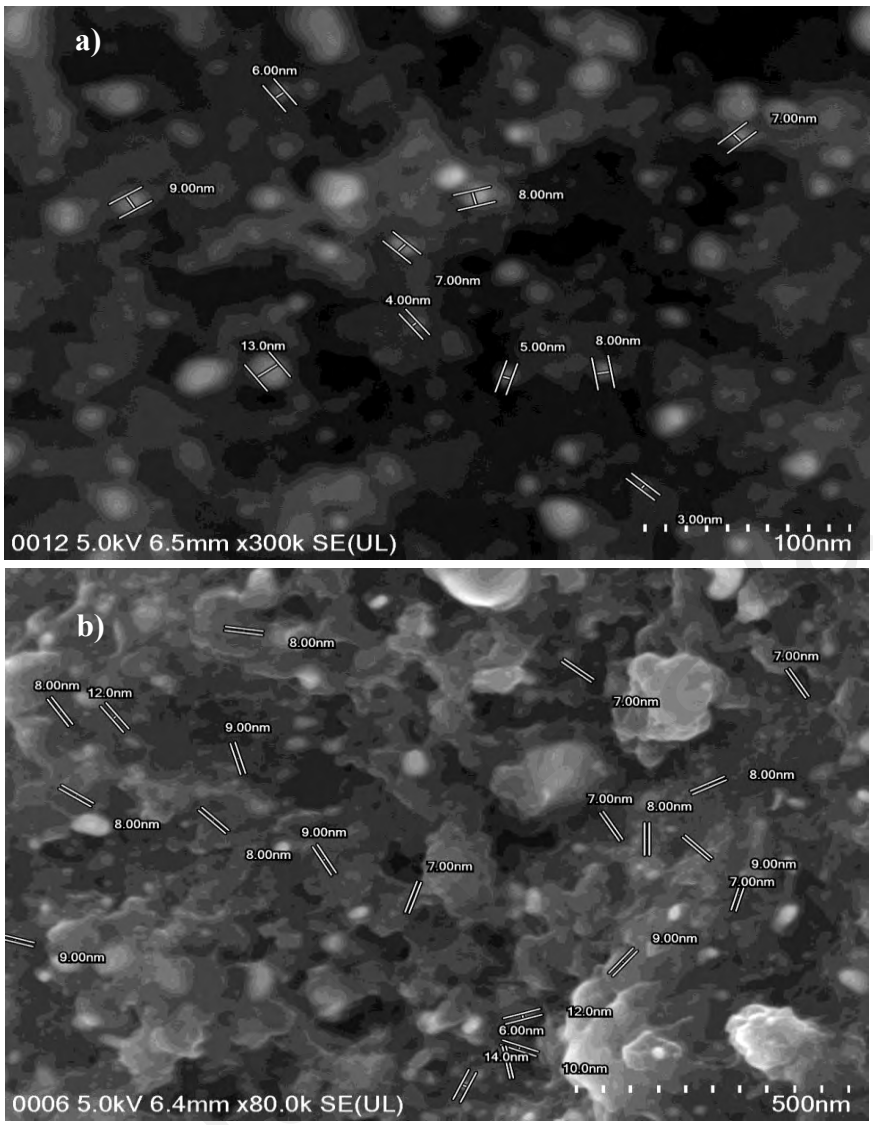

Figure 4.32: The diameter of AuNPs in AuNPs/rGO(B) where (a) fresh catalyst while (b) after recycled.

Whereas AuNPs/rGO(C) the nanoparticle size for fresh catalyst (7 nm – 26 nm) and (8 nm – 54 nm) become larger after recycled. This explains the better catalytic activity of AuNPs/rGO(B) due to the smaller size of catalytic active particles.

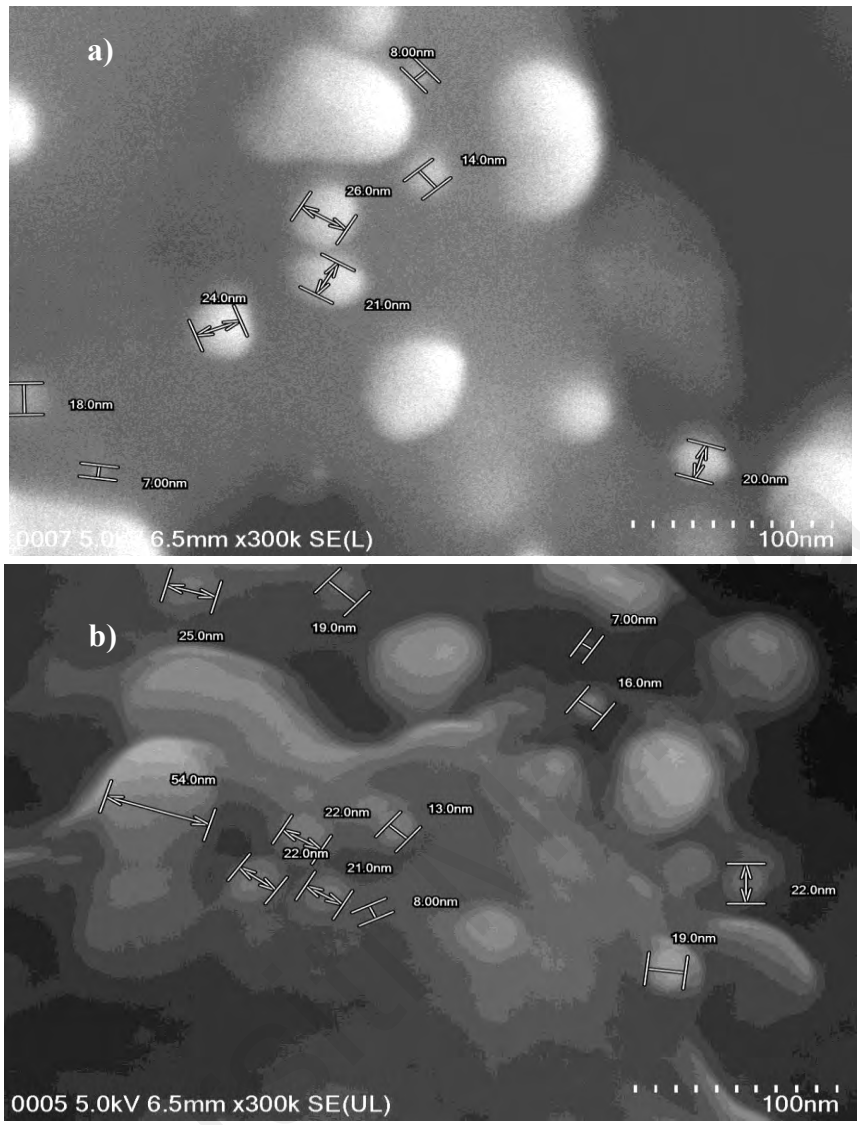

Figure 4.33: The diameter of AuNPs in AuNPs/rGO(C) where (a) fresh catalyst while (b) after recycled.

In both catalysts, the nanoparticles size increased after recycling. This can be attributed due to the agglomeration properties of Au metal (Dheyab et al., 2021). Particle agglomeration is a basic process that reduces surface free energy by increasing particle size and lowering surface area (Gosens et al., 2010).

From the EDS analysis in Figure 4.34 , it is confirmed that all the samples before and after recycled contain Au element. Sodium is present in Figure 4.34 (b) and (d) due to the reducing agent residue on the surface of rGO. Then on both AuNPs/rGO(B) and AuNPs/rGO(C) (Figure 4.34 a-d) after recycled contains silicon which also residue from the substrate used in the reaction. Table 4.6 shows the elemental weight percentage in

the catalysts. The Au weight percentage in fresh AuNPs/rGO(B) is the highest (1.82%) followed by recycled AuNPs/rGO(B) (1.69%), fresh AuNPs/rGO(C) (1.74%) and recycled AuNPs/rGO(C) (1.39%). These significant changes in the catalysts before and after recycling possibly due to either AuNPs leaching or agglomeration after the reaction recycle for five times.

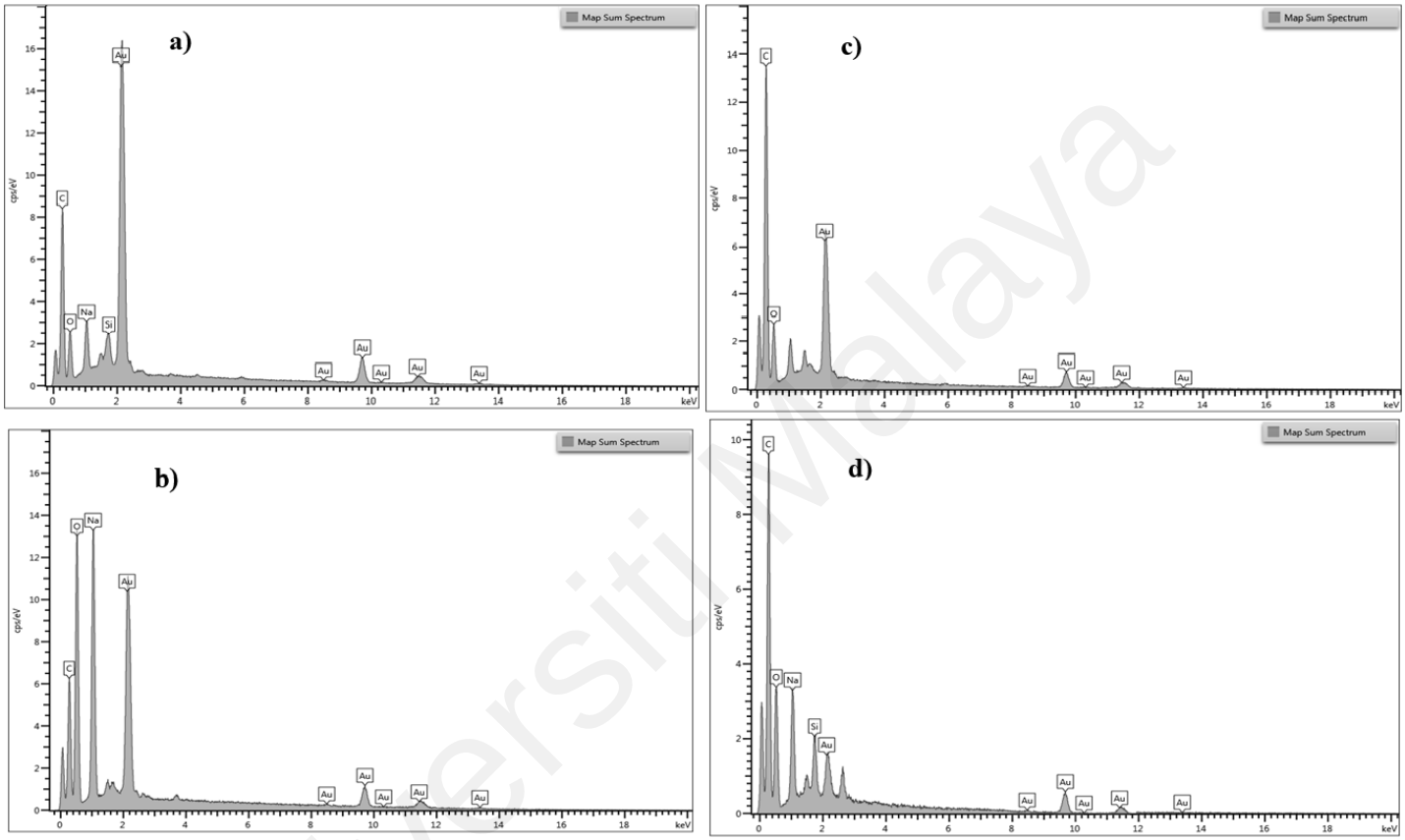

Figure 4.34: EDS spectrum or AuNPs/rGO(B): (a) fresh catalyst;(b) after recycled and EDS spectrum for AuNPs/rGO(C): (c) fresh catalyst; (d) after recycled.

Table 4.6: The weight % of carbon, oxygen, and gold in AuNPs/rGO.

AuNPs/rGO	Weight Percentage (wt%)		
	Carbon (C)	Oxygen (O)	Gold (Au)
(B)-Fresh	3.09	1.83	1. 82
(B)-Recycled	2.58	1.36	1.69
(C)-Fresh	2.34	1.82	1. 74
(C)-Recycled	2.64	1.90	1. 39

4.3.4 Reaction Mechanism

Since the solventless dehydrogenative reaction of DMPS that only produce 1,3-diphenyltetramethyldisiloxane, the reaction mechanism is based on Equation (4.1). There were two reaction pathways possible to produce disiloxane which is classify as organosiloxane product. First, the DMPS was initially generated a conversion of disiloxane product by using AuNPs/rGO catalyst hydration of hydrosilane through hydrosilylation. It has been followed by the dehydrogenation coupling of DMPS to yield of 1,3-diphenyltetramethyldisiloxane as further identified in GC-MS results. According to previous study by Sawama et al. (2016), the second pathway could be dehydrogenative coupling of hydrosilane into disiloxane, followed by hydrolytic dehydrogenative silylation (reaction of catalyst that introduce with water), but the current reaction of solventless are exposed by ambient air (moisture). Where oxygen from the moisture assist in formation of Si-O-Si coupling of the disiloxane product. In this experiment, the reaction of DMPS transformed into disiloxane was limited by the adsorption of substrate on the catalyst due to the absence of solvent. Therefore, it is proposed the reaction pathway of hydrosilane to 1,3-diphenyltetramethyldisiloxane is based on the first possibility which is depicted in Figure 4.35.

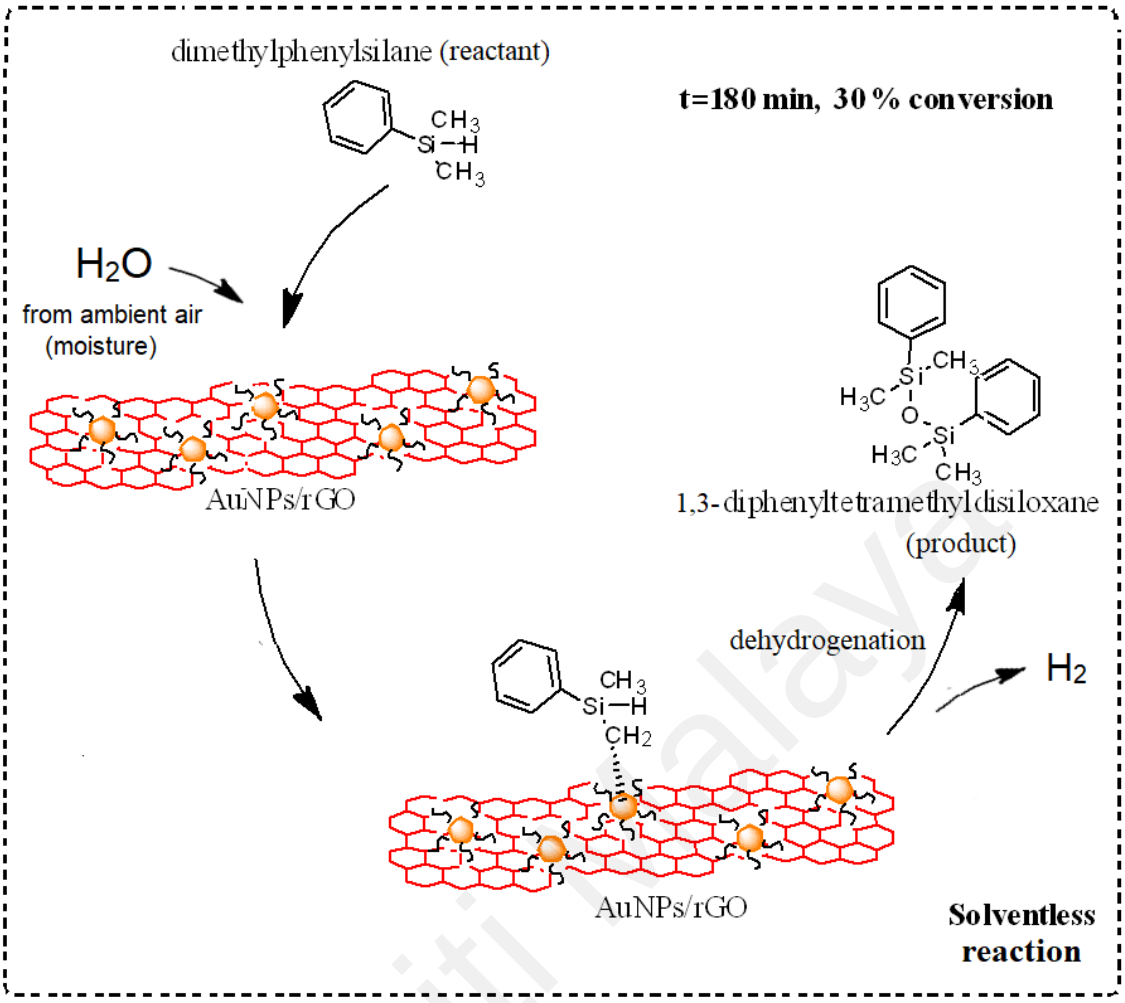

Figure 4.35: Proposed mechanism of Dehydrogenative coupling of DMPS of solventless reaction for a conversion into 1,3-diphenyltetramethyldisiloxane catalysed AuNPs/rGO under reflux at 120 °C.

The hydrogen gas should be released based on Figure 4.35 and Equation (4.1). The presence of hydrogen gas was analyzed using GC-TCD analysis. Figure 4.36(a) shows the GC-TCD spectrum in the H_2 gas calibration with four peaks there are defined as hydrogen, mixture of argon /oxygen, nitrogen and methane. This analysis used 8% to 9% H_2 in helium carrier gas mixture. For the calibration, the gas mixture was mixed with helium carrier gas. It was found that pure helium together was very sensitive to other gas analytes. H_2 peak shows a negative peak because H_2 has high thermal conductivity at 0.1805 $Wm^{-1}K^{-1}$ compared to pure helium at 0.1513 $Wm^{-1}K^{-1}$ (Cowper & Derose, 2013; Detector).

However, there are no H_2 gas observe for overall reaction of solventless as shown in Figure 4.36(b). It was assumed air, nitrogen and carbon monoxide was detected in GC-TCD spectrum. It was assumed H_2 gas produced in solventless reaction was relatively low as the reaction reacted with water from ambient air for the reaction. Besides, it was also assumed the H_2 gas concentration produced from the reaction was possibly less than 5 ppm, which was lower than the detection limit of GC-TCD.

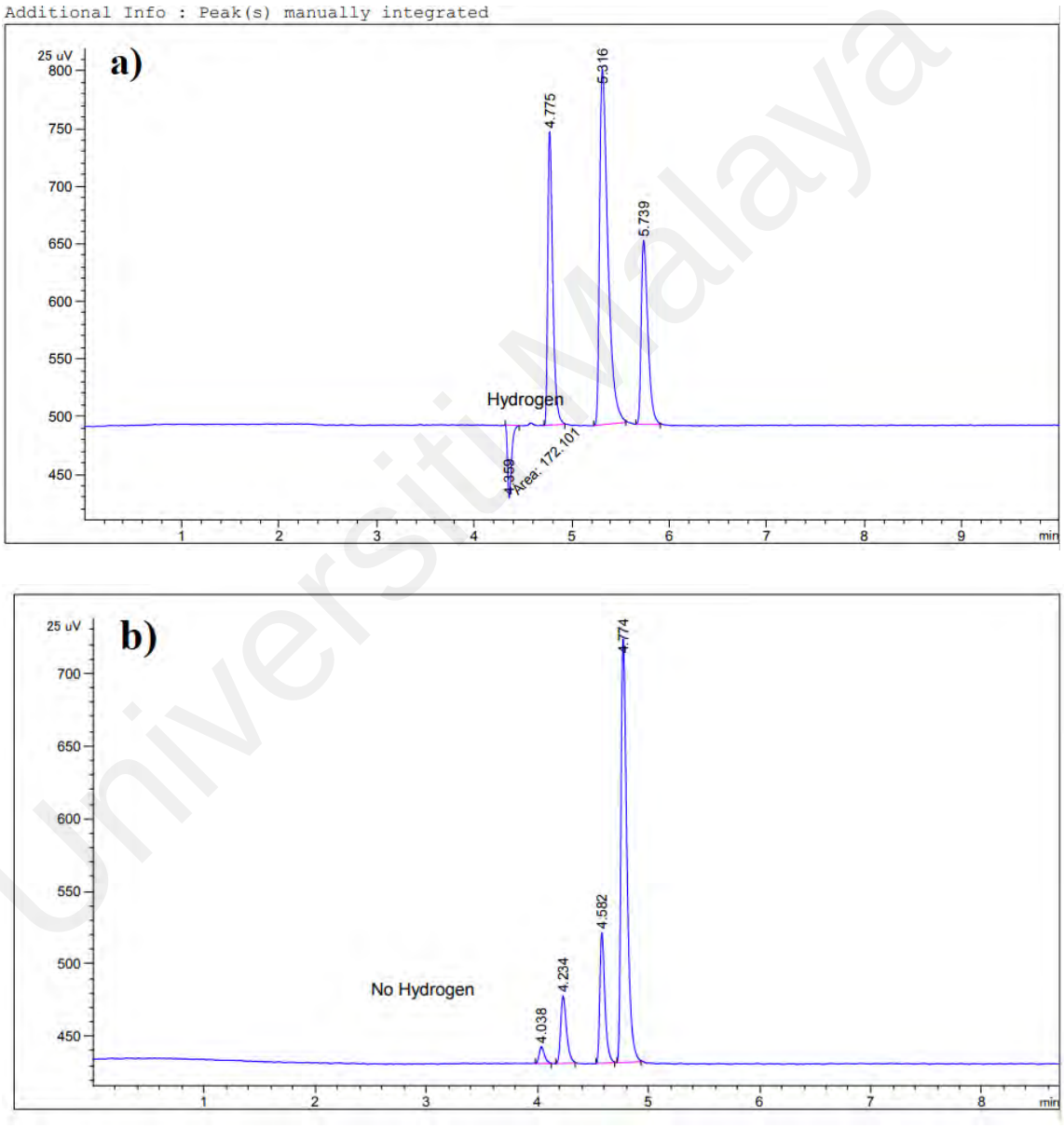

Figure 4.36: GC-TCD analysis (a) Calibration of H_2 gas (b) After reaction observation indicate with no H_2 gas present.

CHAPTER 5: CONCLUSION

5.1 Conclusion

Overall, GO that was used to support the AuNPs was an efficient catalyst for promoting dehydrogenating coupling DMPS especially under solventless reaction for a production of disiloxane. GO as support exerts a noticeable influence on the catalytic activity of optimized using 0.4 mM AuNPs solution in solventless reaction. Initially, the catalyst was optimized by using reducing agent $Na_3C_6H_5O_7$ before further optimized with $NaBH_4$. The catalytic activity of two different reducing agents was analyzed using GC-FID for conversion and selectivity determination and was further analyzed using GC-MS and NMR to confirm the presence of the main product, 1,3-diphenyltetramethyldisiloxane.

The solventless reaction is the most preferable because the reaction produces 100% selectivity and even generates low conversion compared with solvent reaction. The solvent reaction showed high catalytic activity but with less than 90% selectivity. Solventless reaction showed low catalytic activity because the substrate of DMPS's viscosity was higher compared to substrate of DMPS in benzaldehyde solvent. Therefore, the diffusion limitation of DMPS was observed in solventless reaction as the apparent activation energy was lower than 10kJ/mol. The solventless reaction was optimized using reducing agent $NaBH_4$ in AuNPs/rGO(B) catalyst and compared with reducing agent citrate, $Na_3C_6H_5O_7$ in AuNPs/rGO(C) catalyst. Both catalysts showed zero order reaction with the reaction rate of AuNPs/rGO(B) is higher than AuNPs/rGO(C). These catalysts was tested in reaction reproducible for at least five times. It was found the average conversion percentage of both AuNPs/rGO(B) and AuNPs/rGO(C) was around 33% and 29%, respectively. Both catalysts was recycled with no significant loss of conversion. Then the fresh catalysts was tested for 12 hour reaction which showed conversion at 85%

and 70% for AuNPs/rGO(B) and AuNPs/rGO(C) catalysts, respectively. Thus, the catalyst reduced using $NaBH_4$ showed higher catalytic activity compared to the catalyst reduced by citrate, $Na_3C_6H_5O_7$.

All the characterizations successfully showed the presence of AuNPs on rGO by optimized 0.4 mM catalyst when using reducing agent $Na_3C_6H_5O_7$. In UV-Vis analysis, the peak at 550 nm confirmed the presence of Au in both AuNPs/rGO(B) and AuNPs/rGO(C) catalysts. FESEM-EDS confirmed the presence of Au element on rGO for both catalysts. The XRD pattern was perfectly matched with JCPDS of AuNPs for both catalysts which also confirmed the presence of AuNPs crystal plane. To further verify AuNPs on surface rGO, the Au noble metal catalyst was confirmed in nanosized by HR-TEM analysis with relate crystallite size and plane identification of XRD analysis. For XPS analysis, the catalyst already verifies with the present of Au^0 and Au^{3+} on the rGO surface support media that allow Au-O-C and justify the strong bond between AuNPs and rGO.

The reduction of GO to rGO reducing agent was observed in Raman analysis. However, it was found reducing agent citrate, $Na_3C_6H_5O_7$ was not completely reduced GO to rGO since FTIR analysis showed several GO functional groups present in AuNPs/rGO(C) catalysts. Nevertheless, the reducing agent $NaBH_4$ was completely reduced GO in AuNPs/rGO(B) since $NaBH_4$ is stronger reducing agent compared to citrate.

5.2 Future work

Several future directions related to this project were listed as follows:

1. Solvent reaction in this work needs to be analyzed further to find the most optimized parameter to understand overall oxidation reaction.

2. Other reducing agents are to be used to synthesize AuNPs/rGO to increase the catalytic activity in solventless reaction.

3. The catalyst used in this study can be used for hydrogenation reaction since AuNPs/rGO is an active catalyst.

REFERENCES

Abad, A., Corma, A., & García, H. (2007). Supported gold nanoparticles for aerobic, solventless oxidation of allylic alcohols. *Pure and Applied Chemistry, 79*(11), 1847-1854.

Adhikari, B., Biswas, A., & Banerjee, A. (2011). Graphene oxide-based supramolecular hydrogels for making nanohybrid systems with Au nanoparticles. *Langmuir, 28*(2), 1460-1469.

Adib, M., Mahdavi, M., Noghani, M. A., & Bijanzadeh, H. R. (2007). Reaction between isocyanides and chalcones: an efficient solvent-free synthesis of 5-hydroxy-3, 5-diaryl-1, 5-dihydro-2H-pyrrol-2-ones. *Tetrahedron Letters, 48*(45), 8056-8059.

Agrawal, M., Gupta, S., Pich, A., Zafeiropoulos, N. E., & Stamm, M. (2009). A facile approach to fabrication of ZnO− TiO2 hollow spheres. *Chem. Mater., 21*(21), 5343-5348.

Agusu, L., Ahmad, L., Nurdin, M., Mitsudo, S., & Kikuchi, H. (2018). *Hydrothermal Synthesis of Reduced Graphene Oxide Using Urea as Reduction Agent: Excellent X-band Electromagnetic Absorption Properties.* Paper presented at the IOP Conf Ser Mater Sci Eng.

Akyıldırım, O., Yüksek, H., Saral, H., Ermiş, İ., Eren, T., & Yola, M. L. (2016). Platinum nanoparticles supported on nitrogen and sulfur-doped reduced graphene oxide nanomaterial as highly active electrocatalysts for methanol oxidation. *Journal of Materials Science: Materials in Electronics, 27*(8), 8559-8566.

Alshammari, A., & Kalevaru, V. N. (2016). Supported Gold Nanoparticles as Promising Catalysts. In *Catalytic Application of Nano-Gold Catalysts*: InTech.

Amanulla, B., Palanisamy, S., Chen, S.-M., Chiu, T.-W., Velusamy, V., Hall, J. M., . . . Ramaraj, S. K. (2017). Selective colorimetric detection of nitrite in water using chitosan stabilized gold nanoparticles decorated reduced graphene oxide. *Scientific reports, 7*(1), 1-9.

Anastas, P. T., Heine, L. G., & Williamson, T. C. (2000). Green chemical syntheses and processes: introduction. In: ACS Publications.

Anastas, P. T., & Kirchhoff, M. M. (2002). Origins, current status, and future challenges of green chemistry. *Accounts of chemical research, 35*(9), 686-694.

Ansari, R. M., & Bhat, B. R. (2019). Copper (II) Schiff base-graphene oxide composite as an efficient catalyst for Suzuki-Miyaura reaction. *Chemical Physics, 517*, 155-160.

Anwar, A., Ma'amor, A., MAHMUD, H. E., Basirun, W. J., & Abdullah, I. (2022). Catalytic activity of ethylbenzene with product selectivity by gold nanoparticlessupported on zinc oxide. *Turkish Journal of Chemistry, 46*(3), 730-746.

Araki, K., Mizuguchi, E., Tanaka, H., & Ogawa, T. (2006). Preparation of very reactive thiol-protected gold nanoparticles: revisiting the Brust-Schiffrin method. *Journal of Nanoscience and Nanotechnology, 6*(3), 708-712.

Atar, N., Eren, T., & Yola, M. L. (2015). Ultrahigh capacity anode material for lithium ion battery based on rod gold nanoparticles decorated reduced graphene oxide. *Thin Solid Films, 590*, 156-162.

Bagheri, S., Jamal, N., Halilu, A., & TermehYousefi, A. (2018). Novel rGO-T-C(n) Nanosheets developed via click chemistry as a lubricant anti-wear additive. *Scientific Reports, 8*(1), 6221.

Bagheri, S., & Julkapli, N. M. (2018). *Nanocatalysts in Environmental Applications*: Springer.

Bailey, D. L., & Rochow, E. G. (1994). A review of : "Catalyzed direct reactions of silicon. Edited by KM Lewis, Union Carbide Corporation, Tarrytown, NY, USA and DG Rethwisch, University of Iowa, Iowa City, IA, USA; Studies in Organic Chemistry, Volume 49,© 1993, 664 pages Hardbound, Price: DFI 465.(US $265.75), ISBN 0-444-81715-8.". In: Taylor & Francis.

Balwe, S. G., Rokade, A. A., Park, S. S., & Jeong, Y. T. (2019). Green synthesis and characterization of supported gold nanoparticles (Au@ PS) from Schisandra chinensis fruit extract: An efficient and reusable catalyst for the synthesis of chromeno [2, 3-d] pyrimidin-2-yl) phenol derivatives under solvent-free conditions. *Catalysis Communications, 128*, Article#105703.

Biradar, A. V., & Asefa, T. (2012). Nanosized gold-catalyzed selective oxidation of alkyl-substituted benzenes and n-alkanes. *Applied Catalysis A: General, 435*, 19-26.

Bonvicini, S. N., Fu, B., Fulton, A. J., Jia, Z., & Shi, Y. (2022). Formation of Au, Pt, and bimetallic Au–Pt nanostructures from thermal dewetting of single-layer or bilayer thin films. *Nanotechnology, 33*(23), Article#235604.

Boucle, J., & Ackermann, J. (2012). Solid-state dye-sensitized and bulk heterojunction solar cells using TiO2 and ZnO nanostructures: recent progress and new concepts at the borderline. *Polym. Int., 61*(3), 355-373.

Boukhvalov, D., & Katsnelson, M. (2009). Chemical functionalization of graphene. *Journal of Physics: Condensed Matter, 21*(34), Article#344205.

Calvino, V., Picallo, M., López-Peinado, A., Martín-Aranda, R., & Durán-Valle, C. (2006). Ultrasound accelerated Claisen–Schmidt condensation: A green route to chalcones. *Applied Surface Science, 252*(17), 6071-6074.

Chaiseeda, K., Nishimura, S., & Ebitani, K. (2017). Gold Nanoparticles Supported on Alumina as a Catalyst for Surface Plasmon-Enhanced Selective Reductions of Nitrobenzene. *ACS Omega, 2*(10), 7066-7070.

Chauhan, B. P., Sarkar, A., Chauhan, M., & Roka, A. (2009). Water as green oxidant: a highly selective conversion of organosilanes to silanols with water. *Applied Organometallic Chemistry, 23*(10), 385-390.

Chen, X., Zhu, H. Y., Zhao, J. C., Zheng, Z. F., & Gao, X. P. (2008). Visible-light-driven oxidation of organic contaminants in air with gold nanoparticle catalysts on oxide supports. *Angewandte Chemie International Edition, 47*(29), 5353-5356.

Chojnowski, J., Rubinsztajn, S., Cella, J. A., Fortuniak, W., Cypryk, M., Kurjata, J., & Kaźmierski, K. (2005). Mechanism of the B (C6F5) 3-catalyzed reaction of silyl hydrides with alkoxysilanes. Kinetic and spectroscopic studies. *Organometallics, 24*(25), 6077-6084.

Chuang, M.-K., Lin, S.-W., Chen, F.-C., Chu, C.-W., & Hsu, C.-S. (2014). Gold nanoparticle-decorated graphene oxides for plasmonic-enhanced polymer photovoltaic devices. *Nanoscale, 6*(3), 1573-1579.

Clarke, C. J., Tu, W.-C., Levers, O., Brohl, A., & Hallett, J. P. (2018). Green and sustainable solvents in chemical processes. *Chemical reviews, 118*(2), 747-800.

Corma, A., & Garcia, H. (2008). Supported gold nanoparticles as catalysts for organic reactions. *Chemical Society Reviews, 37*(9), 2096-2126.

Corma, A., González-Arellano, C., Iglesias, M., & Sanchez, F. (2007). Gold nanoparticles and gold (III) complexes as general and selective hydrosilylation catalysts. *Angewandte Chemie International Edition, 46*(41), 7820-7822.

Cowper, C. J., & Derose, A. J. (2013). *The analysis of gases by chromatography*: Elsevier.

Daniel, M.-C., & Astruc, D. (2004). Gold nanoparticles: assembly, supramolecular chemistry, quantum-size-related properties, and applications toward biology, catalysis, and nanotechnology. *Chemical reviews, 104*(1), 293-346.

Davies, D., Verde, M., Mnyshenko, O., Chen, Y., Rajeev, R., Meng, Y., & Elliott, G. (2019). Combined economic and technological evaluation of battery energy storage for grid applications. *Nat. Energy., 4*(1), 42.

Della Pina, C., Falletta, E., & Rossi, M. (2012). Update on selective oxidation using gold. *Chemical Society Reviews, 41*(1), 350-369.

Deraedt, C., Salmon, L., Gatard, S., Ciganda, R., Hernandez, R., Ruiz, J., & Astruc, D. (2014). Sodium borohydride stabilizes very active gold nanoparticle catalysts. *Chemical Communications, 50*(91), 14194-14196.

Detector, T. C. Hydrogen Detection with a TCD using Mixed Carrier Gas on the Agilent Micro GC. *Signal, 1*(R2), R3.

Dheyab, M. A., Aziz, A. A., Jameel, M. S., Khaniabadi, P. M., & Mehrdel, B. (2021). Sonochemical-assisted synthesis of highly stable gold nanoparticles catalyst for decoloration of methylene blue dye. *Inorganic Chemistry Communications, 127*, Article#108551.

Ding, M., Tang, Y., & Star, A. (2013). Understanding Interfaces in Metal–Graphitic Hybrid Nanostructures. *J. Phys. Chem. Lett., 4*(1), 147-160.

Dreyer, D. R., Todd, A. D., & Bielawski, C. W. (2014). Harnessing the chemistry of graphene oxide. *Chemical Society Reviews, 43*(15), 5288-5301.

Drisko, G. L., & Sanchez, C. (2012). Hybridization in materials science–evolution, current state, and future aspirations. *European Journal of Inorganic Chemistry, 2012*(32), 5097-5105.

Eigler, S., & Hirsch, A. (2014). Chemistry with graphene and graphene oxide—challenges for synthetic chemists. *Angewandte Chemie International Edition, 53*(30), 7720-7738.

Elbushra, H., Ahmed, M., Wardi, H., & Eassa, N. (2018). Synthesis and characterization of TiO2 using sol-gel method at different annealing temperatures. *MRS Advances, 3*(42-43), 2527-2535.

Elias, D. C., Nair, R. R., Mohiuddin, T., Morozov, S., Blake, P., Halsall, M., . . . Geim, A. (2009). Control of graphene's properties by reversible hydrogenation: evidence for graphane. *Science, 323*(5914), 610-613.

Emiru, T. F., & Ayele, D. W. (2017). Controlled synthesis, characterization and reduction of graphene oxide: A convenient method for large scale production. *Egyptian Journal of Basic and Applied Sciences, 4*(1), 74-79.

Esposito, S. (2019). "Traditional" sol-gel chemistry as a powerful tool for the preparation of supported metal and metal oxide catalysts. *Materials, 12*(4), 668.

Feng, S. H., & Li, G. H. (2017). Chapter 4 - Hydrothermal and Solvothermal Syntheses. In R. Xu & Y. Xu (Eds.), *Modern Inorganic Synthetic Chemistry (Second Edition)* (pp. 73-104). Amsterdam: Elsevier.

Ferrari, A. C., Bonaccorso, F., Fal'Ko, V., Novoselov, K. S., Roche, S., Bøggild, P., . . . Pugno, N. (2015). Science and technology roadmap for graphene, related two-dimensional crystals, and hybrid systems. *Nanoscale, 7*(11), 4598-4810.

Fleming, I., Roberts, R. S., & Smith, S. C. (1998). The preparation and analysis of the phenyldimethylsilyllithium reagent and its reaction with silyl enol ethers. *Journal of the Chemical Society, Perkin Transactions 1*(7), 1209-1214.

Fritz-Langhals, E., Werge, S., Kneissl, S., & Piroutek, P. (2020). Novel Si (II)+ and Ge (II)+ Compounds as Efficient Catalysts in Organosilicon Chemistry: Siloxane Coupling Reaction. *Organic Process Research & Development, 24*(8), 1484-1495.

Ganesh, M., & Ramakrishna, J. (2020). Synthetic Organic Transformations of Transition-Metal Nanoparticles as Propitious Catalysts: A Review. *Asian Journal of Organic Chemistry, 9*(10), 1341-1376.

García, C. P., Sumbayev, V., Gilliland, D., Yasinska, I. M., Gibbs, B. F., Mehn, D., . . . Rossi, F. (2013). Microscopic analysis of the interaction of gold nanoparticles with cells of the innate immune system. *Scientific reports, 3*(1), 1-7.

Glosz, K., Stolarczyk, A., & Jarosz, T. (2020). Siloxanes—Versatile Materials for Surface Functionalisation and Graft Copolymers. *International Journal of Molecular Sciences, 21*(17), Article#6387.

Goncalves, G., Marques, P. A., Granadeiro, C. M., Nogueira, H. I., Singh, M., & Gracio, J. (2009). Surface modification of graphene nanosheets with gold nanoparticles: the role of oxygen moieties at graphene surface on gold nucleation and growth. *Chemistry of Materials, 21*(20), 4796-4802.

Gondal, M. A., Ilyas, A. M., Fasasi, T. A., Dastageer, M. A., Seddigi, Z. S., Qahtan, T. F., . . . Khattak, G. D. (2015). Synthesis of green TiO2/ZnO/CdS hybrid nano-catalyst for efficient light harvesting using an elegant pulsed laser ablation in liquids method. *Appl Surf Sci., 357*, 2217-2222.

Gosens, I., Post, J. A., de la Fonteyne, L. J., Jansen, E. H., Geus, J. W., Cassee, F. R., & de Jong, W. H. (2010). Impact of agglomeration state of nano-and submicron sized gold particles on pulmonary inflammation. *Particle and fibre toxicology, 7*(1), 1-11.

Govindhan, M., & Chen, A. (2015). Simultaneous synthesis of gold nanoparticle/graphene nanocomposite for enhanced oxygen reduction reaction. *Journal of Power Sources, 274*, 928-936.

Gryparis, C., & Stratakis, M. (2012). Gold nanoparticles-catalyzed activation of 1, 2-disilanes: hydrolysis, silyl protection of alcohols and reduction of tert-benzylic alcohols. *Chemical Communications, 48*(87), 10751-10753.

Gualco, P., Ladeira, S., Miqueu, K., Amgoune, A., & Bourissou, D. (2012). Gold-Mediated Insertion of Oxygen into Silicon–Silicon Bond: An Original Au (I)/Au (III) Redox Sequence. *Organometallics, 31*(17), 6001-6004.

Gualteros, J. A., Garcia, M. A., da Silva, A. G., Rodrigues, T. S., Cândido, E. G., Fonseca, F. C., . . . de Moura, C. V. (2019). Synthesis of highly dispersed gold nanoparticles on Al2O3, SiO2, and TiO2 for the solvent-free oxidation of benzyl alcohol under low metal loadings. *Journal of Materials Science, 54*(1), 238-251.

Guo, S., Dong, S., & Wang, E. (2010). Three-dimensional Pt-on-Pd bimetallic nanodendrites supported on graphene nanosheet: facile synthesis and used as an advanced nanoelectrocatalyst for methanol oxidation. *ACS nano, 4*(1), 547-555.

Guo, Y., Yang, X., Ruan, K., Kong, J., Dong, M., Zhang, J., . . . Guo, Z. (2019). Reduced graphene oxide heterostructured silver nanoparticles significantly enhanced thermal conductivities in hot-pressed electrospun polyimide nanocomposites. *ACS applied materials & interfaces, 11*(28), 25465-25473.

Guria, M. K., Majumdar, M., & Bhattacharyya, M. (2016). Green synthesis of protein capped nano-gold particle: an excellent recyclable nano-catalyst for the reduction of nitro-aromatic pollutants at higher concentration. *Journal of Molecular Liquids, 222*, 549-557.

Guzman, J., Carrettin, S., Fierro-Gonzalez, J. C., Hao, Y., Gates, B. C., & Corma, A. (2005). CO Oxidation Catalyzed by Supported Gold: Cooperation between Gold

and Nanocrystalline Rare-Earth Supports Forms Reactive Surface Superoxide and Peroxide Species. *Angewandte Chemie, 117*(30), 4856-4859.

Hackel, T., & McGrath, N. A. (2019). Tris (pentafluorophenyl) borane-catalyzed reactions using silanes. *Molecules, 24*(3), 432.

Haider, A. J., Shabeeb, D. A., & Mohammed, A. T. (2016). Synthesis and stabilization of gold nanoparticles by inverse reduction method using sodium citrate and sodium boro hydride as reducing agent. *Journal of university of Anbar for Pure science, 10*(1).

Halilu, A., Ali, T. H., Atta, A. Y., Sudarsanam, P., Bhargava, S. K., & Abd Hamid, S. B. (2016). Highly selective hydrogenation of biomass-derived furfural into furfuryl alcohol using a novel magnetic nanoparticles catalyst. *Energy & Fuels, 30*(3), 2216-2226.

Halilu, A., Hussein Ali, T., Sudarsanam, P., & Bhargava, S. K. (2019). Synthesis of Fuel Grade Molecules from Hydroprocessing of Biomass-Derived Compounds Catalyzed by Magnetic Fe (NiFe)O_4-SiO_2 Nanoparticles. *Symmetry, 11*(4), 524.

Han, J., Zhuo, Y., Chai, Y. Q., Mao, L., Yuan, Y. L., & Yuan, R. (2011). Highly conducting gold nanoparticles-graphene nanohybrid films for ultrasensitive detection of carcinoembryonic antigen. *Talanta, 85*(1), 130-135.

Hareesh, K., P Joshi, R., N Bhoraskar, V., & D Dhole, S. (2017). Catalytic reduction of 4-nitrophenol by gamma radiation assisted synthesized Au-rGO nanocomposite. *Advanced Materials Letters, 8*(3), 251-255.

Hareesh, K., Williams, J., Dhole, N., Kodam, K., Bhoraskar, V., & Dhole, S. (2016). Bio-green synthesis of Ag–GO, Au–GO and Ag–Au–GO nanocomposites using Azadirachta indica: its application in SERS and cell viability. *Materials Research Express, 3*(7), Article#075010.

Haruta, M. (2003). When gold is not noble: catalysis by nanoparticles. *The Chemical Record, 3*(2), 75-87.

Haruta, M., & Daté, M. (2001). Advances in the catalysis of Au nanoparticles. *Applied Catalysis A: General, 222*(1-2), 427-437.

Hattori, H. (2001). Solid base catalysts: generation of basic sites and application to organic synthesis. *Applied Catalysis A: General, 222*(1-2), 247-259.

Herizchi, R., Abbasi, E., Milani, M., & Akbarzadeh, A. (2016). Current methods for synthesis of gold nanoparticles. *Artificial cells, nanomedicine, and biotechnology, 44*(2), 596-602.

Hernandez, A. G., Cooper-Searle, S., Skelton, A. C., & Cullen, J. M. (2018). Leveraging material efficiency as an energy and climate instrument for heavy industries in the EU. *Energy Policy, 120*, 533-549.

Hu, Y. J., Jin, J. A., Wu, P., Zhang, H., & Cai, C. X. (2010). Graphene-gold nanostructure composites fabricated by electrodeposition and their electrocatalytic activity

toward the oxygen reduction and glucose oxidation. *Electrochimica Acta, 56*(1), 491-500.

Huang, C.-J., Chiu, P.-H., Wang, Y.-H., Chen, K.-L., Linn, J.-J., & Yang, C.-F. (2006). Electrochemically controlling the size of gold nanoparticles. *Journal of The Electrochemical Society, 153*(12), D193.

Huang, L., Zhang, Y., & Wei, H. (2014). Role of the Isolable Hydride Intermediate in the Hydrosilylation of Carbonyl Compounds Catalyzed by the High-Valent Mono-Oxido–Rhenium (V) Complex. *European Journal of Inorganic Chemistry, 2014*(33), 5714-5723.

Humans, I. W. G. o. t. E. o. C. R. t. (2013). Some chemicals present in industrial and consumer products, food and drinking-water. *IARC monographs on the evaluation of carcinogenic risks to humans, 101*, 9.

Huo, Y.-j., Yao, F.-f., & Ma, Y.-s. (2017). Catalytic Performance of Graphite Oxide Supported Au Nanoparticles in Aerobic Oxidation of Benzyl Alcohol: Support Effect. *Chinese Journal of Chemical Physics, 30*(1), 90.

Hussain, M. H., Abu Bakar, N. F., Mustapa, A. N., Low, K. F., Othman, N. H., & Adam, F. (2020). Synthesis of Various Size Gold Nanoparticles by Chemical Reduction Method with Different Solvent Polarity. *Nanoscale Res Lett, 15*(1), 140.

Hutchings, G. J., & Haruta, M. (2005). A golden age of catalysis: a perspective. *Applied Catalysis A: General, 291*(1-2), 2-5.

Iroh, J. O., Zhu, Y., Shah, K., Levine, K., Rajagopalan, R., Uyar, T., . . . Khramov, A. N. (2003). Electrochemical synthesis: a novel technique for processing multi-functional coatings. *PROG ORG COAT, 47*(3), 365-375.

Ishida, T., Murayama, T., Taketoshi, A., & Haruta, M. (2019). Importance of size and contact structure of gold nanoparticles for the genesis of unique catalytic processes. *Chemical reviews, 120*(2), 464-525.

Ison, E. A., Corbin, R. A., & Abu-Omar, M. M. (2005). Hydrogen production from hydrolytic oxidation of organosilanes using a cationic oxorhenium catalyst. *Journal of the American Chemical Society, 127*(34), 11938-11939.

Ito, H., Yajima, T., Tateiwa, J.-i., & Hosomi, A. (2000). First gold complex-catalysed selective hydrosilylation of organic compoundsStudies on Organosilicon Chemistry: no. 152. For no. 151, see K. Miura, K. Tamaki, T. Nakagawa and A. Hosomi, Angew. Chem., Int. Ed., 2000, in press. *Chemical Communications*(11), 981-982.

Jana, N. R., Gearheart, L., & Murphy, C. J. (2001). Seeding Growth for Size Control of 5−40 nm Diameter Gold Nanoparticles. *Langmuir, 17*(22), 6782-6786.

Ji, D., Xi, N., Li, G., Dong, P., Li, H., Li, H., . . . Zhao, Y. (2021). Hydrotalcite-based CoxNiyAl1Ox mixed oxide as a highly efficient catalyst for selective ethylbenzene oxidation. *Molecular Catalysis, 508*, Article#111579.

Jingyue, Z., & Bernd, F. (2015). Synthesis of gold nanoparticles via chemical reduction methods. *Proceedings of the Nanocon, Brno, Czech Republic*, 14-16.

John, J., Gravel, E., Hagège, A., Li, H., Gacoin, T., & Doris, E. (2011). Catalytic oxidation of silanes by carbon nanotube–gold nanohybrids. *Angewandte Chemie International Edition, 50*(33), 7533-7536.

Kalchauer, W., & Pachaly, B. (2008). M üller–R ochow Synthesis: The Direct Process to Methylchlorosilanes. *Handbook of Heterogeneous Catalysis: Online*, 2635-2647.

Kar, P., Sardar, S., Liu, B., Sreemany, M., Lemmens, P., Ghosh, S., & Pal, S. K. (2016). Facile synthesis of reduced graphene oxide–gold nanohybrid for potential use in industrial waste-water treatment. *Science and Technology of advanced MaTerialS, 17*(1), 375-386.

Karthikeyan, P., Kumar, S. S., Jagadeesh, R. V., & Bhagat, P. R. (2012). Solvent Free Synthesis of Substituted-2-Pyrazolines Using Imidazolium Based Ionic Liquid as a Solvent and Catalyst: A Green Route Approach. *Asian Journal of Chemistry, 24*(3).

Kenny, S. L., & Venable, S. L. (2011). *Gold: a cultural encyclopedia*: ABC-CLIO.

Ketabchi, E., Pastor-Pérez, L., Arellano-García, H., & Reina, T. R. (2020). Influence of reaction parameters on the catalytic upgrading of an Acetone, Butanol, and Ethanol (ABE) mixture: Exploring new routes for modern biorefineries. *Frontiers in chemistry, 7*, 906.

Khalil, I., Julkapli, N. M., Yehye, W. A., Basirun, W. J., & Bhargava, S. K. (2016). Graphene–gold nanoparticles hybrid—synthesis, functionalization, and application in a electrochemical and surface-enhanced raman scattering biosensor. *Materials, 9*(6), 406.

Khan, M., Shaik, M. R., Adil, S. F., Kuniyil, M., Ashraf, M., Frerichs, H., . . . Labis, J. P. (2020). Facile synthesis of Pd@ graphene nanocomposites with enhanced catalytic activity towards Suzuki coupling reaction. *Scientific reports, 10*(1), 1-14.

Kimling, J., Maier, M., Okenve, B., Kotaidis, V., Ballot, H., & Plech, A. (2006). Turkevich method for gold nanoparticle synthesis revisited. *The Journal of Physical Chemistry B, 110*(32), 15700-15707.

Koga, H., Kitaoka, T., & Isogai, A. (2011). Development of cellulose nanofiber/metal nanohybrid catalyst. *Polymer Preprints, Japan, 60m*, 4330-4330.

Koledina, K., Koledin, S., Karpenko, A., Gubaydullin, I., & Vovdenko, M. (2019). Multi-objective optimization of chemical reaction conditions based on a kinetic model. *Journal of Mathematical Chemistry, 57*(2), 484-493.

Komiyama, T., Minami, Y., & Hiyama, T. (2017). Recent advances in transition-metal-catalyzed synthetic transformations of organosilicon reagents. *ACS Catalysis, 7*(1), 631-651.

Krishnamurthy, S., Esterle, A., Sharma, N. C., & Sahi, S. V. (2014). Yucca-derived synthesis of gold nanomaterial and their catalytic potential. *Nanoscale research letters, 9*(1), 627.

Kuciński, K., Stachowiak-Dłużyńska, H., & Hreczycho, G. (2022). Catalytic silylation of O–nucleophiles via Si–H or Si–C bond cleavage: A route to silyl ethers, silanols and siloxanes. *Coordination Chemistry Reviews, 459*, Article#214456.

Lancaster, M. (2020). *Green chemistry: an introductory text*: Royal society of chemistry.

Lazar, O.-A., Marinoiu, A., Raceanu, M., Pantazi, A., Mihai, G., Varlam, M., & Enachescu, M. (2020). Reduced Graphene Oxide Decorated with Dispersed Gold Nanoparticles: Preparation, Characterization and Electrochemical Evaluation for Oxygen Reduction Reaction. *Energies, 13*(17), Article#4307.

Lee, A. Y., Yang, K., Anh, N. D., Park, C., Lee, S. M., Lee, T. G., & Jeong, M. S. (2021). Raman study of D* band in graphene oxide and its correlation with reduction. *Applied Surface Science, 536*, Article#147990.

Lewis, K. M., & Rethwisch, D. G. (1993). *Catalyzed direct reactions of silicon*: Elsevier.

Li, Y., Wu, J., Qian, K., Zhang, X., Wan, J., Wang, Y., & Liu, B. (2014). *Janus graphene hybrids: 2D monodispersed gold nanoarrays on graphene with controlled structure and high stability.* Paper presented at the Manipulation, Manufacturing and Measurement on the Nanoscale (3M-NANO), 2014 International Conference on.

Li, Z., Xu, X., & Zhang, X. (2015). Oxidation of Organosilanes with Nanoporous Copper as a Sustainable Non-Noble-Metal Catalyst. *ChemPhysChem, 16*(8), 1603-1606.

Liu, L. H., Metivier, R., Wang, S. F., & Wang, H. (2012). Advanced Nanohybrid Materials: Surface Modification and Applications. *J Nanomater.* , 2.

Liu, W., & Speranza, G. (2021). Tuning the oxygen content of reduced graphene oxide and effects on its properties. *ACS omega, 6*(9), 6195-6205.

Lohse, S. E., Eller, J. R., Sivapalan, S. T., Plews, M. R., & Murphy, C. J. (2013). A simple millifluidic benchtop reactor system for the high-throughput synthesis and functionalization of gold nanoparticles with different sizes and shapes. *ACS Nano, 7*(5), 4135-4150.

Loupy, A. (1999). Solvent-free reactions. In *Modern Solvents in Organic Synthesis* (pp. 153-207): Springer.

Loza, K., Heggen, M., & Epple, M. (2020). Synthesis, structure, properties, and applications of bimetallic nanoparticles of noble metals. *Advanced functional materials, 30*(21), Article#1909260.

Luty-Błocho, M., Fitzner, K., Hessel, V., Löb, P., Maskos, M., Metzke, D., . . . Wojnicki, M. (2011). Synthesis of gold nanoparticles in an interdigital micromixer using ascorbic acid and sodium borohydride as reducers. *Chemical Engineering Journal, 171*(1), 279-290.

Lv, H., Laishram, R. D., Li, J., Shi, G., Sun, W., Xu, J., . . . Fan, B. (2019). Nickel (0) catalyzed oxidation of organosilanes to disiloxanes by air as an oxidant. *Tetrahedron Letters, 60*(14), 971-974.

Lyons, T. W., & Sanford, M. S. (2010). Palladium-catalyzed ligand-directed C− H functionalization reactions. *Chemical reviews, 110*(2), 1147-1169.

Mahyari, M., Shaabani, A., & Bide, Y. (2013). Gold nanoparticles supported on supramolecular ionic liquid grafted graphene: a bifunctional catalyst for the selective aerobic oxidation of alcohols. *RSC Adv., 3*(44), 22509-22517.

Manikandan, B., Endo, T., Kaneko, S., Murali, K., & John, R. (2018). Properties of sol gel synthesized ZnO nanoparticles. *Journal of Materials Science: Materials in Electronics, 29*(11), 9474-9485.

Marcano, D. C., Kosynkin, D. V., Berlin, J. M., Sinitskii, A., Sun, Z., Slesarev, A., . . . Tour, J. M. (2010). Improved synthesis of graphene oxide. *ACS nano, 4*(8), 4806-4814.

Marciniec, B., Gulinski, J., & Urbaniak, W. (1992). ZW Kornetka in Comprehensive Handbook on Hydrosilylation. In: Pergamon Press, Oxford.

Marinoiu, A., Raceanu, M., Andrulevicius, M., Tamuleviciene, A., Tamulevicius, T., Nica, S., . . . Varlam, M. (2020). Low-cost preparation method of well dispersed gold nanoparticles on reduced graphene oxide and electrocatalytic stability in PEM fuel cell. *Arabian Journal of Chemistry, 13*(1), 3585-3600.

Mashayekhi, N. A., Kung, M. C., & Kung, H. H. (2014). Selective oxidation of hydrocarbons on supported Au catalysts. *Catalysis today, 238*, 74-79.

Merhari, L. (2009). *Hybrid nanocomposites for nanotechnology*: Springer.

Mézailles, N., Maigrot, N., Hamon, S., Ricard, L., Mathey, F., & Le Floch, P. (2001). Mixed phosphinine-ether macrocycles. *The Journal of Organic Chemistry, 66*(3), 1054-1056.

Mitsudome, T., Noujima, A., Mizugaki, T., Jitsukawa, K., & Kaneda, K. (2009). Supported gold nanoparticle catalyst for the selective oxidation of silanes to silanols in water. *Chemical Communications*(35), 5302-5304.

Mittal, A. K., Chisti, Y., & Banerjee, U. C. (2013). Synthesis of metallic nanoparticles using plant extracts. *Biotechnology advances, 31*(2), 346-356.

Mohan, J. C., Praveen, G., Chennazhi, K., Jayakumar, R., & Nair, S. (2013). Functionalised gold nanoparticles for selective induction of in vitro apoptosis among human cancer cell lines. *Journal of Experimental Nanoscience, 8*(1), 32-45.

Morimoto, N., Kubo, T., & Nishina, Y. (2016). Tailoring the Oxygen Content of Graphite and Reduced Graphene Oxide for Specific Applications. *Scientific Reports, 6*, 21715.

Naeimi, H., & Farahnak Zarabi, M. (2018). Gold nanoparticles supported on thiol-functionalized reduced graphene oxide as effective recyclable catalyst for synthesis of tetrahydro-4H-chromenes in aqueous media. *Applied Organometallic Chemistry, 32*(4), Article#e4225.

Nandiyanto, A. B. D., Oktiani, R., & Ragadhita, R. (2019). How to read and interpret FTIR spectroscope of organic material. *Indonesian Journal of Science and Technology, 4*(1), 97-118.

Nasrollahzadeh, M., Issaabadi, Z., Tohidi, M. M., & Mohammad Sajadi, S. (2018). Recent progress in application of graphene supported metal nanoparticles in C− C and C− X coupling reactions. *The Chemical Record, 18*(2), 165-229.

Nazari, S., & Shabanian, M. (2014). Novel heterocyclic semi-aromatic polyamides: synthesis and characterization. *Designed Monomers and Polymers, 17*(1), 33-39.

Neto, B. A. D., Eberlin, M. N., & Sherwood, J. (2022). Solvent Screening Is Not Solvent Effect: A Review on the Most Neglected Aspect of Multicomponent Reactions. *European Journal of Organic Chemistry*, Article#e202200172.

Obireddy, S. R., & Lai, W.-F. (2021). Multi-component hydrogel beads incorporated with reduced graphene oxide for ph-responsive and controlled co-delivery of multiple agents. *Pharmaceutics, 13*(3), 313.

Ojea-Jiménez, I., Bastús, N. G., & Puntes, V. (2011). Influence of the sequence of the reagents addition in the citrate-mediated synthesis of gold nanoparticles. *The Journal of Physical Chemistry C, 115*(32), 15752-15757.

Okpala, C. C. (2013). Nanocomposites–an overview. *Int. J. Eng. Res. Dev., 8*(11), 17-23.

Okuhara, T. (2002). Water-tolerant solid acid catalysts. *Chemical reviews, 102*(10), 3641-3666.

Okumura, M., Akita, T., Haruta, M., Wang, X., Kajikawa, O., & Okada, O. (2003). Multi-component noble metal catalysts prepared by sequential deposition precipitation for low temperature decomposition of dioxin. *Applied Catalysis B: Environmental, 41*(1-2), 43-52.

Oznuluer, T., Pince, E., Polat, E. O., Balci, O., Salihoglu, O., & Kocabas, C. (2011). Synthesis of graphene on gold. *Applied Physics Letters, 98*(18), Article#183101.

Pal, B., Rana, S., & Kaur, R. (2015). Influence of different reducing agents on the Ag nanostructures and their electrokinetic and catalytic properties. *Journal of Nanoscience and Nanotechnology, 15*(4), 2753-2760.

Panchakarla, L., Subrahmanyam, K., Saha, S., Govindaraj, A., Krishnamurthy, H., Waghmare, U., & Rao, C. (2009). Synthesis, structure, and properties of boron- and nitrogen-doped graphene. *Advanced Materials, 21*(46), 4726-4730.

Papiya, F., Das, S., Pattanayak, P., & Kundu, P. P. (2019). The fabrication of silane modified graphene oxide supported Ni–Co bimetallic electrocatalysts: a catalytic

system for superior oxygen reduction in microbial fuel cells. *International Journal of Hydrogen Energy, 44*(47), 25874-25893.

Park, J.-E., Atobe, M., & Fuchigami, T. (2006). Synthesis of multiple shapes of gold nanoparticles with controlled sizes in aqueous solution using ultrasound. *Ultrasonics Sonochemistry, 13*(3), 237-241.

Park, M., Kim, N., Lee, J., Gu, M., & Kim, B.-S. (2021). Versatile graphene oxide nanosheets via covalent functionalization and their applications. *Materials Chemistry Frontiers, 5*(12), 4424-4444.

Pascanu, V., González Miera, G., Inge, A. K., & Martín-Matute, B. (2019). Metal–organic frameworks as catalysts for organic synthesis: a critical perspective. *Journal of the American Chemical Society, 141*(18), 7223-7234.

Pattanaik, S., & Gunanathan, C. (2019). Cobalt-catalyzed selective synthesis of disiloxanes and hydrodisiloxanes. *ACS Catalysis, 9*(6), 5552-5561.

Pocklanova, R., Rathi, A. K., Gawande, M. B., Datta, K. K. R., Ranc, V., Cepe, K., . . . Zboril, R. (2016). Gold nanoparticle-decorated graphene oxide: synthesis and application in oxidation reactions under benign conditions. *Journal of Molecular Catalysis A: Chemical, 424*, 121-127.

Prins, R. (2012). Hydrogen spillover. Facts and fiction. *Chemical reviews, 112*(5), 2714-2738.

Radich, J. G., & Kamat, P. V. (2013). Making Graphene Holey. Gold-Nanoparticle-Mediated Hydroxyl Radical Attack on Reduced Graphene Oxide. *ACS Nano, 7*(6), 5546-5557.

Radwan, M. A., & Abbas, E. M. (2009). Synthesis of some pyridine, thiopyrimidine, and isoxazoline derivatives based on the pyrrole moiety. *Monatshefte für Chemie-Chemical Monthly, 140*(2), 229-233.

Rajkumar, C., Thirumalraj, B., Chen, S.-M., & Palanisamy, S. (2016). Novel electrochemical preparation of gold nanoparticles decorated on a reduced graphene oxide–fullerene composite for the highly sensitive electrochemical detection of nitrite. *RSC Advances, 6*(73), 68798-68805.

Rao, B. G., Mukherjee, D., & Reddy, B. M. (2017). Chapter 1 - Novel approaches for preparation of nanoparticles. In D. Ficai & A. M. Grumezescu (Eds.), *Nanostructures for Novel Therapy* (pp. 1-36): Elsevier.

Redón, R., García-Peña, N. G., & Ocampo-Bravo, C. C. (2021). Leaching of Atoms, Clusters, and Nanoparticles. *Recent Patents on Nanotechnology, 15*(2), 125-141.

Rodriguez-Reinoso, F. (1998). The role of carbon materials in heterogeneous catalysis. *Carbon, 36*(3), 159-175.

Rothenberg, G. (2017). *Catalysis: concepts and green applications*: John Wiley & Sons.

Roy, A. K. (2007). A review of recent progress in catalyzed homogeneous hydrosilation (hydrosilylation). *Advances in organometallic chemistry, 55*, 1-59.

Sachdeva, H. (2020). Recent advances in the catalytic applications of GO/rGO for green organic synthesis. *Green Processing and Synthesis, 9*(1), 515-537.

Saha, S., Basak, V., Dasgupta, A., Ganguly, S., Banerjee, D., & Kargupta, K. (2014). Graphene supported bimetallic G-Co-Pt nanohybrid catalyst for enhanced and cost effective hydrogen generation. *International Journal of Hydrogen Energy, 39*(22), 11566-11577.

Sajiki, H., Ito, N., Esaki, H., Maesawa, T., Maegawa, T., & Hirota, K. (2005). Aromatic ring favorable and efficient H–D exchange reaction catalyzed by Pt/C. *Tetrahedron Letters, 46*(41), 6995-6998.

Samantara, A. K., Tripathy, R. K., & Behera, J. (2021). Hybrid nanocomposites based on graphene and gold nanoparticles: From preparation to applications. In *Graphene and Nanoparticles Hybrid Nanocomposites* (pp. 197-211): Springer.

Saquib, M., & Halder, A. (2018). Reduced graphene oxide supported gold nanoparticles for electrocatalytic reduction of carbon dioxide. *Journal of Nanoparticle Research, 20*, 1-12.

Sawama, Y., Masuda, M., Yasukawa, N., Nakatani, R., Nishimura, S., Shibata, K., . . . Takagi, Y. (2016). Disiloxane Synthesis Based on Silicon–Hydrogen Bond Activation using Gold and Platinum on Carbon in Water or Heavy Water. *The Journal of Organic Chemistry, 81*(10), 4190-4195.

Sekhar, K. V. G. C., Sasank, T. V. N. V. T., Nagesh, H. N., Suresh, N., Naidu, K. M., & Suresh, A. (2013). Synthesis of 3, 5-diarylisoxazoles under solvent-free conditions using iodobenzene diacetate. *Chinese Chemical Letters, 24*(12), 1045-1048.

Shang, L., Bian, T., Zhang, B., Zhang, D., Wu, L. Z., Tung, C. H., . . . Zhang, T. (2014). Graphene-supported ultrafine metal nanoparticles encapsulated by mesoporous silica: robust catalysts for oxidation and reduction reactions. *Angewandte Chemie, 126*(1), 254-258.

Shao, L., Huang, X., Teschner, D., & Zhang, W. (2014). Gold supported on graphene oxide: an active and selective catalyst for phenylacetylene hydrogenations at low temperatures. *ACS Catalysis, 4*(7), 2369-2373.

Sharma, S., & Sharma, A. (2009). Solvent Free Synthesis of New-1-acetyl-3-(4-fluoronaphthyl)-5-substituted Aryl Pyrazolines as Spermicides. *ChemInform, 40*(12), Article#no-no.

Sheldon, R. A. (2018). Metrics of green chemistry and sustainability: past, present, and future. *ACS Sustainable Chemistry & Engineering, 6*(1), 32-48.

Siddiqui, Z. N., Musthafa, T. M., Ahmad, A., & Khan, A. U. (2011). Thermal solvent-free synthesis of novel pyrazolyl chalcones and pyrazolines as potential

antimicrobial agents. *Bioorganic & medicinal chemistry letters, 21*(10), 2860-2865.

Singh, M., Kalaivani, R., Manikandan, S., Sangeetha, N., & Kumaraguru, A. (2013). Facile green synthesis of variable metallic gold nanoparticle using Padina gymnospora, a brown marine macroalga. *Applied Nanoscience, 3*(2), 145-151.

Sinkó, K. (2010). Influence of chemical conditions on the nanoporous structure of silicate aerogels. *Materials, 3*(1), 704-740.

Son, S., Nunes, J. F., Shin, Y., Lee, J., & Casiraghi, C. (2018). The roughening kinetics of hydrogenated graphene. *Scientific Reports, 8*(1), Article#8771.

Song, Y., Li, X., Song, Y., Cheng, Z., Zhong, H., Xu, J., . . . Wu, F. (2013). Electrochemical synthesis of gold nanoparticles on the surface of multi-walled carbon nanotubes with glassy carbon electrode and their application. *Russian Journal of Physical Chemistry A, 87*(1), 74-79.

Sridhar, M., Ramanaiah, B. C., Narsaiah, C., Swamy, M. K., Mahesh, B., & Reddy, M. K. K. (2009). An efficient and simple method for the preparation of symmetrical disiloxanes from hydrosilanes by Lewis acid-catalyzed air oxidation. *Tetrahedron Letters, 50*(51), 7166-7168.

Stegelmann, C., Schiødt, N. C., Campbell, C. T., & Stoltze, P. (2004). Microkinetic modeling of ethylene oxidation over silver. *Journal of Catalysis, 221*(2), 630-649.

Stein, J., Lettko, K. X., King, J. A., & Colborn, R. E. (1994). New routes to phenylsilicones. *Journal of applied polymer science, 51*(5), 815-822.

Suchorski, Y., & Drachsel, W. (2007). Catalytic reactions on platinum nanofacets: bridging the size and complexity gap. *Topics in Catalysis, 46*(1), 201-215.

Sudhakar, S., & Santhosh, P. B. (2017). Chapter Six - Gold Nanomaterials: Recent Advances in Cancer Theranostics. In A. Iglič, A. Garcia-Sáez, & M. Rappolt (Eds.), *Advances in Biomembranes and Lipid Self-Assembly* (Vol. 25, pp. 161-180): Academic Press.

Sun, Y., Mayers, B. T., & Xia, Y. (2002). Template-engaged replacement reaction: a one-step approach to the large-scale synthesis of metal nanostructures with hollow interiors. *Nano Letters, 2*(5), 481-485.

Takei, T., Akita, T., Nakamura, I., Fujitani, T., Okumura, M., Okazaki, K., . . . Haruta, M. (2012). Heterogeneous catalysis by gold. In *Advances in catalysis* (Vol. 55, pp. 1-126): Elsevier.

Tanaka, K., & Toda, F. (2000). Solvent-Free Organic Reactions. *Chem. Rev, 100*, 1025-1074.

Tang, L., Li, X., Ji, R., Teng, K. S., Tai, G., Ye, J., . . . Lau, S. P. (2012). Bottom-up synthesis of large-scale graphene oxide nanosheets. *Journal of Materials Chemistry, 22*(12), 5676-5683.

Tene, T., Tubon Usca, G., Guevara, M., Molina, R., Veltri, F., Arias, M., . . . Vacacela Gomez, C. (2020). Toward large-scale production of oxidized graphene. *Nanomaterials, 10*(2), 279.

Toshima, N., Kuriyama, M., Yamada, Y., & Hirai, H. (1981). Colloidal platinum catalyst for light-induced hydrogen evolution from water. A particle size effect. *Chemistry Letters, 10*(6), 793-796.

Tran, T. D., Nguyen, M. T., Le, H. V., Nguyen, D. N., Truong, Q. D., & Tran, P. D. (2018). Gold nanoparticles as an outstanding catalyst for the hydrogen evolution reaction. *Chemical Communications, 54*(27), 3363-3366.

Turcheniuk, K., Boukherroub, R., & Szunerits, S. (2015). Gold–graphene nanocomposites for sensing and biomedical applications. *Journal of Materials Chemistry B, 3*(21), 4301-4324.

Vasilikogiannaki, E., Titilas, I., Gryparis, C., Louka, A., Lykakis, I. N., & Stratakis, M. (2014). Efficient hydrosilylation of carbonyl compounds by 1, 1, 3, 3-tetramethyldisiloxane catalyzed by Au/TiO2. *Tetrahedron, 70*(36), 6106-6113.

Védrine, J. C. (2017). Heterogeneous catalysis on metal oxides. *Catalysts, 7*(11), 341.

Vellaichamy, B., Prakash, P., & Thomas, J. (2018). Synthesis of AuNPs@ RGO nanosheets for sustainable catalysis toward nitrophenols reduction. *Ultrasonics Sonochemistry, 48*, 362-369.

Veziroglu, S., Kuru, M., Ghori, M. Z., Dokan, F. K., Hinz, A. M., Strunskus, T., . . . Aktas, O. C. (2017). Ultra-fast degradation of methylene blue by Au/ZnO-CeO2 nano-hybrid catalyst. *Materials Letters, 209*, 486-491.

Wang, C., Lin, X., Ge, Y., Shah, Z. H., Lu, R., & Zhang, S. (2016). Silica-supported ultra small gold nanoparticles as nanoreactors for the etherification of silanes. *RSC advances, 6*(104), 102102-102108.

Wang, X., Mathis, T. S., Li, K., Lin, Z., Vlcek, L., Torita, T., . . . Sarycheva, A. (2019). Influences from solvents on charge storage in titanium carbide MXenes. *Nat. Energy.*, 1.

Wang, Z. L., Xu, D., Xu, J. J., Zhang, L. L., & Zhang, X. B. (2012). Graphene oxide gel-derived, free-standing, hierarchically porous carbon for high-capacity and high-rate rechargeable Li-O2 batteries. *Advanced functional materials, 22*(17), 3699-3705.

Wen, M. Y. S., Abdullah, A. H., & Ngee, L. H. (2017). Synthesis of ZnO/rGO nanohybrid for improved photocatalytic activity. *Malaysian Journal of Analytical Sciences, 21*(4), 889-900.

Xi, G., Ouyang, S., & Ye, J. (2011). General synthesis of hybrid TiO2 mesoporous "french fries" toward improved photocatalytic conversion of CO2 into hydrocarbon fuel: a case of TiO2/ZnO. *Chem.: Eur. J., 17*(33), 9057-9061.

Xu, S., Man, B., Jiang, S., Wang, J., Wei, J., Xu, S., . . . Li, Z. (2015). Graphene/Cu nanoparticle hybrids fabricated by chemical vapor deposition as surface-enhanced Raman scattering substrate for label-free detection of adenosine. *ACS applied materials interfaces, 7*(20), 10977-10987.

Yamamoto, S.-i., Kinoshita, H., Hashimoto, H., & Nishina, Y. (2014). Facile preparation of Pd nanoparticles supported on single-layer graphene oxide and application for the Suzuki–Miyaura cross-coupling reaction. *Nanoscale, 6*(12), 6501-6505.

Yang, Y., Lei, Q., Li, J., Hong, C., Zhao, Z., Xu, H., & Hu, J. (2022). Synthesis and enhanced electrochemical properties of AuNPs@ MoS2/rGO hybrid structures for highly sensitive nitrite detection. *Microchemical Journal, 172*, Article#106904.

Yang, Y., Zhang, J., Zhang, F., & Guo, S. (2017). Preparation of AuNPs/GQDs/SiO2 Composite and Its Catalytic Performance in Oxidation of Veratryl Alcohol %J Journal of Nanomaterials. *2017*, 8.

Yin, P. T., Shah, S., Chhowalla, M., & Lee, K.-B. (2015). Design, synthesis, and characterization of graphene–nanoparticle hybrid materials for bioapplications. *Chemical reviews, 115*(7), 2483-2531.

Yola, M. L., & Atar, N. (2017). A highly efficient nanomaterial with molecular imprinting polymer: carbon nitride nanotubes decorated with graphene quantum dots for sensitive electrochemical determination of chlorpyrifos. *Journal of The Electrochemical Society, 164*(6), B223-B229.

Yola, M. L., Atar, N., Eren, T., Karimi-Maleh, H., & Wang, S. (2015). Correction: Sensitive and selective determination of aqueous triclosan based on gold nanoparticles on polyoxometalate/reduced graphene oxide nanohybrid. *RSC advances, 5*(89), 72590-72591.

Yola, M. L., Eren, T., Atar, N., Saral, H., & Ermiş, İ. (2016). Direct-methanol fuel cell based on functionalized graphene oxide with mono-metallic and bi-metallic nanoparticles: electrochemical performances of nanomaterials for methanol oxidation. *Electroanalysis, 28*(3), 570-579.

Yoo, W.-J., Ishitani, H., Saito, Y., Laroche, B., & Kobayashi, S. (2020). Reworking organic synthesis for the modern age: Synthetic strategies based on continuous-flow addition and condensation reactions with heterogeneous catalysts. *The Journal of Organic Chemistry, 85*(8), 5132-5145.

Yoshimura, Y., Yasuda, H., Sato, T., Kijima, N., & Kameoka, T. (2001). Sulfur-tolerant Pd-Pt/Yb-USY zeolite catalysts used to reformulate diesel oils. *Applied Catalysis A: General, 207*(1-2), 303-307.

Yousefimehr, F., Jafarirad, S., Salehi, R., & Zakerhamidi, M. S. (2021). Facile fabricating of rGO and Au/rGO nanocomposites using Brassica oleracea var. gongylodes biomass for non-invasive approach in cancer therapy. *Scientific reports, 11*(1), 1-13.

Yu, X., Huo, Y., Yang, J., Chang, S., Ma, Y., & Huang, W. (2013). Reduced graphene oxide supported Au nanoparticles as an efficient catalyst for aerobic oxidation of benzyl alcohol. *Applied Surface Science, 280*, 450-455.

Zabetakis, K., Ghann, W. E., Kumar, S., & Daniel, M.-C. (2012). Effect of high gold salt concentrations on the size and polydispersity of gold nanoparticles prepared by an extended Turkevich–Frens method. *Gold Bulletin, 45*(4), 203-211.

Zangade, S., & Patil, P. (2019). A review on solvent-free methods in organic synthesis. *Current Organic Chemistry, 23*(21), 2295-2318.

Zhang, H., Hines, D., & Akins, D. L. (2014). Synthesis of a nanocomposite composed of reduced graphene oxide and gold nanoparticles. *Dalton Transactions, 43*(6), 2670-2675.

Zhang, Z., Chen, H., Xing, C., Guo, M., Xu, F., Wang, X., . . . Tang, J. (2011). Sodium citrate: A universal reducing agent for reduction/decoration of graphene oxide with au nanoparticles. *Nano Research, 4*(6), 599-611.

Zhang, Z., Fan, L.-P., & Wang, Y.-J. (2020). Applications of Chemical Kinetics in Heterogeneous Catalysis. In *Advanced Oxidation Processes-Applications, Trends, and Prospects*: IntechOpen.

Zhao, P., Li, N., & Astruc, D. (2013). State of the art in gold nanoparticle synthesis. *Coordination Chemistry Reviews, 257*(3-4), 638-665.

Zhou, F., Hearne, Z., & Li, C.-J. (2019). Water—the greenest solvent overall. *Current Opinion in Green and Sustainable Chemistry, 18*, 118-123.

Zhu, L., Zhang, C., Guo, C., Wang, X., Sun, P., Zhou, D., . . . Xue, G. (2013). New insight into intermediate precursors of Brust–Schiffrin gold nanoparticles synthesis. *The Journal of Physical Chemistry C, 117*(21), 11399-11404.

Zuber, A., Purdey, M., Schartner, E., Forbes, C., Van der Hoek, B., Giles, D., . . . Ebendorff-Heidepriem, H. (2016). Detection of gold nanoparticles with different sizes using absorption and fluorescence based method. *Sensors and Actuators B: Chemical, 227*, 117-127.